12-2010

Sequence and Chemostratigraphy of the Middle Cambrian Succession in Nevada and Utah

Robyn A. Howley
University of Nevada, Las Vegas

SEQUENCE AND CHEMOSTRATIGRAPHY OF THE MIDDLE CAMBRIAN SUCCESSION IN NEVADA AND UTAH

by

Robyn Allyn Howley

Bachelor of Science
Salem State College
1999

Master of Science
University of Nevada, Las Vegas
2002

A dissertation submitted in partial fulfillment of
the requirements for the

Doctor of Philosophy in Geoscience
Department of Geoscience
College of Science

Graduate College
University of Nevada, Las Vegas
December 2010

UNLV
UNIVERSITY OF NEVADA LAS VEGAS

THE GRADUATE COLLEGE

We recommend the dissertation prepared under our supervision by

Robyn A. Howley

entitled

Sequence and Chemostratigraphy of the Middle Cambrian Succession in Nevada and Utah

be accepted in partial fulfillment of the requirements for the degree of

Doctor of Philosophy in Geoscience

Ganqing Jiang, Committee Chair

Andrew Hanson, Committee Member

Matthew Lachniet, Committee Member

Steve Rowland, Committee Member

Vernon Hodge, Graduate Faculty Representative

Ronald Smith, Ph. D., Vice President for Research and Graduate Studies
and Dean of the Graduate College

December 2010

ABSTRACT

Sequence and Chemostratigraphy of the Middle Cambrian Succession in Nevada and Utah

by

Robyn A. Howley

Dr. Ganqing Jiang, Examination Committee Chair
Associate Professor of Geoscience
University of Nevada, Las Vegas

The House Range Embayment of western Utah and eastern Nevada was a prominent topographic feature on the passive margin of western North America during the middle and late Cambrian. In this study, detailed documentation of sequence boundaries, and their intervening sequences across a platform-to-basin transect of the House Range Embayment was used to establish a sequence-stratigraphic framework from which the depositional history of the embayment was deciphered. This framework was then used to test the hypothesis that the House Range Embayment formed by tectonic subsidence. In addition, the chemostratigraphic ($\delta^{13}C_{carb}$) record across the embayment was analyzed within this framework to (1) document the relationship between the FAD of *P. atavus* and the negative $\delta^{13}C$ Drumian Carbon Isotope Excursion (DICE), (2) clarify the relationship between sea-level change and the DICE, (3) refine the definition of the DICE event in a sequence stratigraphic framework, (4) test the hypothesis that the embayment was a restricted anoxic basin, and (5) explore the possibility of using carbon isotope excursions for regional/global stratigraphic correlation.

Five sequence boundaries were identified in the platform and correlated with condensed intervals in the basin within the known biostratigraphic framework. These sequence boundaries document the initial tectonic formation of the embayment and its subsequent infilling during tectonic quiescence. Five carbon isotope profiles indicate that the DICE is located stratigraphically above the FAD of *Ptychagnostus atavus* in the

embayment, associated with transgressive deposits on the southern platform, and with stratigraphic condensation in the basin. Two longer carbon isotope profiles do not reveal significant isotopic variability that can be attributed solely to local carbon cycling in an anoxic basin but they do reveal the effect of diagenetic alteration of platform values. The results also indicate that chemostratigraphic correlation in poorly dated successions deposited from significantly different paleoenvironments should be approached with caution.

PREFACE

Late Neoproterozoic rifting events led to rift-to-drift phase passive margin subsidence of the western margin of North America (northwest margin of Laurentia) during the Cambrian (Bond and Kominz, 1984; Levy and Christie-Blick, 1991; Prave, 1999). The rift-to-drift transition is characterized by a broad continental shelf composed of lower Cambrian terrigenous sediments. By the Cambrian Epoch 3 (formerly the 'middle' Cambrian), a broad carbonate platform developed in a passive margin setting along western Laurentia (Palmer, 1971). Siliciclastic sediment that was shed off the craton was deposited in coastal regions and in the deep-water basin. By the end of Epoch 3, a narrow deeper-water embayment, the House Range Embayment, formed on the carbonate-dominated shelf and extended as far east as the Canyon Range in western Utah. This deep-water embayment became the site of fine-grained carbonate and siliciclastic deposition, and strata from this interval contain exceptionally well-preserved Burgess Shale-type fossils that indicate the embayment contained a basinal anoxic water mass (Gaines and Droser, 2005; Gaines et al., 2005). Both Kepper (1976) and Rees (1986) interpreted the southern boundary of this embayment as a high-angle normal fault, although physical evidence of this interpretation is not available due to the lack of outcrop and of a precise palinspastic reconstruction. The northern margin of the embayment had a low angle ramp geometry that laterally fluctuated until the embayment was finally filled during the Furongian (Rees, 1986). Although the stratigraphic differences between the HRE and the equivalent shallow-water carbonate platform have long been recognized and lithostratigraphic correlations have been proposed (Robison, 1960, 1964; Palmer, 1971; Kepper, 1972; Hintze and Robison, 1975; Kepper, 1976; Rees, 1986; Hintze, 1988; Hintze and Davis, 2003), the evolution of the House Range Embayment and its influence on geochemical variability and stratigraphic architecture have remained largely unknown. The sequence and chemostratigraphic analyses

performed in this study were used to decipher the paleotectonic setting of the House Range Embayment and it's affect on sedimentation and fossil preservation.

In Chapter 1, the hypothesis that the House Range Embayment was formed by tectonic subsidence of the region surrounding and extending east of the House Range in west-central Utah was tested using a newly proposed sequence stratigraphic framework from the House Range Embayment to the southern carbonate platform. Stratigraphic sections were measured and analyzed from 5 geographic locations across the middle Cambrian shelf. From these sections, five sequence boundaries were identified and correlated between the platform and basin using the known biostratigraphic framework and vertical facies trends. Data from the interval surrounding sequence boundary 1 reveal formation of the House Range Embayment as a typical half-graben type basin in a carbonate-dominated setting with increased subsidence of the hanging wall recorded by basinal strata, and uplift and exposure of the footwall recorded by southern platform strata. Data from the remainder of Series 3 is less equivocal and may reflect either a complete cessation of tectonic subsidence or the influence of antithetic faults that limited tectonic subsidence to the region within the embayment. The results of this study represent one example of the application of sequence stratigraphic methods to correlation of laterally discontinuous outcrop sections over a large region in which biostratigraphic data is limited and highlight the applicability of sequence stratigraphic analyses to understand paleogeographic settings with more than one depositional controller.

Chapter 2 provides a detailed documentation of the negative Drumian Carbon Isotope Excursion (DICE) between the House Range Embayment and the southern carbonate platform in transgressive strata that overlie a regional sequence boundary. $\delta^{13}C_{carb}$ samples were collected from 5 sections in the interval surrounding sequence boundaries 1 and 2 from Chapter 1 to (1) document the relationship between the first

appearance datum (FAD) of *Ptychagnostus atavus* and the DICE, (2) clarify the relationship between sea-level change and the DICE, and (3) refine the definition of the DICE event in a sequence stratigraphic framework. Results indicate that the DICE is located stratigraphically above the FAD of *P. atavus,* associated with retrogradation of the shallow-water carbonate platform and with stratigraphic condensation in the basin and that in future global correlations, the DICE should be restricted to the negative carbon isotope anomaly slightly post-dating the Drumian GSSP. Identification and correlation of the DICE from the interval immediately above the Drumian Stage Global Stratotype Section and Point (GSSP) horizon in the Drum Mountains, Utah, to strata deposited on the southern carbonate platform is the first clear documentation of the DICE event globally in shallow-water strata. This documentation dramatically increases the applicability of use of the DICE as a global correlation tool, however further data is needed to truly distinguish whether the DICE in Nevada and Utah could be a local phenomena. Chapter 2 comprises a manuscript that was published in Palaeogeography, Palaeoclimatology, Palaeoecology in October 2010 (refer to Howley and Jiang, 2010; Elsevier License to reproduce # 25351711288042).

Chapter 3 presents data from two new carbon isotope profiles for the Cambrian Drumian Stage, one from the House Range Embayment basinal section at Marjum Pass in the House Range, Utah and one from the Panaca Hills platform section in eastern Nevada. . These profiles were used within the sequence stratigraphic framework documented in Chapter 1 to test the hypothesis that the House Range Embayment was a restricted, anoxic basin with a surface-to-deep carbon isotopic gradient larger than that of the modern ocean (~2‰) and similar to those gradients documented in other anoxic basins, and to examine the possibility of using carbon isotope excursions for regional/global stratigraphic correlation. Results however do not show systematic $\delta^{13}C_{carb}$ changes that would be expected if local carbon cycling in a prolonged anoxic

basin dominated the isotopic record. Results from the Wheeler Formation interval indicate either a history of periodic basin water anoxia or alternatively the effects of burial diagenesis of organic-rich sediments on the $\delta^{13}C_{carb}$ values of basin carbonate strata. Results from the Marjum Formation interval reveals a pattern opposite of that expected for an anoxic basin in that platform values are more negative than the basin indicating a history of meteoric diagenesis of platform carbonates in response to frequent exposure and karstification. The DICE excursion that was well documented in Chapter 2 is one of only two isotopic excursions that are correlated between these two new profiles. The second isotopic event is present below a sequence boundary on the platform and below its correlative conformity in the basin leading to the possibility that the excursion is a local phenomenon related to diagenetic alteration of platform sediments during exposure and transportation of these altered sediments to the basin during regression. Documentation of this event in other locations is necessary to determine its significance. No other easily identifiable isotopic trends are present in the section indicating that either isotopic trends were modified by later diagenesis or that isotopic excursions were limited during the latter half of the Drumian Stage. The results of this study indicate that carbon isotope chemostratigraphy should be used with caution in poorly dated successions.

ACKNOWLEDGMENTS

Most PhD students are told that a dissertation is an effort in perseverance as much as it is a scientific endeavor. This idea is only fully realized when it comes time to thank all those who helped guide and encourage you along the way. It seems almost impossible to express my appreciation for those who have helped me to this point, but I will do my best. First and foremost, I would not have made it this far without the constant support of my advisor Dr. Ganqing Jiang. As his first PhD student, who appeared unexpectedly in his office door, as he was first moving onto campus as a new faculty member, Ganqing has given me constant support and guidance. I would also like to thank my committee members, Drs. Andrew Hanson, Matthew Lachniet, Steve Rowland and Vernon Hodge for their time, advice, and support. My MS advisor, Dr. Peg Rees has also provided invaluable support and advice over the course of both my PhD and MS programs and I've definitely enjoyed reminding her of her Cambrian roots! Drs. Brenda Buck, Jean Cline and Michael Wells I would like to thank for their motivational support. The office staff, as usual, has been invaluable. Maria Figueroa, Liz Smith, Nicholle Booker and all the student workers who have graced the office were a life raft many times.

Any graduate research requires significant financial support and I would like to thank the following organizations for their support of mine: UNLV Foundation, UNLV Geoscience Department, AAPG, GSA, The Nevada Petroleum Society, Geological Society of Nevada, Institute for Cambrian Studies, and the American Chemical Society (PRF 43382-G8 to G. Jiang). I would also like to thank those scientists who at one point or another provided crucial assistance in my research: Clay Crow for constant assistance in the rock lab, Million Hailemichael for tireless work in the UNLV LVIS lab, and Drs. Pete Palmer, Dick Robison, Loren Babcock, Dave Osleger, and Melissa Hicks with knowledge of the Cambrian. I also need to express my gratitude to Lael Vetter and

Marty Erwin for field support, and also to all those geo students and trilobite hunters who I've interacted with along the way.

Last but certainly not least, I want to express my sincere appreciation to my family and friends who have put up with me in my latest quest. Their constant faith in me was truly a gift. Drs. Amy Brock and Kim Howell were true lifelines! I don't know what I would have done without their shoulders to lean on. The ECP's at ExxonMobil provided the right amount of encouragement in the form of 'are you done yet?'. My parents, my sisters and best friends, well I love them for always knowing the right things to say. Finally, I have to say thank you to my husband Scott. There are no words to describe how much he has sacrificed so that I could make it this far.

TABLE OF CONTENTS

LIST OF FIGURES

CHAPTER 1

STRATAL PATTERNS OF A SYNDEPOSITONAL FAULT-CONTROLLED CARBONATE PLATFORM: AN EXAMPLE FROM THE MIDDLE CAMBRIAN HOUSE RANGE EMBAYMENT IN THE GREAT BASIN, WESTERN UNITED STATES

Abstract

The middle Cambrian stratigraphic succession in eastern Nevada and western Utah recorded deposition on a passive continental margin where normal sedimentation patterns were disrupted by formation of a deep-water basin, the House Range Embayment, that intersected the carbonate-dominated shallow-water shelf and continued to affect sedimentation for nearly 6 million years. In this study, detailed documentation of sequence boundaries and their intervening sequences across the platform-to-basin transect of the House Range Embayment were used to establish a sequence-stratigraphic framework from which the depositional history of the embayment was deciphered. This framework was then used to test the hypothesis that the House Range Embayment was formed by tectonic subsidence of the region surrounding and extending east of the House Range in west-central Utah.

Five sequence boundaries were identified in the platform and correlated with condensed intervals in the basin within the known biostratigraphic framework. An abrupt change in depositional facies across sequence boundary 1 documents the initiation of tectonic subsidence during formation of the House Range Embayment. This interpretation differs from previous interpretations of a major eustatic rise above this sequence boundary. The remaining 4 sequence boundaries and their internal facies variations record the influences of both sea-level change and tectonic subsidence on sedimentation across the region until the end of the middle Cambrian when similar facies across the basin indicate infilling of the House Range Embayment. The results of this

study represent one example of applying sequence stratigraphic methods to correlate physical stratigraphic surfaces across discontinuous outcrop sections of varying depositional environments and to understand sequence development in paleogeographic settings with more than one depositional controller.

Introduction

Sequence boundaries were originally defined to explain large-scale stratal geometries observed in seismic data (Mitchum et al., 1977; Vail et al., 1977; Nystuen, 1988). In outcrop however, stratal patterns that are easily recognizable in seismic data require large-scale laterally extensive mountainside exposures such as the Book Cliffs in Utah or the Dolomites in Italy. Unfortunately, not all outcrops have exposure over the lateral distance necessary to observe these stratal geometries and features typically used to identify sequence boundaries in seismic data, such as toplap of underlying strata and onlap of overlying strata, are difficult or nearly impossible to discern (Cartwright et al., 1993; Myers and Milton, 1996; Catuneanu et al., 2009). In the absence of these features, predictive models of internal stratigraphic and facies relationships are used as a guide for identifying sequences, sequence boundaries and correlative conformities (Koerschner and Read, 1989; Van Wagoner et al., 1990; Goldhammer et al., 1990, 1992, 1993; Posamentier et al., 1992; Montañez and Osleger, 1993; Lehrmann and Goldhammer, 1999; Overstreet et al., 2003). This study represents an outcrop-based example of the identification and correlation of sequence boundaries across a shallow-water carbonate platform and a coeval fault-controlled deep-water basin in a carbonate-dominated, poorly fossiliferous depositional setting.

The middle Cambrian House Range Embayment in western Utah and eastern Nevada (Fig. 1) is hypothesized to have formed by tectonic subsidence along a series of normal faults and affected sedimentation across the region for nearly 6 million years

(Palmer, 1971; Kepper, 1976; Rees, 1986; Smith, 2007), although direct evidence of this fault is not available due to a lack of outcrop and lack of an accurate palinspastic reconstruction. Robison (1964) identified this basin based on the abrupt appearance of fine-grained shales and carbonate strata containing deep-water fossils in the region of the House Range in Utah, and in several mountain ranges across central Nevada. The vertical and lateral juxtaposition of these deep-water rocks in the shallow-water carbonate section indicated that there was a restricted basin that intersected the passive margin during the middle Cambrian. Kepper (1981) described evidence for syndepositional faulting along a north-northeast trending normal fault in southeastern California and western Nevada that he proposed as the southern extent of the House Range Embayment. Rees (1986) also supported a syndepositional tectonic control for formation of the House Range Embayment by documenting large-scale facies changes across the embayment in western Utah and central Nevada. The southern fault of the House Range Embayment is hypothesized to be located somewhere south of the Marjum Pass region of the House Range and north of the northern Wah Wah Mountains where rocks of the southern carbonate platform are exposed (Robison, 1964; Brady and Koepnick, 1979; Rees, 1986; Miller et al., 2003). Rees argued that the structural setting of the House Range, with the House Range and northern Wah Wah Mountains being situated on the same thrust sheet as documented by seismic reflection profiles beneath the Sevier Desert (Allmendinger et al., 1983), did not support post-Cambrian regional tectonic deformation as a cause for the lateral juxtaposition of basin and platform strata. In fact, more recent studies across west-central Utah support this interpretation (Levy and Christie-Blick, 1989; Hintze and Davis, 2003).

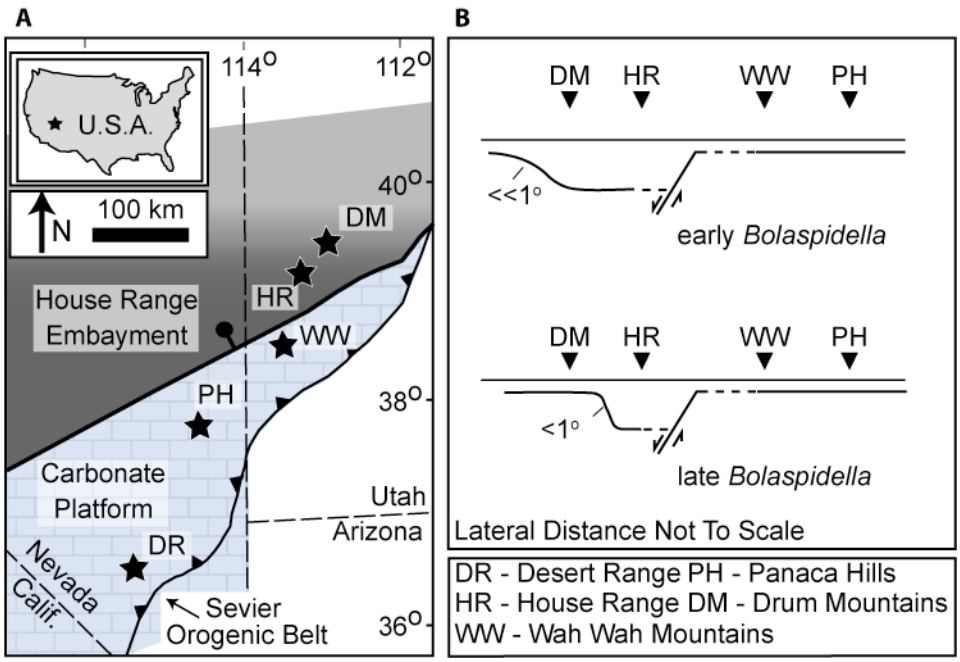

Figure 1. Non-palinspastic reconstruction (A) and cross section (B) of the House Range Embayment during the latest Ehmaniella and Bolaspidella trilobite zones (modified from Palmer, 1971; Rees, 1986; Elrick and Snider, 2002), with location of measured sections indicated.

Recently, studies have focused on the sequence stratigraphic framework of the HRE and southern platform. Montañez and Osleger (1993), Osleger and Montañez (1996), Osleger et al. (1996), Howley (2002) and Howley et al. (2006) used cycle stacking patterns to correlate strata of the *Bolaspidella* zone from southeastern California to the Wah Wah Mountains in central Utah. Langenberg (2003), Smith (2007), Brett et al. (2009), and Halgedahl et al. (2009) used cycle stacking patterns, gamma ray analysis, and carbon isotopes to correlate *Ehmaniella* and *Bolaspidella* zone strata between the House Range and Drum Mountains. None of these studies however attempted to correlate sequence boundaries or sequences between the southern platform and House Range Embayment and therefore a complete understanding of the affects of regional

tectonics on the sedimentation patterns across the margin remain unresolved. In this study, the hypothesis that the middle Cambrian House Range Embayment in western Utah and eastern Nevada formed by tectonic subsidence along a normal fault and affected sedimentation not only in the basin but also on the southern platform for nearly 6 million years is tested within a sequence-stratigraphic framework. The objective of this paper is to discuss how sequence boundaries were identified and correlated in this common outcrop setting and to integrate these sequence boundaries and intervening depositional sequences into a comprehensive model for evolution of the House Range Embayment.

Geologic background

Cambrian strata of western North America were deposited on a passive continental margin that developed over the rift associated with the breakup of the supercontinent Rodinia during the late Neoproterozoic (Bond and Kominz, 1984; Levy and Christie-Blick, 1991; Burchfiel et al., 1992; Poole et al., 1992). A broad continental shelf composed of terrigenous strata was formed on top of the rifted margin. By the middle half of the Cambrian, a northwest-facing carbonate platform covered most of present day Utah, Nevada, and southeastern California. During the latest *Ehmaniella* Chron, the carbonate platform was dissected by the formation of deep-water mixed carbonate-siliciclastic basin known as the House Range Embayment and was argued to have formed as the result of faulting along a northeast trending series of normal faults situated south and southwest of the House Range in Utah (Fig. 1). The depocenter of this basin was close to the present day Marjum Pass region of the House Range (Palmer, 1971; Kepper, 1976; Rees, 1986). Further north, a gentle carbonate ramp with a topographic gradient of approximately <1° existed between the Drum Mountains and Marjum Pass (Rees, 1986; Elrick and Snider, 2002). This asymmetric basin extended for more than

400 km from the shelf edge across the margin, was likely more than 100 m deep, and controlled the distribution of depositional facies through the early Ordovician (Rees, 1986; Miller et al., 2003). In regions to the south (a region herein referred to as 'the southern platform'), shallow-water carbonate deposition continued unimpeded (Palmer, 1971; Kepper, 1972; 1976; Rees, 1986).

Stratigraphic units associated with the Cambrian succession across the House Range Embayment are presented in Figure 2. The diverse stratigraphic nomenclature associated with units on the carbonate platform is the result of regional differences in naming conventions and is not related to significant differences in lithologic facies. Although the stratigraphic differences between the House Range Embayment and the southern platform have long been recognized and lithostratigraphic and sequence stratigraphic correlations have been proposed (Robison, 1960; 1964; Palmer, 1971; Kepper, 1972; Hintze and Robison, 1975; Kepper, 1976; Rees, 1986; Hintze, 1988; Hintze and Davis, 2003; Langenberg, 2003; Howley et al., 2006; Smith, 2007), no study has examined the stratigraphic correlation from strata of the House Range Embayment to strata of the southern carbonate platform over the entire stratigraphic interval covering the infilling history of the House Range Embayment. As a result, interpretations regarding the evolution of the House Range Embayment and the sea level versus tectonic control on stratigraphic and facies patterns are incomplete and remain untested and unresolved.

Biostratigraphic zonation

Biostratigraphic data were obtained from numerous literature sources and correlation schemes that are based on both polymerid (restricted shelf and open-shelf) and agnostoid (cosmopolitan) trilobites (Fig. 2; Robison, 1964, 1976, 1982; Rowell et al., 1982; Robison, 1984; Sundberg, 1991; 1996; Peng and Robison, 2000; Hintze and Davis, 2003; Babcock et al., 2004; 2007). Trilobites are rare in shallow-water carbonate

platform strata and are restricted to specific intervals that contain low diversity polymerid species. Specifically, two distinct trilobite faunas (e.g., *Ehmaniella* and *Eldoradia*) bracket the late Stage 5 and Drumian Stage strata investigated in this study. The widespread occurrence of *Ehmaniella* zone fauna provides a lower biostratigraphic control prior to formation of the House Range Embayment (Robison, 1964; Tschanz and Pampeyan, 1970; Kopaska-Merkel, 1988; Sundberg, 1991; 1996). In contrast, slope and basin strata of the House Range Embayment contain well-preserved polymerid and agnostoid species that have been successfully used in both regional and global biostratigraphic correlations (Robison, 1964, 1976, 1982; Rowell et al., 1982; Robison, 1984; Peng and Robison, 2000; Babcock et al., 2004; 2007). The Global Stratotype Section and Point (GSSP) for the Drumian Stage is defined at the first appearance datum (FAD) of the globally occurring agnostoid *Ptychagnostus atavus* within the Wheeler Formation in the Drum Mountains, and correlation with the FAD of *P. atavus* in the Wheeler Formation in the House Range provides a key horizon for global correlation. The FAD of *Lejopyge laevigata* (*calva*) is defined as the base of the Guzhangian Stage (Babcock et al., 2004; 2005; 2007) and has been tentatively correlated with the open-shelf polymerid *Eldoradia* and provides an important control for correlation in the mostly barren carbonate platform sections (Hintze and Robison, 1975; Robison, 1976; Hintze and Davis, 2003). Strata of the *Crepicephalus* and younger trilobite zones are highly fossiliferous and have tightly-constrained the biostratigraphic zonation of Gunzhangian Stage strata (Palmer, 1965; Hintze and Palmer, 1976; Lohmann, 1977; Cooper et al., 1982; Palmer, 1984). The top of the Guzhangian Stage and base of the overlying Paibian Stage of the Furongian Series is closely associated with the *Crepicephalus*-*Aphelaspis* boundary at the base of the Pterocephaliid biomere (Geyer and Shergold, 2000).

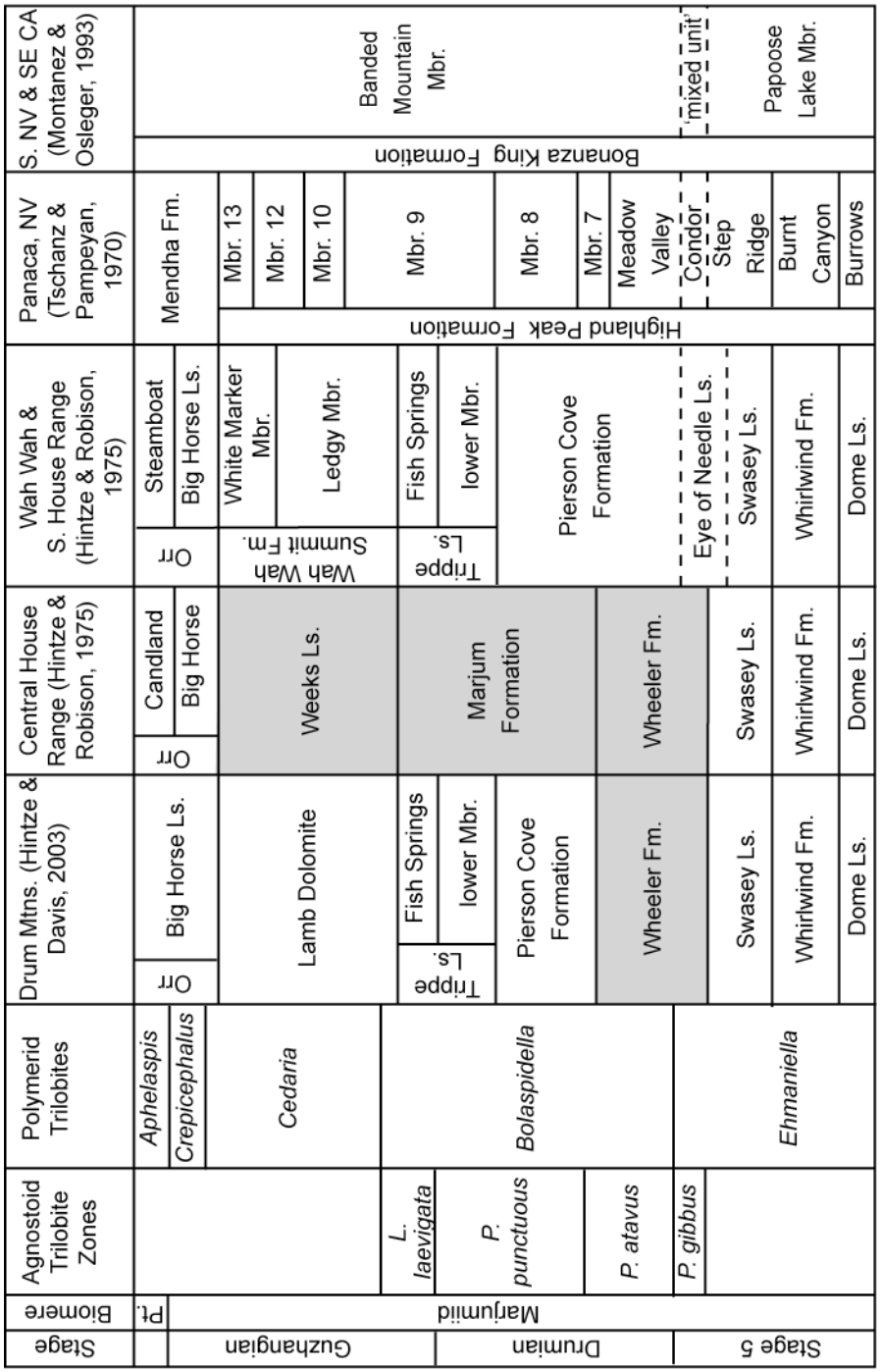

Figure 2. Correlation for stratigraphic units associated with the House Range Embayment based on a combination of previously published correlations (see references in chart) and the new sequence stratigraphic framework. Shaded units are deep-water strata.

Methods

Five composite stratigraphic sections, up to 1.4 km thick and covering a lateral distance of over 400 km, were measured and analyzed through bed-by-bed sedimentological analysis and lateral tracing of surfaces and facies, and placed into a new sequence stratigraphic framework for the middle Cambrian succession in Nevada and Utah. This new sequence stratigraphic framework was composed based on correlation of both newly described sequence boundaries and reinterpretated regional surfaces. Sequence boundaries documented in this study were integrated with published stratigraphic and biostratigraphic correlation schemes (Tchanz and Pampeyan, 1970; Hintze and Robison, 1975; Hintze and Palmer, 1976; Lohmann, 1977; Rees, 1986; Montañez and Osleger, 1993; Langenburg, 2003; Smith, 2007) to create the most up-to-date stratigraphic correlation for the interval surrounding House Range Embayment strata. This new correlation provides the most accurate data currently available for understanding the depositional history of the House Range Embayment and will allow for improved global correlation of this interval.

Sequence stratigraphy

Facies

Fourteen lithofacies are identified based on outcrop and petrographic analysis of the 5 sections measured across the House Range Embayment (Fig. 3; Table 1). Lithofacies were delineated based on composition, grain size and type, sedimentary structures, diagenetic fabric and vertical lithologic associations. The lithologic composition of middle Cambrian strata associated with the House Range Embayment include (1) predominantly pure carbonates with rare siliclcastic-rich intervals on the southern platform, and (2) interbedded fine-grained carbonates, and calcareous and non-calcareous shales with rare flat-pebble conglomerate in the House Range Embayment.

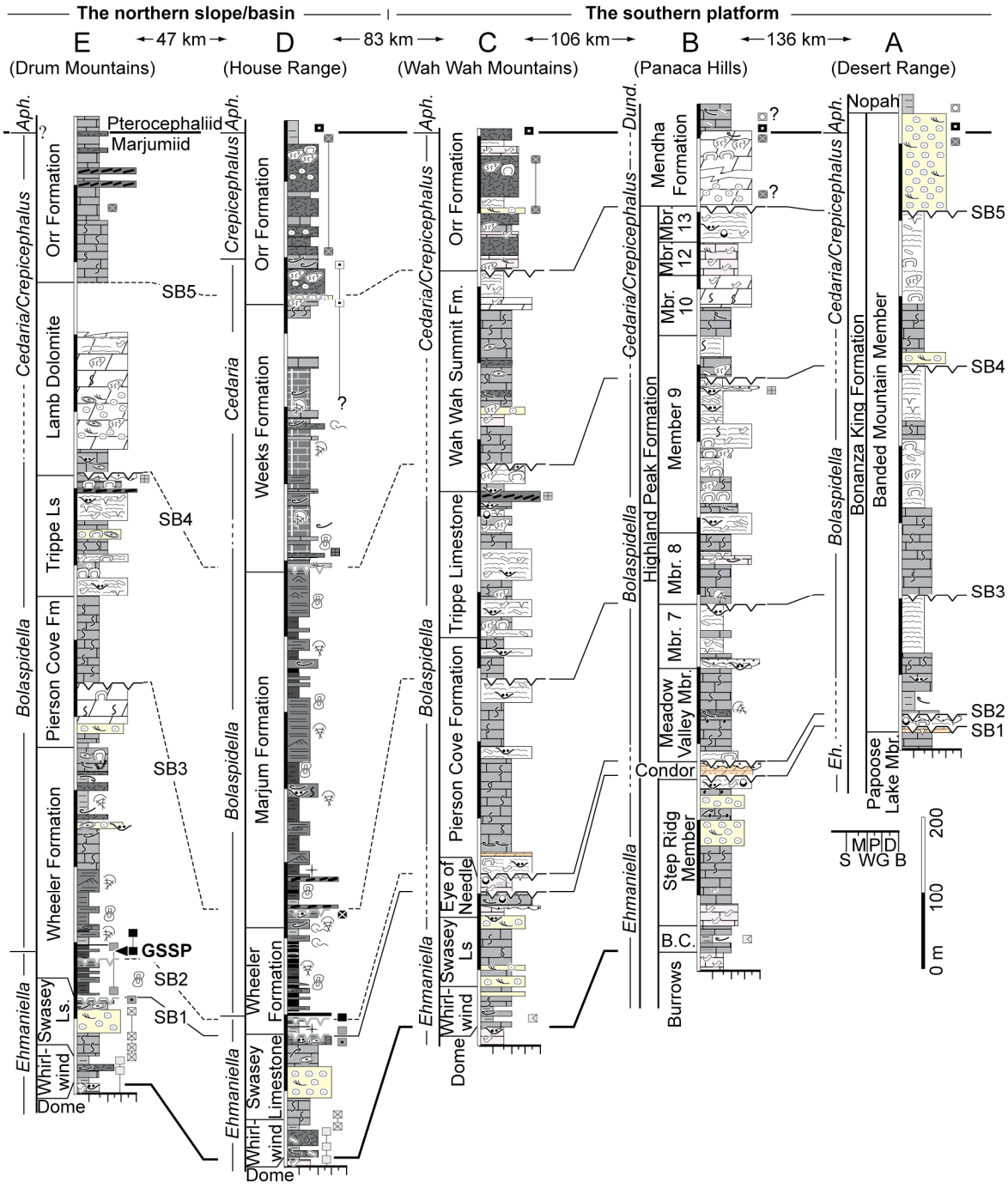

Figure 3. Sequence stratigraphic cross section across the middle Cambrian House Range Embayment. SB1-SB5 are sequence boundaries. Refer to the legend on the following page for symbol descriptions.

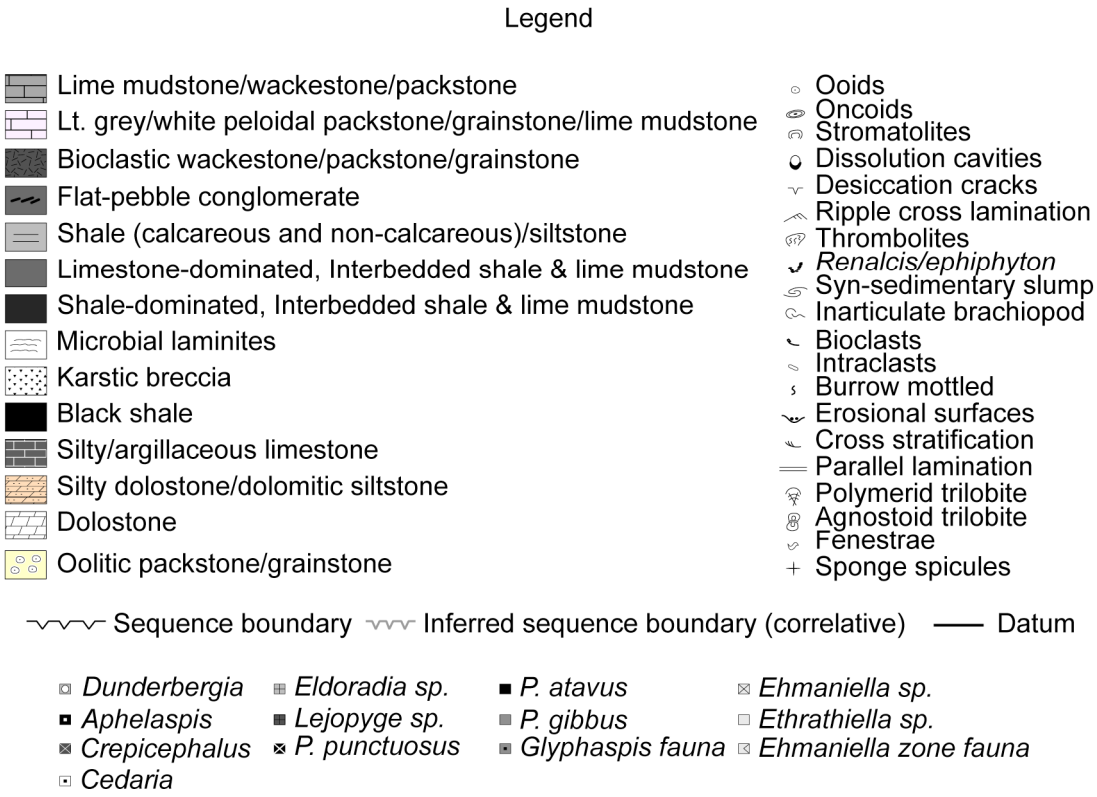

Figure 3 continued.

Table 1. Facies descriptions and interpretations.

Lithofacies	Description	Interpretation
Microbial laminites	Thin-bedded to finely-laminated; tabular beds; tan, light-grey to white; laminae of peloidal packstone/wackestone and grainstone are typical as are laminae of lime mudstone; thin laminae are typically wavy or crinkly; original mineralogy is commonly replaced by finely crystalline dolomite; upper surfaces of laminae and beds are commonly irregular and truncated by an erosional or dissolution surface; fenestrae and intraclasts are typical; dissolution cavities, desiccation cracks and evaporites are rare; fossils are absent except for *girvanella* and low-relief stromatolites..	Restricted intertidal to supratidal with elevated temperature and/or salinity.
Oolitic packstone/ grainstone	Medium-to-very thick bedding; medium grey; well-sorted; ooid nuclei are predominantly silt-sized peloids; cross-stratification is abundant; recrystallization of layers resulted in a 'tiger-striped' appearance; hardgrounds are common; fossils are rare but when present are predominately abraded trilobite fragments.	Open-marine shallow-subtidal platform margin or tidal bars.
Karstic breccia	Laterally discontinuous lenses and layers; light grey to white; angular to subangular clasts of microbial laminites, lime mudstone, peloidal packstone, and/or chert; poorly sorted; matrix is either wackestone or microcrystalline dolomite or clasts are cemented with calcite; microcrystalline calcite is also common; lower surfaces are irregular over the underlying topography; commonly infill underlying dissolution surfaces and cavities.	Supratidal dissolution features.
Black shale	Finely-laminated; calcareous and non-calcareous shale; silt is common; fossils are restricted to disarticulated algae.	Anoxic basin below SWWB.
Silty/ argillaceous limestone	Thin-to-medium bedded; tabular; medium grey; commonly laminated; argillaceous lime mudstone, silty lime mudstone and wackestone; silty and argillaceous laminated calcisiltite; micro-graded beds are common; interbedded with very-thin bedded lime mudstone, calcareous shale, or bioclastic grainstone; in places interbedded with laterally discontinuous lenses of trough cross-stratified grainstone; fossils are predominantly articulated agnostoid and polymerid trilobites.	Mid to outer slope and basin.
Silty dolostone/ dolomitic siltstone	Fine-grained; tabular; Medium-bedded to thickly laminated; tan to orange; laminated peloidal wackestone, lime mudstone, dolomudstone, silty dolomite, dolomitic siltstone and very fine-grained sandstone; most beds are replaced by finely crystalline dolomite; mottled textures, flaser bedding, planar and ripple-cross lamination, and trace fossils are typical; mudcracks, ripple marks and fossils are rare.	Shallow-subtidal to intertidal platform interior; siliciclastic-rich tidal flats.
Dolostone	Coarsely-crystalline dolomite; thick to massively bedded; white, light-to-medium grey, slightly pink; varying crystal sizes in seams and vugs parallel to bedding; in some locations follows fractures but predominately beds are laterally continuous; oncoids, ooids and microbial structures are common in some locations but in other locations the replacement was fabric destructive.	Replacement feature in most horizons but predominately shallow-subtidal to intertidal platform interior or platform margin.

Table 1 continued.

Lithofacies	Description	Interpretation
Lime mudstone/ wackestone/ packstone	Fine grained; tabular, thin-to-thick bedded; medium-to-dark grey; mottled texture with frequent dolomitization of mottles; hardgrounds are typical; peloids and intraclasts are common; fossils are rare except in certain beds.	Restricted subtidal platform interior; open-marine subtidal below FWWB.
Lt. grey/white peloidal packstone/ grainstone/ lime mud-stone	Fine-to-medium grained; tabular, thin-to-very thick bedded; light grey to white; graded bedding common; small-scale tabular cross-stratification common in some beds; fenestrae are typical; fossils are rare; peloids are typically well-sorted silt-to-very fine sized, rounded to subrounded, micrite but aggregate grains are also present in less well-sorted beds.	Shallow-subtidal to intertidal, restricted to open-marine platform interior.
Bioclastic wackstone/ packstone/ grainstone	Fine-to-coarse grained; thin-to-medium bedded; medium-to-dark grey; hardgrounds are common, bioclasts range from articulated to broken and abraded; rarely associated with small rounded oncoids; fossils include trilobites, echinoderm plates, sponge spicules and brachiopods.	Open-marine subtidal above and/or near FWWB.
Flat-pebble conglomer-ate	Very-thin to thin-bedded; tabular to lenticular beds; medium-to-dark grey; discoidal to tabular rounded to subrounded clasts of pebble-to-cobble sized lime mudstone; imbrication is common in certain beds; matrix is lime mudstone; calcite-filled shelter porosity is rare; conglomerate beds are interbedded with calcareous shale or lime mudstone.	Where interbedded with shale: gravity flow deposited along the outer slope below SWB; where interbedded with lime mudstone: restricted shallow-subtidal platform interior.
Shale/siltsto ne	Green, brown, beige, grey and black calcareous and non-calcareous shale and siltstone; very thin-bedded to laminated; interbedded with predominantly very thin-bedded lime mudstone and calcisiltite, or bioclastic grainstone; fossil content varies but commonly associated with trilobites, algae, inarticulate brachiopods and rarely soft-bodied fossils such as annelid worms and arthropods.	Deep-subtidal outer slope and basin below SWWB; semi-restricted shallow-subtidal platform interior.
Limestone-dominated, interbedded shale and lime mud-stone	Thin-bedded to finely-laminated; tabular beds; intervals of rhythmitic bedding are common; medium grey; lime mudstone or calcisiltite interbedded with calcareous shale, argillaceous lime mudstone, silty lime mudstone or silty dolomite; ls>sh; micro-graded bedding and ripple cross-stratification are common; syn-sedimentary slump structures and hardgrounds are rare; finely disemminated pyrite is common; associated fossils are predominantely trilobites (both articulated and disarticulated).	Outer slope and basin below SWWB; mostly turbidites.
Shale-dominated, interbedded shale and lime mud-stone	Thin-bedded to finely-laminated; tabular beds; light grey to beige on weathered surface and dark grey on fresh surface; calcareous and non-calcareous shale (and rare siltstone) intercalated with very-thin beds of lime mudstone argillaceous lime mudstone; sh>ls; associated fossils are predominantely trilobites (both articulated and disarticulated agnostoid and polymerid), algae, sponge spicules and inarticulate brachiopods.	Outer slope and basin below SWWB.

Sequence boundaries

Five sequence boundaries were documented on the southern carbonate platform and correlated with five correlative conformities in the basin (Fig. 3). The criteria used for identifying sequence boundaries on the platform include: (1) localized karstic breccias filling in shallow paleokarstic depressions or cavities, (2) reworked karstic breccias as lenticular intraclastic grainstone/packstone lags along the surface, (3) intensified cm-sized dissolution cavities and desiccation cracks below the surface and disappearance of such features in overlying strata, and (4) abrupt facies changes and facies stacking patterns representing a change from shallower-water to deeper-water deposits, although the magnitude of change may not be large (Fig. 4). Criteria for identifying sequence boundaries in the basin are more subtle than on the platform but include: (1) submarine hardgrounds with iron oxide and/or phosphate coatings and truncated bioclasts, (2) abrupt increase in skeletal lags with abraded and reworked bioclasts, (3) an increase in grain size and texture of carbonate particles, and (4) abrupt facies changes and stacking patterns from carbonate-dominated below the sequence boundary to either siliciclastic-dominated or siliciclastic-rich above (Fig. 5). Individual criteria in basinal sequences are not singularly indicative of a sequence boundary, and in fact both criteria 1 and 2 can also be present at maximum flooding surfaces, but when one of these criteria is combined with criteria number 3 and 4, the surface is interpreted as a sequence boundary.

Platform sequence boundaries

On the southern platform, sequence boundary (SB) 1 and SB2 are closely associated with a stratal thickness of <20 meters between them (Fig. 6). SB1 is present at the top of a shallowing-upward sequence of peritidal strata that is predominately composed of finely laminated and fenestral peloidal packstone, dolostone, and dolomitized microbial laminites, with dolomitic siltstone abundant in the Desert Range.

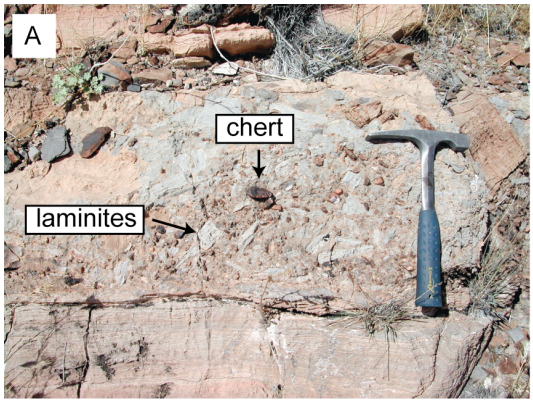
A
chert
laminites

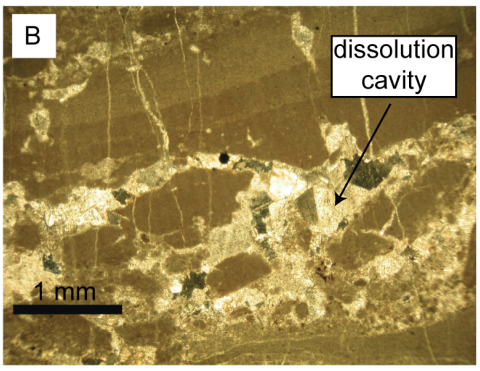
B
dissolution cavity
1 mm

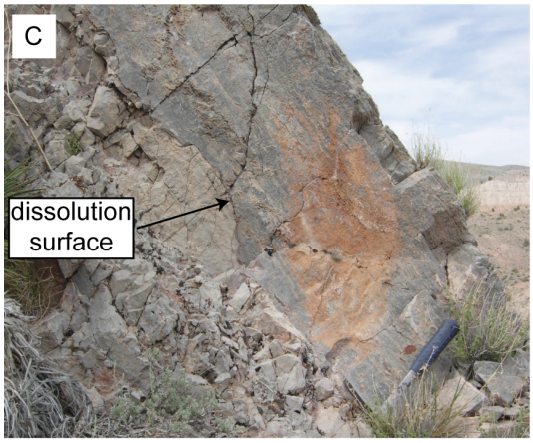
C
dissolution surface

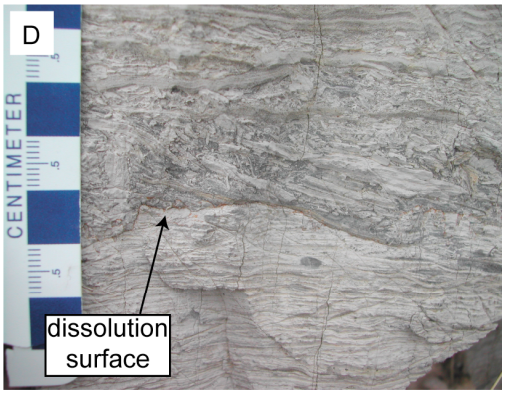
D
CENTIMETER
dissolution surface

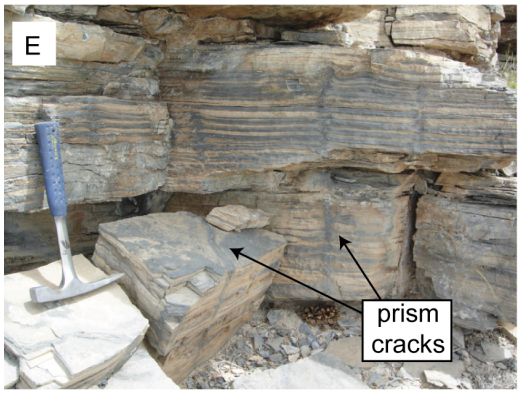
E
prism cracks

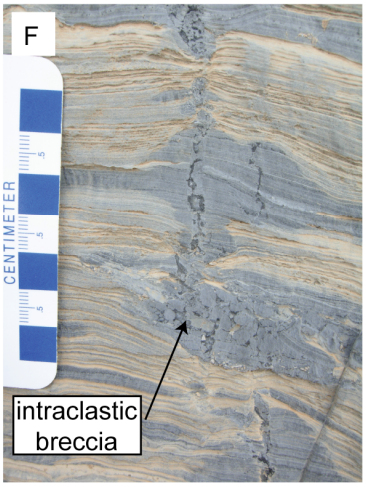
F
CENTIMETER
intraclastic breccia

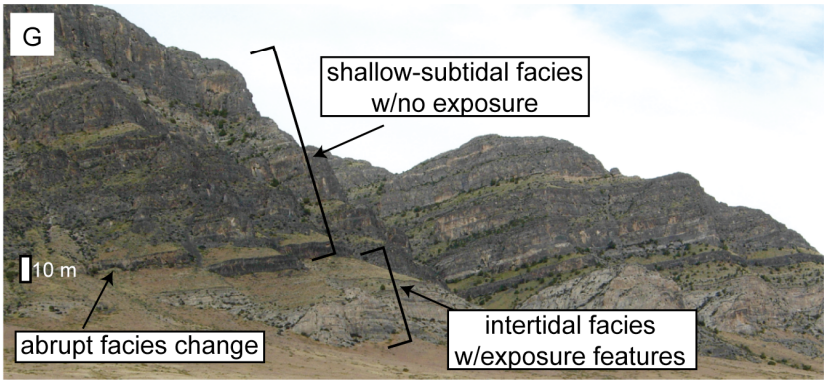
G
shallow-subtidal facies w/no exposure
10 m
abrupt facies change
intertidal facies w/exposure features

Figure 4. Examples of criteria for identifying sequence boundaries in platform strata. (A) Karstic breccia at SB1, Bonanza King Formation, Indian Ridge, Nevada. (B) Dissolution cavity and breccia in laminated lime mudstone below SB1, Step Ridge Member, Highland Peak Formation. Crossed Nicols. (C) Dissolution surface separating dolomitized microbial laminite beds, Step Ridge Member, Highland Peak Formation. Hammer for scale. (D) Intraclastic breccia overlying an irregular dissolution surface below SB3, Pierson Cove Formation, Wah Wah Mountains. (E) Dissolution feature penetrating laminated lime mudstone and microbial laminae from SB4 in the Fish Springs Member, Trippe Limestone, Wah Wah Mountains. (F) Close-up of a dissolution feature from E with internal intraclastic breccia in calcite cement. (G) An example of a large-scale abrupt change in facies across a sequence boundary. SB2, Eye of Needle Limestone and basal Pierson Cove Formation, Wah Wah Mountains.

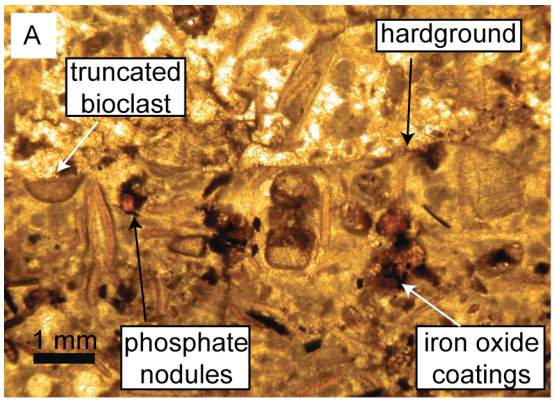
A
truncated bioclast
hardground
1 mm
phosphate nodules
iron oxide coatings

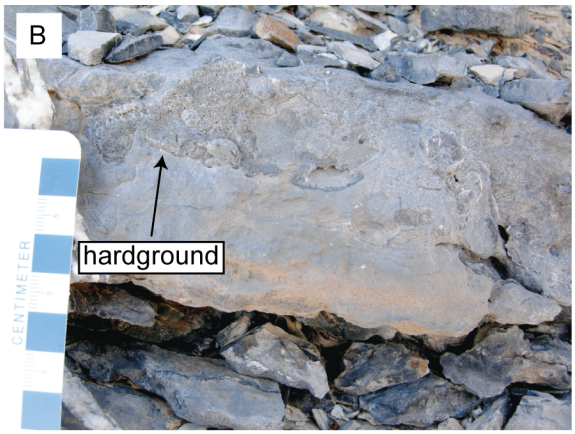
B
hardground


C

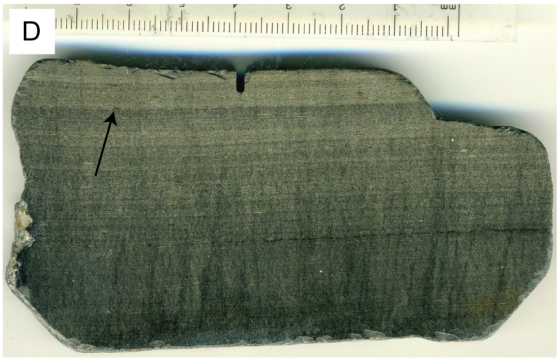
D

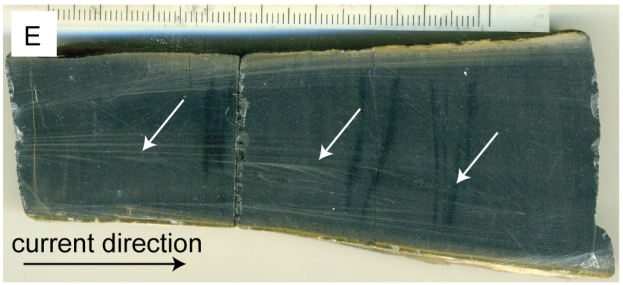
E
current direction

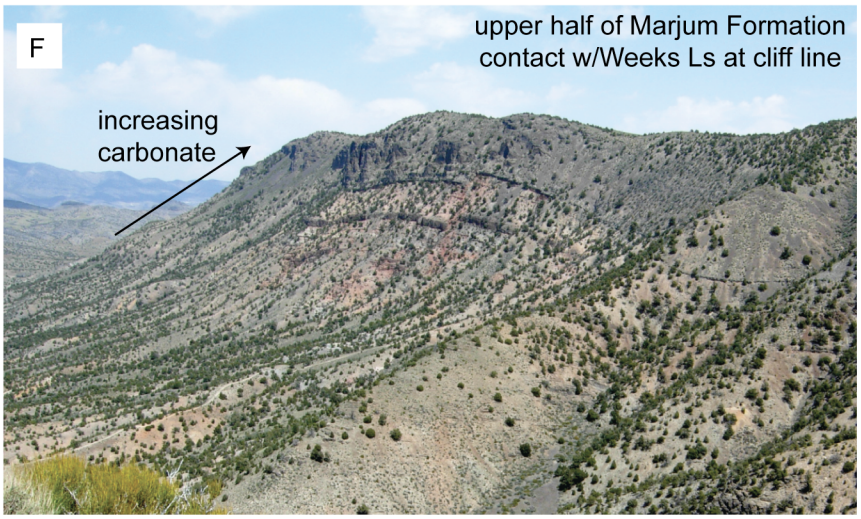
F
upper half of Marjum Formation
contact w/Weeks Ls at cliff line
increasing carbonate

Figure 5. Examples of criteria used to identify sequence boundaries (correlative conformities) in the basin. (A) Truncated grains associated with a submarine hardground in a bioclastic wackestone/packstone, Swasey Limestone, Drum Mountains. (B) Submarine hardground surface in lime mudstone, Marjum Formation, House Range. (C) Very thinly bedded rhythmites in the basal Marjum Formation below SB3. Gray beds are lime mudstone and calcisiltite, and orange layers are argillaceous lime mudstone. (D) Planar laminated calcisiltite with bedding plane aligned agnostoid trilobites (arrow). Sample has normally graded bedding, Wheeler Formation, House Range. (E) Ripple (arrows) cross-laminated lime mudstone and calcisiltite in a very thinly bedded turbidite from the Wheeler Formation, House Range. (F) Example of increasing carbonate component of sequences towards a sequence boundary. SB4 is present at the cliff line contact between the Marjum Formation and argillaceous-rich Weeks Limestone. Marjum Pass, House Range.

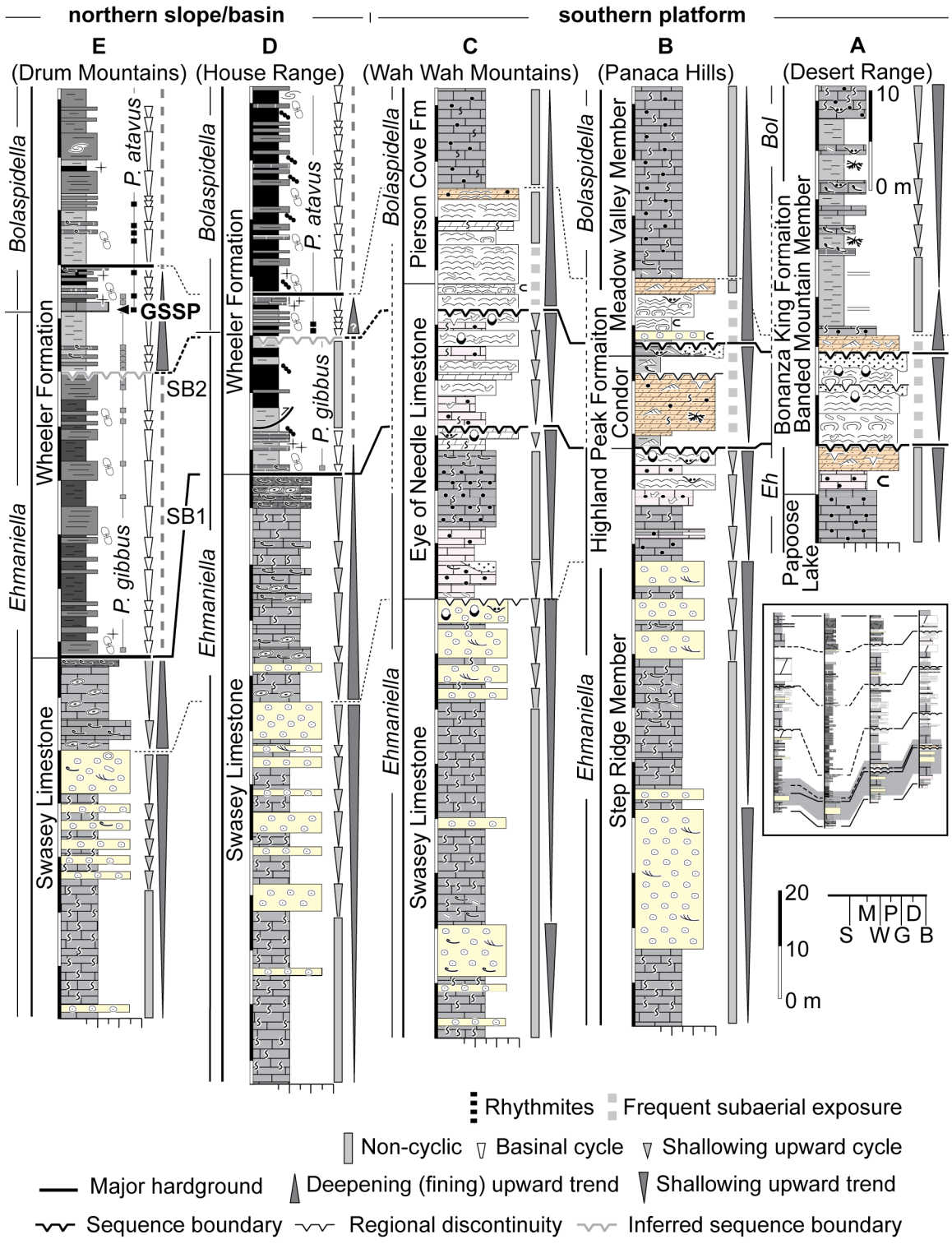

Figure 6. Sequence stratigraphic cross-section across SB1 and SB2 and associated with formation of the House Range Embayment. Inset of Figure 3 shows the interval highlighted in gray.

Intensified dissolution cavities and fissures mark the surface itself, with irregular dissolution surfaces having surficial relief ranging from centimeters to meters. In the Wah Wah Mountains, pockets of dolomudstone and wackestone breccia fill possible paleokarstic dykes that penetrate downwards up to 10 m below the surface. In the Desert Range, mudcracks are a common feature in the interval below SB1. SB2 is present at the top of the interval above SB1 that is dominated by finely laminated and dolomitic microbial laminates in the Desert Range and Wah Wah Mountains, and finely laminated dolomitic siltstone and silty dolostone in the Panaca Hills. The SB2 surface is marked by laterally discontinuous karstic breccia that vary in grain size and vertical thickness across the southern platform. The most extensive breccias are present in the Desert Range where they are composed of pebble- to cobble-sized angular clasts of microbial laminites and chert that fills in the underlying paleokarstic depressions. In each section, this surface is abruptly overlain by a deepening upward succession of facies that are devoid of exposure features.

The sequence boundaries SB3, SB4 and SB5 are fairly similar in characteristics across the southern platform and in the Drum Mountains (Figs. 3, 7 and 8). Strata above SB2 and below SB3 in the Drum Mountains change from fine-grained carbonates and shale near SB2 to coarse-grained carbonates and dolostone near SB3 and therefore by SB3 the Drum Mountains section records deposition in environments similar to those of the southern platform. SB3, SB4 and SB5 are all abrupt contacts at the top of shallowing-upward sequences of carbonate strata where dolomitic and non-dolomitic microbial laminites are the dominant lithology immediately below the sequence boundary. The only exception is SB3 in the Drum Mountains that overlies a laterally extensive crystalline dolomite. Common to each sequence boundary are the presence of multiple surfaces with exposure-related features in the interval directly below the sequence boundary. Features associated with these sequence boundaries include thin

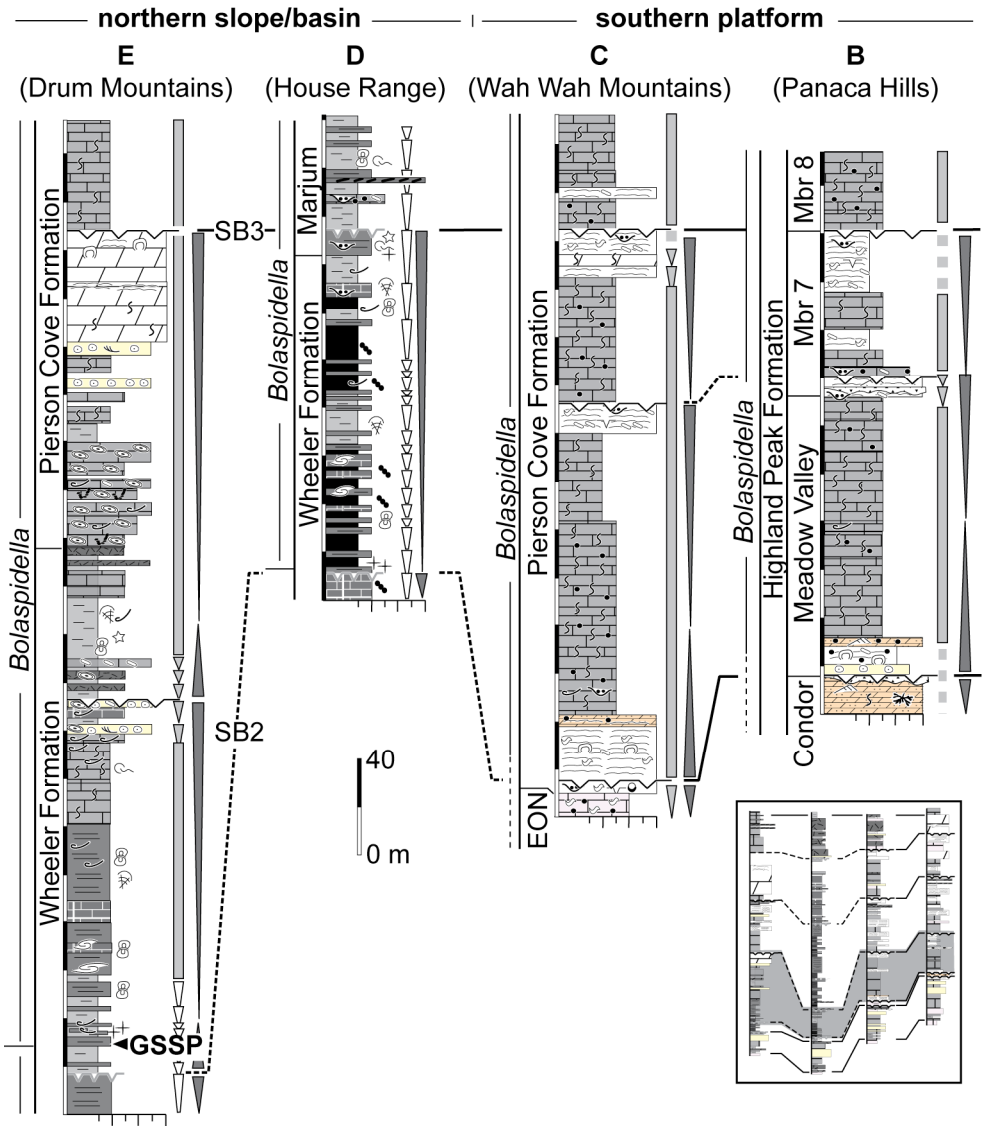

Figure 7. Sequence stratigraphic cross-section across the interval between SB2 and SB3. Inset of Figure 3 shows highlighted interval. Refer to Figure 3 for lithologic symbols and Figure 6 for cycle and surface symbols.

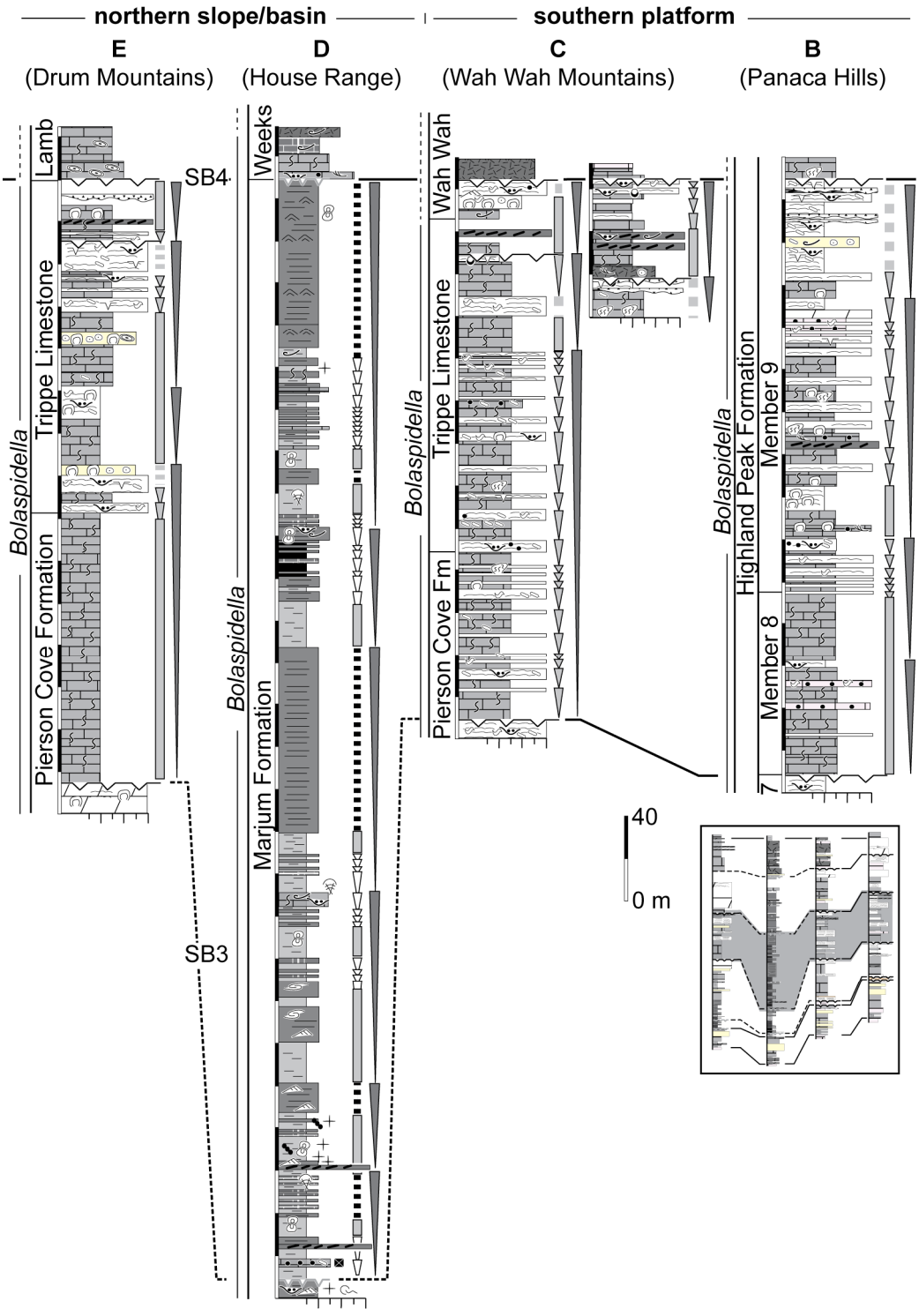

Figure 8. Sequence stratigraphic cross-section for the sequence between SB3 and SB4. Inset of Figure 3 shows highlighted interval. Refer to Figure 3 for lithologic symbols and Figure 6 for surfaces and cycles.

paleokarstic depressions, truncated microbial laminae, minor erosional surfaces, dissolution features, desiccation cracks, and reworked karstic breccias. Exposure features are most well developed at SB4 where thin-bedded peritidal cycles dominate and are interbedded with flat-pebble conglomerate layers and laterally discontinuous karstic breccias. Each sequence boundary is abruptly overlain by lithologic facies that are devoid of exposure features, typically mottled mudstone and wackestone or bioclastic/oolitic grainstone.

Basin sequence boundaries

In the House Range Embayment, SB1 and SB2 are not as closely associated as on the southern platform (Fig. 6). SB1 is the abrupt contact between the Swasey Limestone and Wheeler Formation in both the House Range and Drum Mountains. This surface is marked by a major hardground that contains truncated bioclasts cemented with fibrous calcite cement and many grains are coated with iron oxide and phosphate. The upper beds of the Swasey Limestone are dominated by thinly bedded oncolitic wackestone/packstone, interbedded with thin beds of bioclastic packstone/grainstone and wackestone that contain a diverse open-marine fauna (Fig. 9; Glyphaspis fauna; Randolph, 1973; White, 1973; Robison, 1976). Above SB1, the lower Wheeler Formation is dominated by parallel-laminated calcareous shale interbedded with subordinate amounts of very thin-bedded lime mudstone and argillaceous lime mudstone (Fig. 10). The overlying SB2 is subtle in both basinal sections but is marked by a change in strata from a sequence of increasing fine-grained carbonate below to an interval of shale and more argillaceous limestone above.

No exposure features are present at any of the sequence boundaries in the basinal section in the House Range, however, SB3, SB4, and SB5 each are present at the top of sequences of strata where the amount of carbonate layers increases upsection and shale decreases. SB3 is the upper surface of a 10-m-thick interval of carbonate-

dominated rhythmites of the basal Marjum Formation. This interval contains abundant submarine hardgrounds and a diversity of fossil content including sponge spicules, inarticulate brachiopods, articulated echinoderms, disarticulated polymerid trilobites and agnostoid trilobites indicating an active infauna. SB4 is also at the top of an interval of carbonate-dominated rhythmites, in this case containing intercalated carbonate mud mounds that are composed of peloidal wackestone and calcite cement layers. SB5 is present at the top of a shallowing-upward sequence of carbonate strata that culminate with a thin oolitic grainstone layer capping a thrombolitic biostrome. Abruptly overlying SB3 and SB4, lithologies become more argillaceous. Above SB5 strata are composed of coarse-grained bioclastic wackestone and packstone.

Sequence stratigraphic framework

The fragmented nature of Cambrian strata in the Basin and Range Province makes physical tracing of sequence boundaries impossible between mountain ranges; however, the trilobite-based biostratigraphic control present in the studied interval provides a solid enough framework for correlation between the platform and basin. The five sequence boundaries identified occur within a succession that is bracketed at its base by (1) a sequence boundary present at the top of the Dome Limestone that formed prior to initiation of the HRE and is constrained by fauna of the *Ehmaniella* biozone (lower datum in Fig. 3; Tchanz and Pampeyan, 1970; Hintze and Robison, 1975; Kopaska-Merkel, 1988; Sundberg, 1991; 2005), at its top by (2) the tightly constrained Marjumiid - Pterocephaliid biomere boundary near the base of the Candland and Steamboat Pass Shale members of the Orr Formation, base of the Mendha Formation, and top of the Bonanza King Formation (upper datum in Fig. 3; Palmer, 1964; 1965; 1979, Ludvigsen and Estrop, 1985, Evans, 1997), and in its middle by (3) the proposed *Eldoradia* – *Lejopyge laevigata* correlation (Hintze and Robison, 1975; Robison, 1976; Hintze and Davis, 2003).

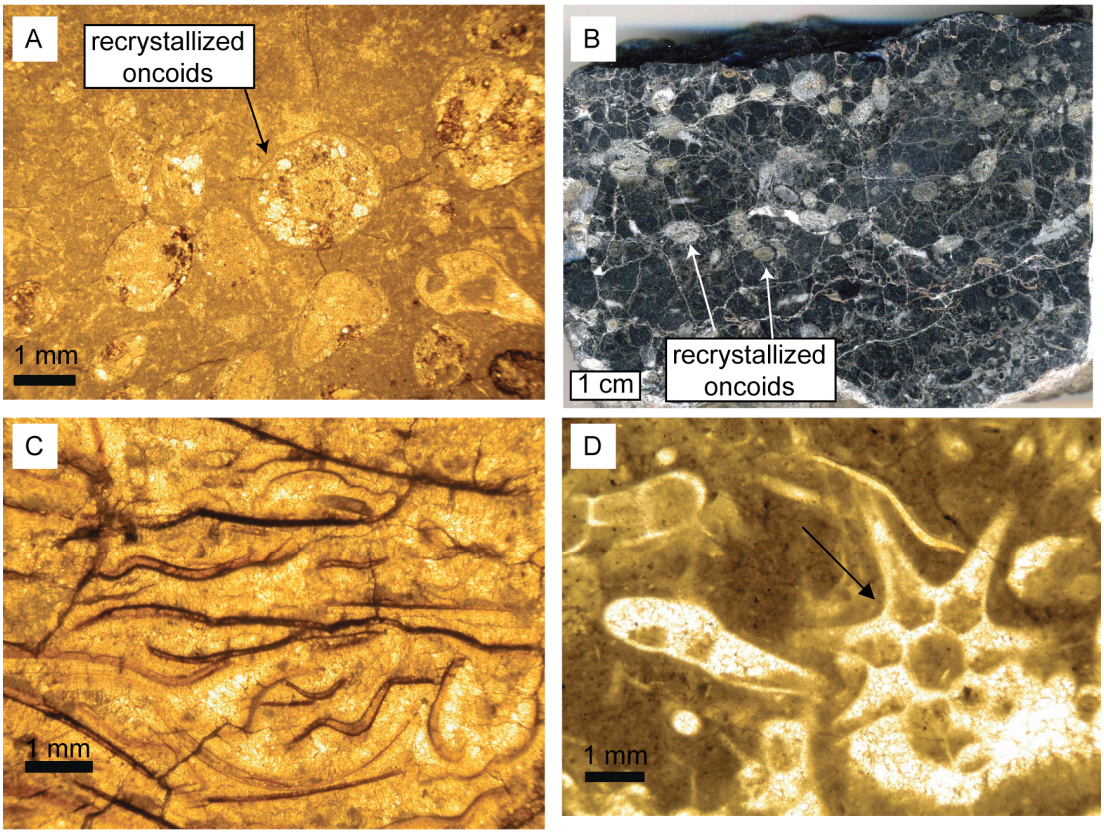

Figure 9. Examples of facies associated with the deepening of the House Range Embayment recorded in the upper beds of the Swasey Limestone. (A) Recrystallized micritic oncoids in a wackestone matrix, Drum Mountains. (B) Recrystallized oncoids in a wackestone matrix, House Range. (C) Bioclastic grainstone (skeletal lag) composed of trilobite fragments, Drum Mountains. (D) Sponge spicules (*chancelloria* – arrow) and other bioclasts in a wackestone matrix, House Range.

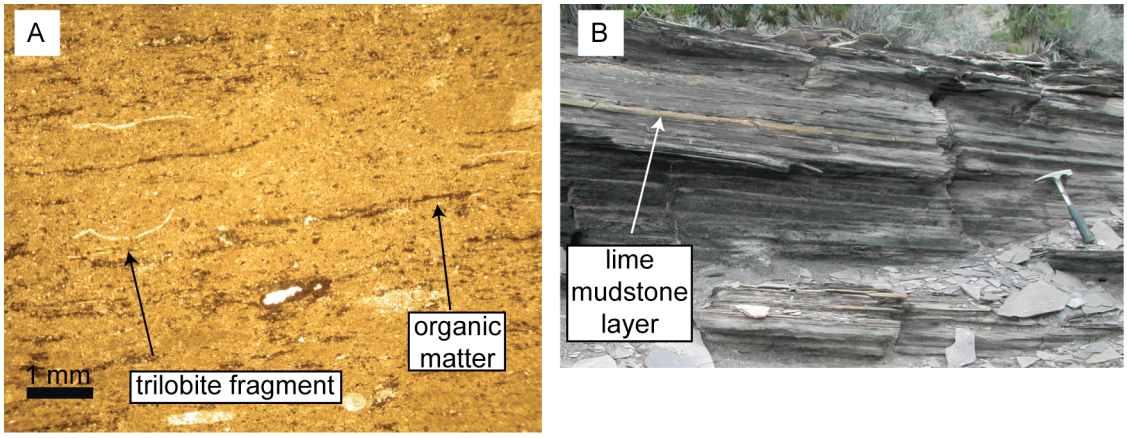

Figure 10. Examples of the shale-rich lower Wheeler Formation in the House Range. (A) Argillaceous lime mudstone with trilobite fragments and organic matter aligned with laminae. (B) Black and gray paper shale with very thin beds of lime mudstone.

The stratigraphic patterns of individual sequences were examined within the framework of the previously described sequence boundaries (Fig. 3). The intervening sequences are characterized primarily by large-scale shallowing-upward trends in facies. In carbonate platform strata, these shallowing-upward sequences are expressed in the lower portion by thick packages of mottled wackestone and peloidal wackestone and in the upper portion by increasing amounts of microbial laminites, many of which have been dolomitized (Fig. 11). Deviations from this general trend include (1) the sequence between SB1 and SB2 where strata are composed of interbedded microbial laminites and peloidal wackestone and mudstone, with dolomitic siltstone common in some locations and exposure surfaces abundant throughout; and (2) the sequence between SB4 and SB5 in the Drum Mountains where strata are composed of coarse-grained oolitic and oncolitic grainstone/packstone at the base and fine-grained, fenestral microbial dolostone at the top; all of which have been heavily altered to coarsely crystalline dolomite.

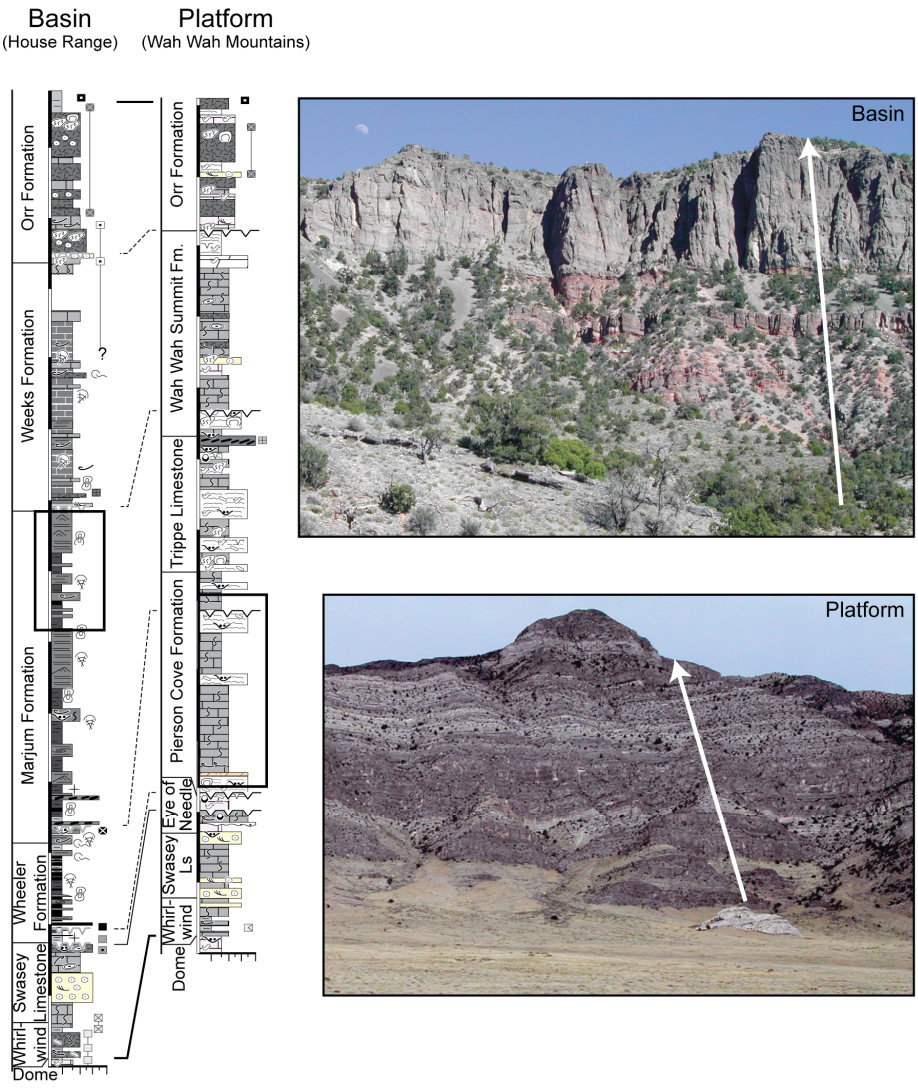

Figure 11. Examples of the difference between a shallowing-upward sequence in the basin compared to one on the platform. Basin example is from the upper Marjum Formation in the House Range (see inset on left stratigraphic column). Platform example is from the Pierson Cove Formation in the Wah Wah Mountains (see inset on left).

In the basinal strata, shallowing-upward sequences are primarily composed of shale-rich lower portions (argillaceous-rich in the case of the Weeks Limestone) and carbonate-rich upper portions, with increasing amounts of coarse-grained carbonates towards the top (Fig. 11). A deviation in this pattern is present in the lower Wheeler

Formation in both the Drum Mountains and House Range where carbonate strata above SB1 decrease in frequency upsection to a shale-rich interval and then increase in frequency again towards SB2, although this trend is less apparent in the Drum Mountains.

Examination of the overall pattern of facies between SB1 and SB5 reveals an even larger-scale shallowing-upward trend. In southern platform strata, dolomitized microbial laminites and other intertidal facies increase upsection. In the House Range Embayment, the amount of carbonate increases upsection corresponding with a decrease in the amount of shale or argillaceous limestone. Bioturbation features and platform-derived grains such as ooids, peloids and bioclasts also increase towards the top of the overall sequence. In the Drum Mountains section, the transition from basinal strata to shallow-water platform strata is most pronounced between SB2 and SB3.

Above SB5, coarse-grained oolitic and bioclastic grainstones dominate the southern platform and extend across the previously existed basinal sections of the House Range Embayment. Below SB1 however, the overall pattern of facies above the lower datum is not consistent between sections (Fig. 3 and 6). An overall shallowing-upward trend is expressed by vertical changes from non-cyclic intervals of mottled wackestone and oolitic grainstone, to intervals that contain cyclic repetition of the same facies and increasing amounts of oolitic grainstone. In southern platform strata, this trend continues upsection to SB1 with an increase in microbial laminae and exposure features. In sections containing subsequent basinal strata however, the shallowing-upward trend identified on the southern platform is not observed and instead an abrupt irregular surface marks a change from shallowing-upward to deepening-upward strata. This abrupt transition is documented in Figure 6 by a dotted line in the Swasey Limestone. Above this horizon, thinly bedded oncolitic-bioclastic wackestone beds grade vertically into thinly bedded bioclastic packstone/grainstone facies that contain a diversity of fossil

material. Capping this deepening-upward sequence is the major submarine hardground at SB1.

Discussion

Formation of the House Range Embayment

Formation of the House Range Embayment is documented in strata associated with SB1 (Figs. 3 and 6). Above the lower datum, all sections contain thick packages of oolitic grainstone and mottled wackestone. These deposits were likely formed in the shoreface portion of an oolitic sand shoal that expanded/migrated into a semi-restricted subtidal back-barrier lagoon. On the southern platform, these lagoonal and shoreface deposits are replaced upsection by thin-bedded fenestral peloidal packstone and dolomitized microbial laminites. These deposits, with their abundant exposure features, record decreasing accommodation and shallowing to tidal flat environments on the southern platform culminating in prolonged exposure at SB1.

In contrast, lagoonal and oolitic shoal deposits in the House Range and Drum Mountains are abruptly replaced upsection by thin-bedded oncolitic-bioclastic wackestone beds that grade vertically into thin-bedded bioclastic packstone/grainstone beds. These coarse-grained carbonate beds were formed under subtidal, open-marine conditions and most likely represent deposition in lower shoreface to foreshore environments at the seaward edge of an oolitic shoal. This interpretation is based on the presence of small (< 1 cm diameter) spherical micritic oncoids with concentric laminae and bioclastic nuclei which indicate formation under high-energy conditions, and their presence in bioclastic wackestone beds indicate transportation downslope into quieter-water conditions in the lower shoreface. Less spherical and well-rounded oncoids indicate deposition under intermittent high-energy conditions (Flugel, 2004). The diversity of bioclastic material associated with these beds, consisting of trilobites,

echinoderm sclerites, sponge spicules and inarticulate brachiopods indicate that a diverse open-marine fauna was active during deposition. Bioclastic packstone and grainstone beds that cap the sequence are interpreted as reworked bioclastic lag deposits due to the abraded texture of bioclasts and formed when fine-grained material was winnowed away from the seafloor by high-energy currents or moderate but consistent currents; consistent with interpretations made by White (1973) and Caldwell (1980). These deposits represent a phase of sediment starvation and condensation in the basin associated with SB1.

The contrasting records below SB1 reveal decreasing accommodation on the southern platform and increasing accommodation in the House Range Embayment, all occurring prior to SB1. This juxtaposition is interpreted as recording the initial tectonic subsidence in the region of the House Range, and uplift of the southern platform that accommodated vertical movement along a normal fault, or series of normal faults (Fig. 12A). Uplift of the southern platform eventually resulted in negative accommodation and formation of SB1. Increased subsidence in the basin, in conjunction with exposure of the platform resulted in sediment starvation and condensation in the basin at SB1. This interpretation is based on the fact that in carbonate-dominated systems with minimal siliciclastic input, early lithification of sediments results in decreased transport of carbonate material during lowstands and adjacent basins are typically sediment starved (Leeder and Gawthorpe, 1987; James and Kendall, 1992; Berra, 2007).

Strata present between SB1 and SB2, consisting of (1) a thin interval of intertidal to supratidal facies with intensified exposure surfaces on the southern platform, (2) a thick interval of fine-grained and finely laminated carbonates and shales with common pelagic fossils in the Drum Mountains, and (3) a thin interval of calcareous and black shale with intercalated very thin beds of fine-grained argillaceous carbonate, indicate a major shift in depositional environments across the region. While the initial activation

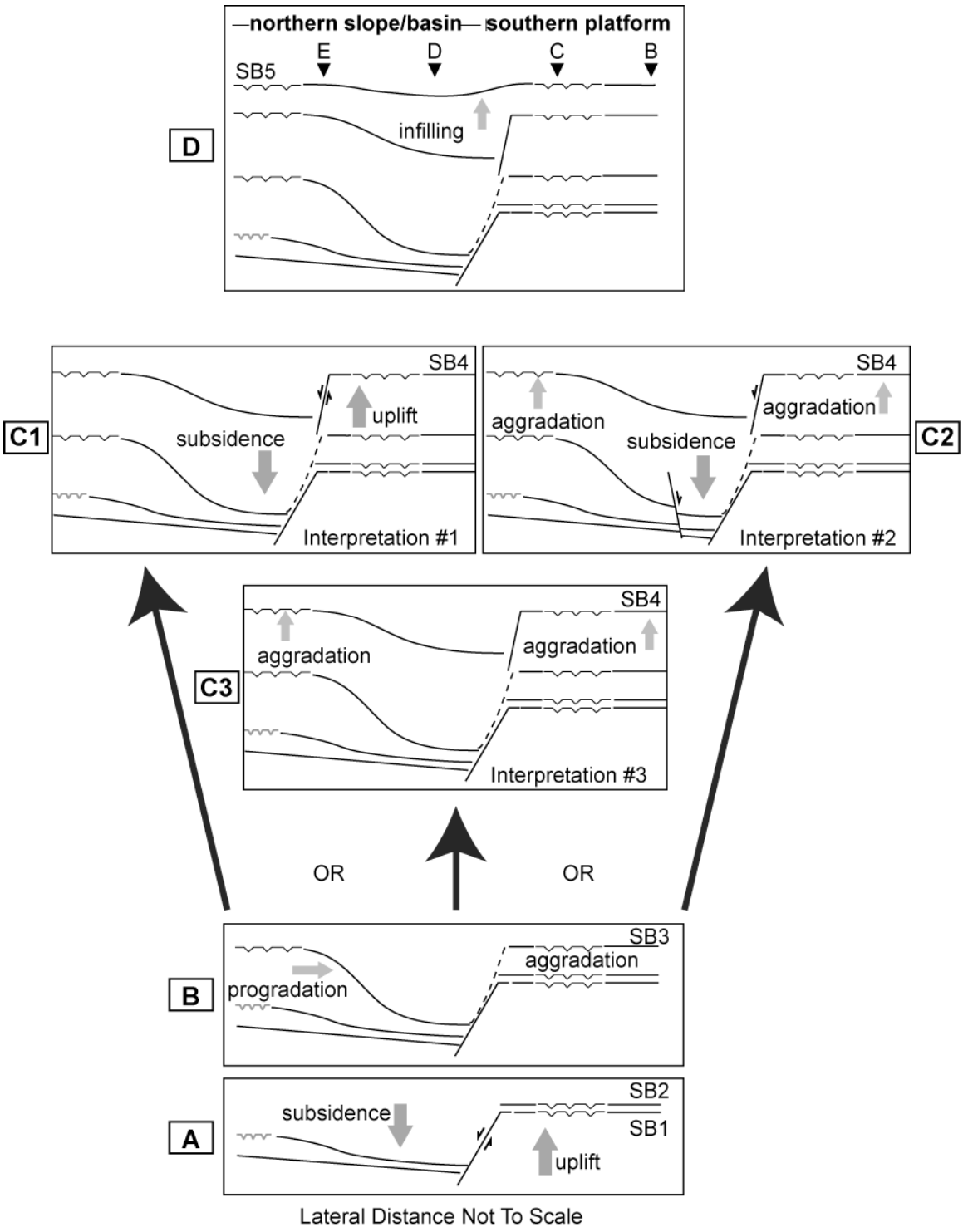

Figure 12. Schematic diagram illustrating the evolution of the House Range Embayment and southern platform from the late Ehmaniella zone through the Crepicephalus zone. C1-C3 represent the 3 interpretations for the Marjum Formation stratigraphic interval.

surface of the House Range Embayment is interpreted to slightly pre-date formation of SB1, the abrupt increase in water depth associated with deep-water strata directly overlying SB1 indicates a major increase in subsidence that resulting in the carbonate platform drowning in region surrounding the House Range and Drum Mountains. The House Range section is highly condensed and its thickness may be underestimated due to irrecoverable offsets caused by low-angle faults (Hintze and Robison, 1975; Babcock et al., 2007). The Drum Mountains section is more than twice as thick and contains more carbonate layers indicating that the primary source for carbonate into the basin was from the north; an interpretation also supported by Elrick and Snider (2002). In each basinal section, the amount of carbonate increases upsection towards SB2.

Correlative strata on the southern platform, with multiple exposure surfaces from SB1 upsection, are interpreted as reflecting uplift of the southern platform during formation of the House Range Embayment. Field studies of recent extensional basins have documented that during active faulting, uplifted footwalls are characterized by numerous exposure surfaces, thin sequences, and sequence boundaries that either coalesce or are closely spaced (Leeder and Gawthorpe, 1987; Gawthorpe et al., 1994; Bosence et al., 1998; Zeechin et al., 2004; Zecchin, 2005; George et al., 2009). Most fault-controlled basins contain carbonate breccias derived from uplift and erosion of the footwall along the basin-bounding fault (Leeder and Gawthorpe, 1987; MacLeod et al., 2000; Nagy et al., 2005). In House Range Embayment strata, carbonate breccia and conglomerate are rare and do not consist of platform-top carbonate facies. The lack of footwall-derived carbonate breccia in the House Range Embayment is not a deterrent to support for the fault-controlled model because the lateral distance between outcrops that bracket the basin bounding fault is > 70 km; a distance that could easily contain buried outcrop of both an eroded footwall and hanging wall with footwall-derived carbonate breccias based on modern and ancient analogs of similar structural settings where

affected areas of footwall uplift and erosion span < 20 km (Bosence et al., 1998; MacLeod et al., 2000; Zecchin, 2005; Jiang, 2007). A similar pattern to that of the House Range Embayment surrounding SB1 including fault-controlled backstepping of carbonate strata was documented in lower Frasnian shelf strata of the Canning Basin in Australia (George et al., 2009). Uncertainties remain regarding the precise correlation and timing of formation of individual surfaces in this interval because the surfaces are below the available biostratigraphic resolution. However, the contrasting facies trends across SB1, and similar features in other extensional basins, support the hypothesis that the House Range Embayment formed due to tectonic subsidence and argues against a major eustatic rise at SB1.

Evolution of the House Range Embayment

Evolution of the House Range Embayment after its initial formation is summarized in Figure 12B-D which reflects the infilling of the basin in the Drum Mountains, prolonged deep-water sedimentation in the House Range, and continued shallow-water carbonate sedimentation on the southern platform. The relatively simple stratigraphic trends between SB2 and SB3 are interpreted as a record of tectonic quiescence during which sedimentation was controlled primarily by carbonate production and sea level (Fig. 12B). Directly overlying SB2 on the southern platform, thin-bedded microbial laminites with an absence of exposure features reflects increasing accommodation during the early stages of transgression. Upsection, the predominately non-cyclic, bioturbated, fine-grained carbonates that dominate much of the southern platform represent sedimentation on a healthy carbonate platform. The non-cyclic characteristic within much of this interval indicates that sedimentation mostly kept pace with rising sea level and that the southern platform shoaled to sea level in two large shallowing-upward sequences as evidenced by two large non-cyclic intervals capped by thin-bedded microbial laminites with common subaerial exposure-related features such as microkarstic depressions, erosional

surfaces, and fenestrae. While the second shallowing-upward sequence is correlated between each southern platform section and correlated with both basinal sections, the first shallowing-upward sequence can only be correlated between the Wah Wah Mountains and the Panaca Hills sections, with only a questionable correlation to the Drum Mountains. The limited lateral extent of this sequence boundary indicates that the first shoaling event was likely of only limited regional significance. Correlation of this sequence boundary to the Desert Range section is uncertain because the top of the shoaling sequence may actually be located within the thick package of microbial laminites in the lower portion of the Banded Mountain Member of the Bonanza King Formation. Without higher resolution biostratigraphic data, or any other means of precisely correlating this surface, the magnitude and extent of this shoaling event remains unknown.

On the northern slope of the House Range Embayment in the Drum Mountains, the interval between SB2 and SB3 contains strata that record the transition from a low-angle ramp with deposition below storm wave base to an active carbonate platform that shoaled to sea level by SB3. Above SB2, the shallowing-upward sequence is recorded in the following sequence: transition from a shale-rich interval in the lower Wheeler Formation; to an interval characterized by limestone-dominated rhythmites with interbedded syn-sedimentary slump structures and increasing amounts of bioturbation features in the middle Wheeler; to an interval with increasing amounts of bioclastic and oncolitic packstone and grainstones in beds that contain abundant submarine hardgrounds. This vertical sequence of strata records the reestablishment of the carbonate factory on the northern slope of the embayment. Tentative correlation with the lower sequence of this interval on the southern platform indicates that this shoaling event might at least be of regional significance. A second sequence begins with the appearance of fossiliferous shale directly over the underlying oncolitic-bioclastic

grainstone. The presence of this fossiliferous shale abruptly overlying a grainstone indicates that accommodation increased during retrogradation of the carbonate platform to the north. This increase in accommodation could reflect a time when sea-level rise outpaced carbonate production, or a time when a decrease in carbonate production caused the platform to retrograde and hence increased accommodation by decreasing sedimentation rates. Brett et al. (2009) and Halgedahl et al. (2009) suggested that this fossil-rich shale horizon marks the maximum flooding surface that formed during maximum transgression. They based this interpretation on an increase in gamma radiation and an increase in the diversity of fossil content that suggest the most open-marine conditions of the sequence. Their interpretation would support the suggestion in this study that the shoaling up to SB3 was due to progradation during sea-level highstand and that the shale-rich interval below SB3 represented maximum transgression. However, the alternative scenario of a retrograded carbonate factory caused by a decrease in carbonate production is also likely. Further research on the precise correlation of this sequence in sections to the north would aid in deciphering the significance of this event.

The sequence of strata above this shale-rich interval in the Drum Mountains contains decreasing amounts of shale as the number of bioclastic grainstone and packstone beds increases. Bioclastic beds are interbedded with and overlain by oncolitic wackestone/packstone beds that contain small microbial bioherms. This sequence of facies reflects the transition from low-energy subtidal ramp to moderate energy mid-ramp shoals that were seaward of an inner quiet-water lagoon. The entire sequence is capped by a thick coarsely crystalline dolostone that contains small domal stromatolites and microbial laminae that reflect deposition on extensive tidal flats below SB3. The shallowing-upward sequence and the primarily non-cyclic pattern of facies on the northern slope reflect progradation of the carbonate factory towards the basin during

sea-level highstand at the same time that the southern platform was aggrading to sea level (Fig. 12B).

In the deepest portion of the basin, the strata between SB2 and SB3 reflect sedimentation of mostly pelagic silt and clay and hemipelagic fine-grained carbonate into a basin that remained below storm wave base and was restricted from bottom currents. The stratigraphic pattern of the Wheeler Formation in the House Range comprises one shallowing-upward sequence. The two sequences present on the northern slope and southern platform do not appear in the basin. Basinal cycles in this interval are thin and form no specific patterns or trends until they thicken upsection and as the percentage of carbonate increases towards SB3. This increase in carbonate towards the sequence boundary most likely reflects increased carbonate production on the adjacent carbonate platform and shedding of fine-grained carbonate downslope from the northern margin of the basin through turbidity currents during sea-level highstand. Modern studies of marine carbonate slopes have shown that while turbidites are common in all sea-level positions; they are most commonly associated with sea-level highstand (Schlager et al., 1994; Melim et al., 2002). On carbonates ramps such as likely existed between the Marjum Pass region of the House Range and regions to the north of Drum Mountains, increased carbonate transport would occur more prevalently during late highstand and early lowstand when the carbonate factory moved downslope towards the basin (Burchette and Wright, 1992; Elrick and Snider, 2002; MacNeil and Jones, 2006). Both of these interpretations fit the pattern of increasing carbonate transport by progradation of the carbonate platform into the basin towards SB3 during a period of tectonic quiescence.

The pattern of sedimentation that existed during tectonic quiescence was altered during deposition of late *Bolaspidella* zone strata between SB3 and SB4. Shallow-water carbonate facies in the Drum Mountains, and on the southern platform reflect sedimentation on a carbonate platform that experienced frequent subaerial exposure,

particularly on the southern platform. On the southern platform, carbonate cycles are common but difficult to discern directly below SB4 where facies are amalgamated and exposure surfaces are closely stacked. Where present, cycles are composed of mottled peloidal wackestone bases and microbial laminite caps that are composed of replacement microcrystalline dolomite and subaerial exposure features. Cycle stacking patterns do not appear to fit with one systematic pattern of shallowing, but certain intervals do contain cycles that thin towards the sequence boundary. Closely spaced exposure surfaces and the variability of stacking patterns makes correlation of individual cycles or shallowing-upward trends difficult between sections. Correlation of individual shallowing-upward trends between the northern slope and southern platform is also complicated by the presence of two thick non-cyclic intervals in the Drum Mountains. In all sections, it is the larger pattern of increasing exposure towards the uppermost interval close to SB4 that helps correlate the sequence between sections. In the Drum Mountains, exposure-related features are restricted primarily to two intervals, one of which is the interval at SB4.

In contrast to the exposure-feature dominated shallow-water stratigraphic interval on the northern slope and southern platform, the same stratigraphic interval in the House Range is doubled in thickness and includes facies such as laminated, fine-grained lime mudstone and calcisiltite that are interbedded with calcareous shale, with pelagic agnostoid trilobites, limited bioturbation features, and carbonate mud mounds. These facies all indicate prolonged sedimentation on a deep subtidal ramp below storm wave base, and rates of accommodation that either kept pace with or exceeded rates of sedimentation. Thick stratigraphic packages of rhythmites, basinal cycles, and non-cyclic intervals comprise several shallowing-upward trends. Basinal cycles are common but have no consistent relationship with the larger-scale stacking patterns or facies trends. Non-cyclic strata commonly form the base of a shallowing-upward trend and contain

large amounts of shale, whereas carbonate-dominated rhythmites form the upper portion of such trends. The increase in carbonate content towards SB4 reflects increased input of detrital carbonate into the basin during highstand shedding from the adjacent carbonate platforms.

Depositional patterns recorded in strata between SB3 and SB4 lead to three interpretations for the differences in facies and thickness between Marjum Formation and equivalent strata on the adjacent carbonate platforms. Interpretation 1 is that syn-sedimentary normal faulting resulted in increased accommodation in the House Range Embayment due to tectonic subsidence, and decreased accommodation on the southern platform due to platform uplift (Fig. 12C1). This scenario is the classic half-graben model for basin formation described by Leeder and Gawthorpe (1987) in which sediments on the footwall are characterized by numerous exposure surfaces and the thickest packages of sediment are in the axial portion of the hanging wall. The second interpretation is a modified version of the first interpretation in that syn-sedimentary normal faulting resulted in increased accommodation in the House Range Embayment due to tectonic subsidence, however, in this scenario footwall uplift was minimized and southern platform accommodation unaffected due to deformation in the hanging wall by antithetic normal faults north of the basin axis (Fig. 12C2). This scenario is modeled after extensional basins where Coulomb collapse of the hanging wall accommodated movement along listric normal faults (Hamblin, 1965; Xiao and Suppe, 1992; Tearpock and Bischke, 2002). In this interpretation, the thickest sediment packages would be found in the axial region of the half-graben between the major basin-bounding normal fault and the antithetic faults that accommodate collapse of the hanging wall onto the footwall, although sediment packages that dip into the basin on the hanging wall would thicken towards the basin. Footwall uplift is minimized in this type of basin. The third interpretation is that vertical and lateral facies differences between the House Range

Embayment and adjacent carbonate platforms were not the result of continued or renewed tectonic subsidence but were the result of the complex interaction between rates of sea-level rise, passive margin subsidence, and sedimentation over pre-existing topography (Fig. 12C3). In this scenario, rates of sedimentation in the House Range Embayment would be equal to or less than the creation of accommodation through the combined rates of sea-level rise/fall and passive margin subsidence. The driving factors in this model for basin infilling would be sediment supply and sea level.

Although each scenario is plausible within the current data for formation of the House Range Embayment, the second interpretation is preferred because it matches not only the current data but also substantiates previously published interpretations for sedimentation in the basin and on the southern platform. In the current data, features that are used for interpreting basin history include the abundance of exposure surfaces present on the southern platform, the variability in thickness and facies content of meter-scale cycles on the southern platform and northern ramp, and the dramatic thickness and facies difference of sedimentary packages between the platform and basin.

In the preferred model (Fig. 12C2), both the abundance of exposure surfaces and variability in meter-scale cycles on the southern platform are explained by sedimentation on a shallow, flat-topped carbonate platform under high-frequency, low amplitude sea-level fluctuations that were common during greenhouse climates, and not the result of frequent uplift of the southern platform due to faulting. Under these highstand conditions, subaerial exposure of the platform top would be frequent but individual surfaces would be laterally discontinuous creating a cryptic and complex record of cyclicity (Spence and Tucker, 2007). Bond et al. (1991; 1993), Montañez and Osleger (1993), and Howley (2002) all suggested based on detailed analysis of stacking patterns and cyclostratigraphy of the southern platform interval between SB3 and SB4, that deposition on the southern platform was controlled primarily by eustatic fluctuations during a time of

global sea-level highstand. Bond et al. (1991; 1993) further suggested that these eustatic fluctuations were consistent with Milankovitch orbital periodicities. Results of Embedded Markov Chain and gamma analyses of the Panaca section by Howley et al. (2001), however, revealed no conclusive evidence of periodicity and/or forcing of sea level by Milankovitch orbital variations. The authors suggested that either syn- or post-depositional geologic processes masked the signal, or that autocyclic processes resulted in the lateral thickness and facies variability that dominate platform stratigraphy. In fact, autocyclic migration of extensive tidal flats under low amplitude sea-level change is a common mechanism proposed for meter-scale cyclicity in the geologic record (Ginsburg, 1971; Pratt and James, 1986; Tucker and Wright, 1990). The hypothesis that the orbital signal was masked in some southern platform sections is supported by the fact that Elrick and Snider (2002) documented Milankovitch periodicities in strata of the basinal Marjum Formation. Overall the evidence indicates that sedimentation on the southern platform was controlled primarily by sea level and that any tectonic influence was minor.

The third piece of evidence used in basin analysis is the major difference in stratigraphic thickness and facies type between platform and basin. Typical half-graben basins have thicker packages of sediment deposited on the hanging wall than on the footwall, and facies content reflects gradual infilling of these basin types. The data from the House Range Embayment do match this basin model, however the stratigraphic record of infilling present in the Drum Mountains section by SB3, and in the Wheeler Amphitheater region of the central House Range (just 10 km north of the Marjum Pass section examined in this study) by the middle of the sequence between SB3 and SB4, as documented by Smith (2007), reveals that progradation and infilling of the basin to just north of the axial region occurred over a period of 2-3 million years (based of current estimates of the middle Cambrian time scale). Yet, with an active carbonate platform only several kilometers to the north, the axial region of the basin continued to reflect only

deposition on a low-angle ramp below storm wave base. A study by Burchette and Wright (1992) revealed that carbonate factories that exist on ramps prograde rapidly during base level fall. In addition, very limited shallowing of facies is present below SB4 and the transition from basin to shallow-water platform occurs within the upper half of the Weeks Limestone up to SB5. From the evidence in this study, it seems likely that the hanging wall in the basin contained faults that were antithetic to the major basin-bounding fault and that this caused the pronounced and prolonged sedimentation of deep-water strata in the basin axis while surrounded by active carbonate platforms. Progradation of the carbonate factory from the Wheeler Amphitheater region of the House Range into the basin axis at Marjum Pass would have been hindered by a sharp topographic change across the antithetic faults. The interpretation would support the hypothesis by Rees (1986) that the northern margin of the embayment was a distally steepened ramp.

Arguably, interpretation 2 (Fig. 12C2) is not that different from interpretation 3 (Fig. 13C3) where no tectonic control was evoked. The presence of antithetic faults in the basin is hypothetical, and a scenario where sedimentation rates in the basin were less than or equal to the rates of creation of accommodation (based on combined rates of sea-level change and passive margin subsidence) could easily explain how the axial region of the basin could remain below storm wave base for such an extended period of time with infilling not occurring until a time when sedimentation rates exceeded the creation of accommodation. To test the distinction between these two scenarios, a higher resolution chronostratigraphic framework and age control is needed to determine likely sedimentation rates, and a higher-resolution correlation scheme is needed to directly link individual sedimentation events in the basin with individual surfaces on the southern platform and northern ramp.

Controls on sequence boundary formation

Sequence boundaries are unconformities that formed at times of maximum rate of sea-level fall in typical sea-level controlled basins (Posamentier et al., 1988), however, similar surfaces have been known to form by decreases in accommodation caused by basement uplift (Bosence et al., 1988; Miall and Miall, 2001; George et al., 2009). In addition, sequence boundaries identified in seismic data are unlikely to result from 'regionally correlatable discrete surfaces' but instead form a closely related series of surfaces (Cartwright et al., 1993). Furthermore, many authors have illustrated the varying physical expressions of sequence boundaries, from the well-defined erosional unconformity to gradational intervals without a clearly identifiable erosional surface in between the highstand and transgressive phases (Vail et al., 1984, Sarg, 1988, Schlager, 1999). While in outcrop direct evidence for subaerial exposure is the best evidence for accurately identifying sequence boundaries related to base-level fall (Posamentier et al., 1992; Myers and Milton, 1996), not all sequences are bounded by this type of sequence boundary and their expression also varies with location in the basin. In many cases, the flooding surface between highstand (progradational) and transgressive (aggradational or retrogradational) deposition, sometimes with limited to no subaerial exposure, represents a good regionally correlatable sequence boundary (Goldhammer et al., 1990; Embry, 1993; Montañez and Osleger, 1993; Saller et al., 1993; Schlager, 1999). The key to deciphering the cause of these unconformities is accurate correlation of surfaces and sequences and a detailed understanding of stratigraphic and facies patterns that surround these surfaces. George et al. (2009) found that vertical trends in stacking patterns surrounding a sequence boundary on the lower Frasnian Hull Platform in the Canning Basin did not match the trends predicted by conventional sequence stratigraphic models and were more likely related to footwall uplift of a tilted basement block. In the House Range Embayment, the sequence

boundary associated with formation of the basin (SB1) is similar to the Hull Platform in that the major exposure surface is overlain by a thin sequence of shallow-water strata that contain multiple surfaces of subaerial exposure. In addition, correlation of SB1 to a major flooding surface in the basin indicates opposing trends in water depth change that was likely caused by footwall uplift and hanging wall subsidence along a normal fault. Whether this tectonic activity was coincident with a eustatic fall in sea level is unknown, but the Cambrian was a period of greenhouse climate conditions with high sea levels and an absence in ice sheets that are necessary for eustatic fluctuations of the glacioeustatic magnitudes necessary for such a significant facies change (Frakes et al., 1992; Miller et al., 2005). Gawthorpe et al. (1994) suggested that the effects of tectonically controlled relative sea-level change would be more pronounced during greenhouse climates because rates and magnitudes of eustatic fluctuations on any scale would be much less than during our present icehouse climate. In fact, the question of what caused greenhouse eustatic change has long confounded sequence stratigraphers (Miall and Miall, 2001).

A dominant causal mechanism for sequence boundaries is not always obvious and may indicate a dual control. SB2 is one such boundary because of the short vertical association with the fault-controlled surface at SB1 and intervening surfaces. Facies above SB2 in both the platform and basin do deepen upward but in both locations facies do not change significantly above the exposure surface. In this instance, minimal uplift and subsidence in the basin in conjunction with early transgression could produce the stratigraphic patterns of this interval. Alternatively the lack of a significant facies change across SB2 could reflect the limited accommodation on the southern platform and a period of non-deposition in the basin. In contrast, SB3, SB4 and SB5 are all present at the top of shallowing-upward sequences and most likely formed as a result of regional or eustatic sea-level fall, although of low magnitude, because the facies patterns match the

predicted model for sea-level driven deposition. In this study, SB1 is the only sequence boundary that formed due to tectonic uplift of the southern platform, and subsidence at a flooding surface in the basin. The primary result of this analysis is that while sequence boundaries can easily be identified in many locations, the cause of these sequence boundaries is not always related to eustasy and care must be taken to fully understand the paleotectonic setting before trying to correlate surfaces to regions outside of the basin that they are located.

Conclusions

A sequence stratigraphic study was conducted to understand the stratal patterns of a syndepositional fault-controlled basin, the House Range Embayment, on the middle Cambrian passive margin. Five sequence boundaries were identified and correlated between platform and basin sections of the House Range Embayment within the known biostratigraphic framework. An abrupt change in depositional facies across sequence boundary 1 documents the initiation of tectonic subsidence during formation of the House Range Embayment. This interpretation differs from previous interpretations of a major eustatic rise above sequence boundary 1. The remaining 4 sequence boundaries and their internal facies variations record the influences of both sea-level change and tectonic subsidence on sedimentation across the region until the end of the middle Cambrian when similar shallow-water facies platform and basin indicates infilling of the House Range Embayment. The results of this study represent one example of the application of sequence stratigraphic methods to correlation of laterally discontinuous outcrop sections over a large region in which biostratigraphic data is limited and highlight the applicability of sequence stratigraphic analyses to understand paleogeographic settings with more than one depositional controller.

CHAPTER 2

THE CAMBRIAN DRUMIAN CARBON ISOTOPE EXCURSION (DICE) IN THE GREAT BASIN, WESTERN UNITED STATES

Abstract

The Global boundary Stratotype Section and Point (GSSP) of the Cambrian Series 3 (formerly the Middle Cambrian) Drumian Stage is defined by the first appearance datum (FAD) of the agnostoid trilobite *Ptychagnostus atavus* in the deep-water Wheeler Formation of the Drum Mountains in Utah, USA. In the Great Basin (USA), China and Scandinavia the FAD of *P. atavus* is associated with transgression and with a negative carbon isotope excursion named the Drumian Carbon Isotope Excursion (DICE). However, the relationship between the FAD of *P. atavus*, sea-level changes, and the DICE is tentative, mainly due to the paucity of biostratigraphic data in shallow-water sections that limit correlation between deep- and shallow-water chemostratigraphic sections. An integrated sequence and chemostratigraphic study across a platform-to-basin transect in western Utah and southern Nevada indicates that the DICE is stratigraphically located above the FAD of *P. atavus,* associated with retrogradation of the shallow-water carbonate platform and with stratigraphic condensation in the basin. The results suggest that in future global correlations, the DICE should be restricted to the negative carbon isotope anomaly slightly post-dating the Drumian GSSP.

Introduction

The Global boundary Stratotype Section and Point (GSSP) of the Cambrian Series 3 Drumian Stage (ca. 506.5–503 Ma) is defined by the first appearance datum (FAD) of the cosmopolitan agnostoid trilobite *Ptychagnostus atavus* (Babcock et al., 2004, 2007; Zhu et al., 2006). This guide fossil is commonly found in slope to basinal successions where it is associated with other cosmopolitan agnostoids and open-shelf polymerid

trilobites (Robison, 1982; Rowell et al., 1982; Sundberg, 1991; Peng and Robison, 2000; Ahlberg et al., 2009). The association of basin-dwelling agnostoid species with shelf- and basin-dwelling polymerid species is important because it provides for both regional and global correlation (Babcock et al., 2004, 2007). However, correlation of *P. atavus* to shallow-water facies has been hampered in many locations by poor biostratigraphic control in shallow-water sections. Consequently, integration of techniques such as sequence stratigraphy and carbon isotope chemostratigraphy with the known biostratigraphy greatly increases our ability to carry out high-resolution correlation regionally and globally. Enormous effort has been invested in Cambrian chronostratigraphic studies from different continents (e.g., Brasier and Sukhov, 1998; Montañez et al., 2000; Buggisch et at., 2003; Babcock et al., 2004, 2007; Zhu et al., 2004, 2006; Gomez et al., 2007; Álvaro et al., 2008; Kouchinsky et al., 2008; Ahlberg et al., 2009) and preliminary sequence stratigraphic studies (Montañez and Osleger, 1993; Osleger and Montañez, 1996; Babcock et al., 2004, 2007; Peng et al., 2004; Howley et al., 2006; Brett et al., 2009). In summary of existing data, it has been suggested that the Drumian GSSP is associated with the base of a transgressive event and a negative carbon isotope excursion named the Drumian Carbon isotope Excursion (DICE in Fig. 13A; Babcock et al., 2004, 2007; Zhu et al., 2006), but the exact relationship between these events remains elusive.

The transgressive event associated with the FAD of *P. atavus* was inferred by Babcock et al. (2004, 2007) primarily from variations in the amount and characteristics of shale and carbonate strata in the basal Wheeler Formation across the Drumian GSSP in the Drum Mountains of western Utah. These fine-grained deposits most likely represent deposition below storm wave base on the lower slope (Rees, 1986; Babcock et al., 2004, 2007; Brett et al., 2009). This information was supplemented by stratigraphic observations from elsewhere, most notably South China. In the Great Basin, the

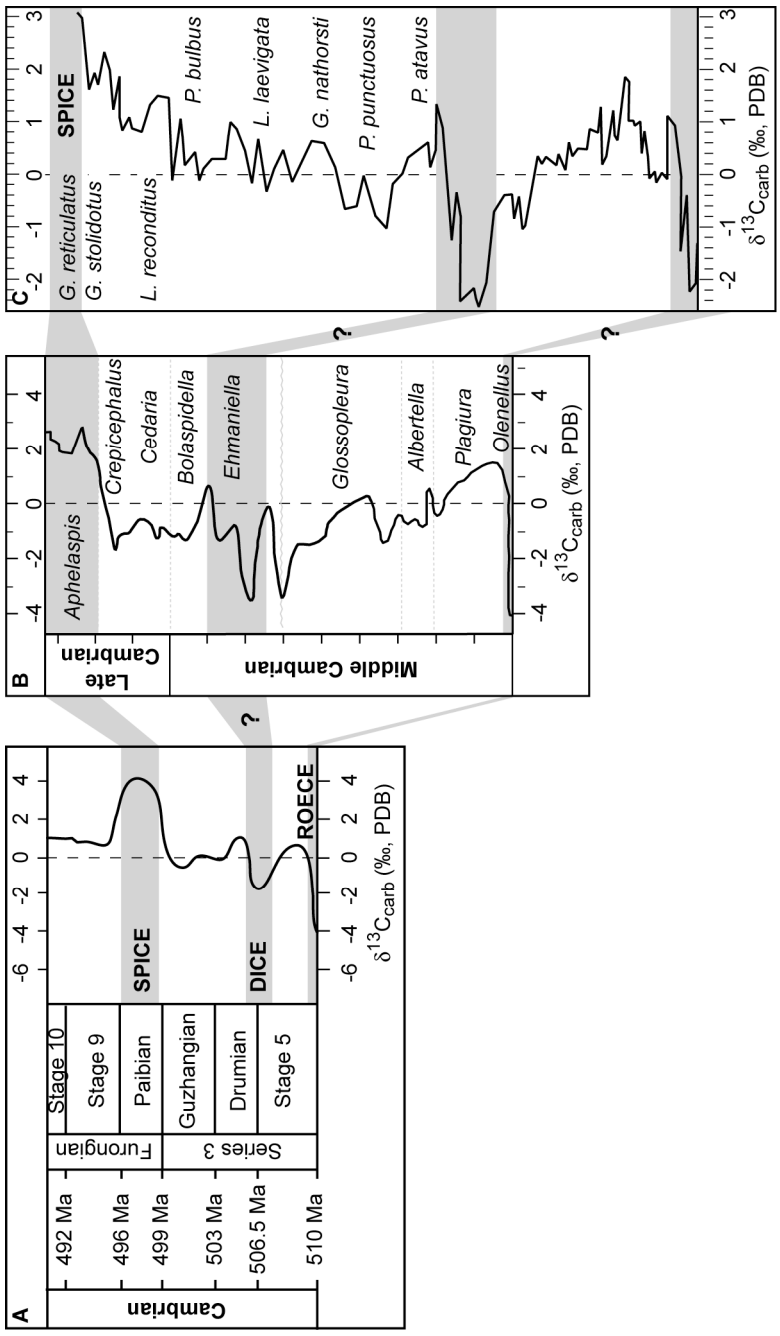

Figure 13. (A) Generalized global standard chronostratigraphic scale and $\delta^{13}C$ record that defines the Drumian Carbon Isotope Excursion (DICE), modified from Zhu et al. (2006); (B) Composite $\delta^{13}C$ record potentially covering the DICE in the Great Basin (Montañez et al., 2000). The FAD of *P. atavus* nearly coincides with the base of the *Bolaspidella* Zone (Babcock et al., 2004, 2007), it seems that the DICE is correlated with one of the excursions below the *Bolaspidella* and *Ehmaniella* boundary; (C) mid-Cambrian $\delta^{13}C$ record from the Wangcun section in South China (Zhu et al., 2004). The major negative $\delta^{13}C$ excursion is below the first recognized appearance of *P. atavus* in this section.

interplay of tectonic subsidence with low-amplitude sea-level fluctuations during greenhouse climate conditions has obscured the sea-level change signal in the stratigraphic record of the Wheeler Formation. Correlation to shallow-water facies is crucial for deciphering the most accurate sea-level record. In addition to questions surrounding the sequence stratigraphic interpretation of the GSSP, published chemostratigraphic data across this interval are primarily derived from shallow-water carbonate-rich successions and their precise correlation with the FAD of *P. atavus* is questionable. The DICE is defined as being associated with the FAD of *P. atavus*, but in the section containing the GSSP horizon, only one data point represents the DICE negative $\delta^{13}C$ shift and it occurs 10 m above the GSSP (Babcock et al., 2007). However, in the Montañez et al. (2000) composite $\delta^{13}C$ curve summarized from shallow-water sections of the Great Basin and Canadian Rockies, notable negative $\delta^{13}C$ shifts were located below the polymerid trilobite *Bolaspidella* Zone (Fig. 13B), the base of which is thought to be nearly equivalent to the FAD of *P. atavus* (Ludvigsen and Westrop, 1985; Babcock et al., 2004). In slope sections of South China, a major negative $\delta^{13}C$ excursion was located below the FAD of *P. atavus* (Fig. 13C; Zhu et al., 2004), although a small shift in $\delta^{13}C$ was also documented above *P. atavus*. In Siberia, stratigraphic intervals across the FAD of *P. atavus* are highly condensed and negative $\delta^{13}C$ values were found both below and above the FAD of *P. atavus* (Brasier and Sukhov, 1998). In Sweden, a negative shift in organic $\delta^{13}C$ values occurs in a thin limestone bed within a highly condensed interval of dark gray to black mudstone and shale near the base of the *P. atavus* zone (Ahlberg et al., 2009). These inconsistencies make the definition of the DICE uncertain and require calibration of the relationships between the FAD of *P. atavus*, sea-level change, and the DICE in the deep-water section that hosts the GSSP and its adjacent shallow-water carbonate platform.

In this paper, we present an integrated sequence and chemostratigraphic study of the basal Drumian strata across a platform-to-basin transect in western Utah and southern Nevada, USA, including the Stratotype Ridge section in the Drum Mountains that defines the Drumian GSSP (Fig. 14). The purpose of this study is to (1) document the relationship between the FAD of *P. atavus* and the negative $\delta^{13}C$ excursion, (2) clarify the relationship between sea-level change and the negative $\delta^{13}C$ excursion, and (3) refine the definition of the DICE event in a sequence stratigraphic framework.

Geologic setting

Cambrian strata of western North America were deposited on a passive continental margin that was developed over the rift associated with the breakup of supercontinent Rodinia during the late Neoproterozoic (Bond and Kominz, 1984; Levy and Christie-Blick, 1991; Burchfiel et al., 1992; Poole et al., 1992). By Cambrian Series 3, a northwest-facing carbonate platform covered most of present day Utah, Nevada, and southeastern California. Fine-grained terrigenous sediments accumulated in deep-water to the west of the carbonate platform and in shallow water to the east (Palmer, 1971). This stratigraphic pattern was disrupted during the Stage 5 *Ehmaniella* Chron (provisional Age 5) by the development of a syndepositional, fault-controlled basin known as the House Range Embayment (Fig. 14A; Rees, 1986). This basin extended for more than 400 km from the shelf edge across the margin and controlled the distribution of depositional facies through the Early Ordovician (Rees, 1986; Miller et al., 2003).

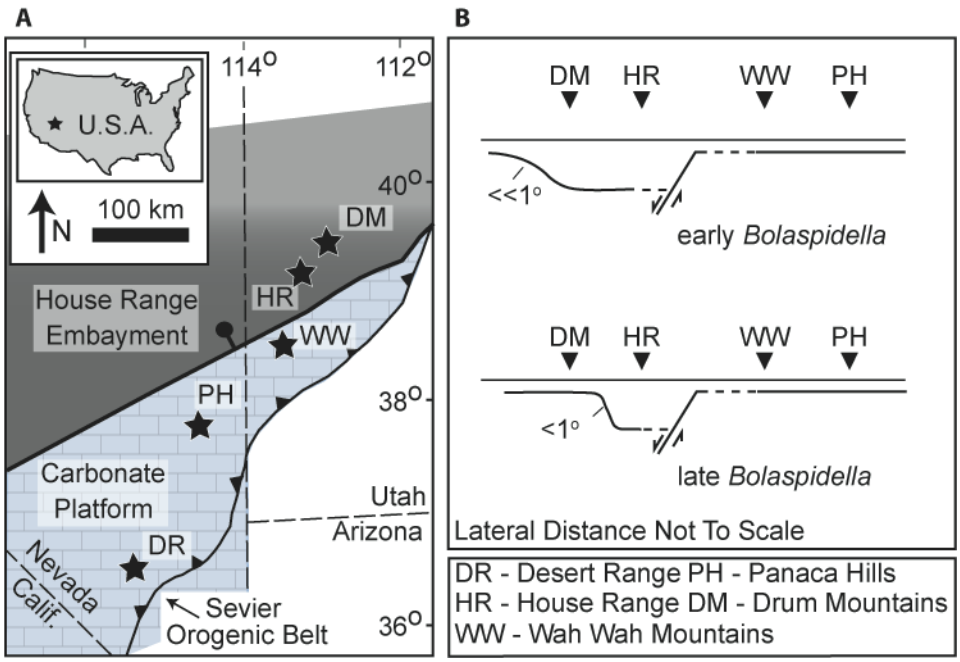

Figure 14. Non-palinspastic paleogeographic reconstruction (A) and cross section (B) of the House Range Embayment during the latest Ehmaniella and Bolaspidella trilobite zones (modified from Palmer, 1971; Elrick and Snider, 2002), with location of measured sections indicated.

Syndepositional fault activity within the House Range Embayment is inferred to have started during the latest *Ehmaniella* Chron (Rees, 1986). On the northern (downthrown) side of the fault, deep-water shale and fine-grained carbonates span most of Cambrian Series 3, with the depocenter close to the present day Marjum Pass region of the House Range in western Utah (Fig. 14). Further north, a gentle carbonate ramp with perhaps < 1° topographic gradient was developed towards the basin during the latest *Ehmaniella* Chron and early *Bolaspidella* Zone (Fig. 14B; Rees, 1986; Elrick and Snider, 2002), although detailed documentation of shallow ramp facies is lacking due to the limited availability of outcrop. The Drum Mountains section that hosts the Drumian GSSP was likely deposited along the lower slope environment of this south-facing carbonate ramp

(White, 1973; Grannis, 1982; Kepper, 1981; Rees, 1986; Elrick and Snider, 2002; Babcock et al., 2007). On the southern side of the inferred fault (a region herein referred to as the southern platform), however, shallow-water carbonate deposition continued through the Cambrian Epoch 3 and the Furongian Epoch (Palmer, 1971; Kepper, 1972, 1976; Rees, 1986; Montañez and Osleger, 1993).

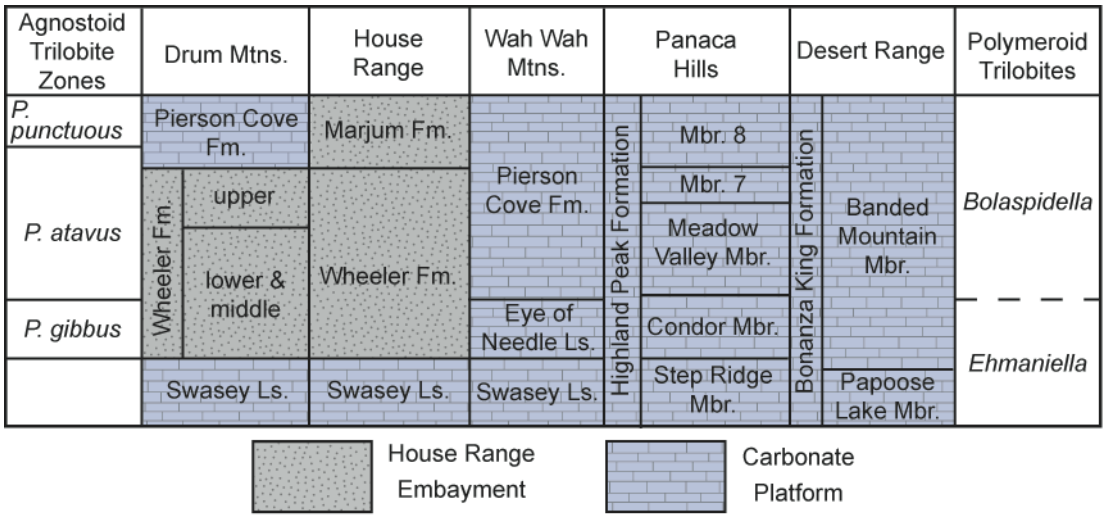

Figure 15. Nomenclature of stratigraphic units and their biostratigraphic correlation. Note that the boundary between Ehmaniella and Bolaspidella biozones is poorly defined due to a lack of sufficient fossils in platform sections.

Stratigraphic units associated with the FAD of *P. atavus* in the basin and across the transition between the *Ehmaniella* and *Bolaspidella* biozones in the southern platform are summarized in Figure 15. The basinal sections contain both polymerid and agnostoid trilobites, and the FAD of *P. atavus* nearly coincides with the base of the polymerid *Bolaspidella* Biozone (Ludvigsen and Westrop, 1985; Babcock et al., 2004, 2007). However, in the platform sections the boundary between the *Ehmaniella* and *Bolaspidella* biozones can only be approximately defined or inferred due to the paucity of

fossils in general and the facies-dependent distribution of polymerid trilobites (Robison, 1976; Palmer, 1977; Robison et al., 1977; Rowell et al., 1982; Geyer and Shergold, 2000).

Sequence stratigraphy

Through bed-by-bed sedimentological analysis, and lateral tracing of surfaces and facies in available outcrops surrounding each measured section, two sequence boundaries are identified within the southern platform sections (Fig. 16A–C). These sequence boundaries are expressed by the following features: (1) localized karstic breccias filling in shallow paleokarstic depressions or cavities, (2) reworked karstic breccias as lenticular intraclastic grainstone/packstone lags along the surface, (3) intensified cm-sized dissolution cavities and desiccation cracks below the surface and disappearance of such features in overlying layers, and (4) abrupt change in facies and facies stacking patterns. Between these two sequence boundaries are mostly fine-grained carbonates and calcareous siltstone with abundant fenestrae, minor erosional surfaces and desiccation cracks indicative of intertidal to supratidal environments. Localized discontinuities are present within this interval, but their correlation between sections is uncertain. In the deep-water sections (Fig. 16D and E), the expression of sequence boundaries is subtle, and their identification is guided by the presence of a major hardground at the top of a deepening-upward trend, which may record reduced sediment supply during transgression.

In the Desert Range (Fig. 16A), the lower sequence boundary is located at the base of the Banded Mountain Member of the Bonanza King Formation, which has been

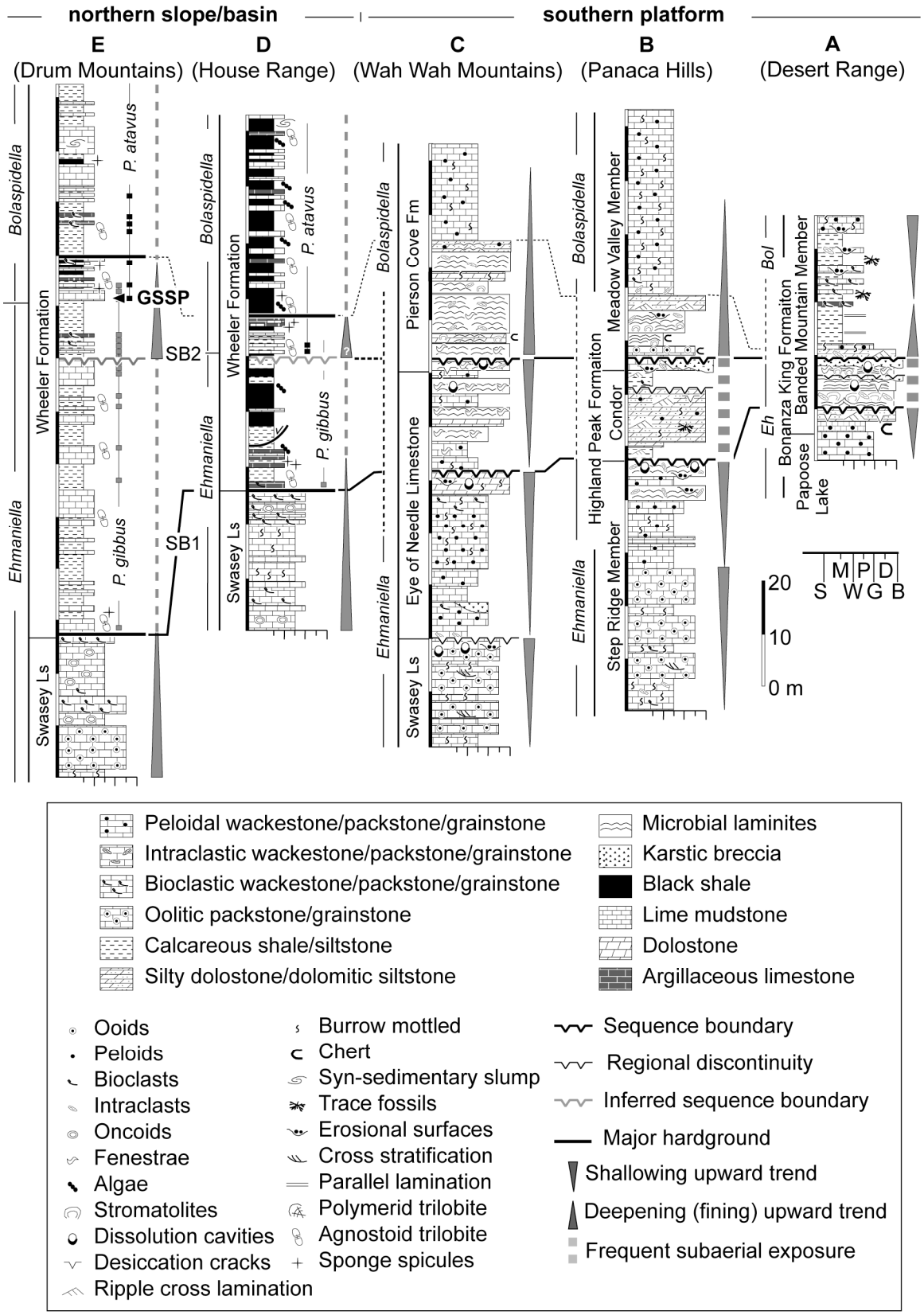
northern slope/basin
southern platform
E
(Drum Mountains)
D
(House Range)
C
(Wah Wah Mountains)
B
(Panaca Hills)
A
(Desert Range)
Bolaspidella
Ehmaniella
Wheeler Formation
Swasey Ls
P. atavus
P. gibbus
GSSP
SB2
SB1
Pierson Cove Fm
Eye of Needle Limestone
Meadow Valley Member
Highland Peak Formaiton
Condor
Step Ridge Member
Bol
Eh
Bonanza King Formaiton
Banded Mountain Member
Papoose Lake
M P D
S W G B
20
10
0 m
Peloidal wackestone/packstone/grainstone
Intraclastic wackestone/packstone/grainstone
Bioclastic wackestone/packstone/grainstone
Oolitic packstone/grainstone
Calcareous shale/siltstone
Silty dolostone/dolomitic siltstone
Microbial laminites
Karstic breccia
Black shale
Lime mudstone
Dolostone
Argillaceous limestone
Ooids
Peloids
Bioclasts
Intraclasts
Oncoids
Fenestrae
Algae
Stromatolites
Dissolution cavities
Desiccation cracks
Ripple cross lamination
Burrow mottled
Chert
Syn-sedimentary slump
Trace fossils
Erosional surfaces
Cross stratification
Parallel lamination
Polymerid trilobite
Agnostoid trilobite
Sponge spicules
Sequence boundary
Regional discontinuity
Inferred sequence boundary
Major hardground
Shallowing upward trend
Deepening (fining) upward trend
Frequent subaerial exposure

Figure 16. Sequence stratigraphic framework across the platform-to-basin transect, with available biostratigraphic data indicated. See Figure 2 for location of measured sections.

informally referred to as the lower “mixed unit” (Osleger and Montañez, 1996; Osleger et al., 1996). This sequence boundary is marked by (1) intensified desiccation cracks in the silty dolomudstone, (2) local karstic breccias that range from 5 to 20 cm thick and fill in small depressions along the surface, and (3) reworked karstic breccias as intraclasts in the overlying dolomitic siltstone and microbial dolostone. The upper sequence boundary is characterized by a laterally discontinuous karstic breccia, up to 2 m thick and composed of pebble- to cobble-sized angular clasts of microbial laminites and chert. This breccia fills the underlying topographic lows (paleokarstic depressions), along with abundant centimeter-scale dissolution cavities that disappear above the sequence boundary. The overlying strata show an upward-deepening trend from cross-laminated silty dolostone, to peloidal packstone, and to parallel-laminated shale with a rare open-marine fauna including polymerid trilobites and inarticulate brachiopods. Between the two sequence boundaries are shallow-water deposits dominated by fenestral microbial dolostone with domal stromatolites having 3-10 cm of synoptic relief. Desiccation cracks and dissolution cavities are common, suggesting upper intertidal to supratidal environments. A few meters below the upper sequence boundary, there is another interval that contains localized karstic breccias up to 20 cm thick. This surface may record another paleokarst surface with intensified subaerial exposure that is present in the Desert Range and adjacent areas such as the Indian Ridge (Montañez and Osleger, 1993; Osleger and Montañez, 1996; Osleger et al., 1996).

In the Panaca Hills of southern Nevada, the lower sequence boundary is located at the contact between the Step Ridge and Condor members of the Highland Peak Formation (Fig. 16B). The uppermost part of the Step Ridge Member shows an increase in fenestral microbial dolostone and dissolution cavities. Dissolution cavities and fissures are intensified at the sequence boundary and irregular dissolution surfaces have centimeters of surficial relief. Also present along this surface are random evaporite

(halite) pseudomorphs. The upper sequence boundary in this section is close to the base of the Meadow Valley Member (Fig. 16B) and is marked by laterally discontinuous, ≤ 0.5 m thick karstic breccias that are either clast-supported or supported by reddish dolomudstone. Laterally, breccias are replaced by intraclastic dolowackestone-dolomudstone or by localized intraclastic grainstone that contain reworked clasts from karstic breccias. A partially silicified oolitic grainstone caps the paleokarst surface, followed by an overall deepening-upward trend from microbial lime mudstone-packstone to thick, peloidal wackestone. Between the two sequence boundaries lies the Condor Member, which is primarily composed of cross-laminated silty dolostone or dolomitic siltstone with rare calcareous siltstone. An exposure surface marked by desiccation cracks and thin (≤ 2 cm) hematite-rich crust is present 5 m below the upper sequence boundary, which record at least a localized stratigraphic discontinuity in the Panaca area.

In the Wah Wah Mountains of western Utah, the lower sequence boundary is located in the middle of the Eye of Needle Limestone (Fig. 16C). This sequence boundary is expressed by brecciation of dolomudstone and wackestone, pockets of breccias filling paleokarstic dikes that penetrate downwards as deep as 10 m below the surface, and common dissolution cavities. Localized erosional depressions with 5-8 m relief were observed along laterally traced surfaces and are filled with peloidal wackestone. Overlying this sequence boundary, shallow-water (intertidal-supratidal) facies composed of peloidal wackestone and fenestral microbial dolostone constitute the upper part of the Eye of Needle Limestone. The upper sequence boundary in this section is near the base of the Pierson Cove Formation (Fig. 16C). Evidence for intensified exposure and depositional base-level fall at this sequence boundary include microkarstic features represented by thin (≤ 10 cm), laterally discontinuous karstic breccias and reworked breccias in the overlying intraclastic dolopackstone, dissolution cavities below the

surface, and desiccation cracks filled with silty dolostone and brecciated dolostone clasts. The irregular contact between the Swasey and Eye of Needle limestones in this section contains dissolution cavities and brecciation of oolitic grainstone/packstone, which may also record a depositional base-level fall of regional significance.

In the House Range and Drum Mountains (Fig. 16D and E), the contact between the Swasey Limestone and overlying Wheeler Formation is marked by a major hardground that records a significant increase in water depth above a reworked skeletal lag deposit (Grannis, 1982; Rees, 1986). The uppermost Swasey Limestone in both locations shows an overall deepening-upward trend from thick oolitic grainstone/packstone to thinly bedded oncolitic-bioclastic packstone/wackestone that contains a diverse open-marine fauna (*Glyphaspis* fauna; Randolph, 1973; White, 1973). The thick oolitic grainstone/packstone was deposited in an oolitic sand shoreface, whereas the oncolitic packstone and wackestone were deposited in lower shoreface to foreshore environments. This interpretation is consistent with the increase in bioclasts of open-marine fauna (echinoderm ossicles, trilobite sclerites, sponge spicules and inarticulate brachiopods) and oncoids in the uppermost beds of the Swasey, suggesting lower energy conditions away from the influence of the more proximal oolitic shoreface but still susceptible to moderate energy events (Randolph, 1973; White, 1973). The hardground at the Swasey-Wheeler contact shows truncated bioclasts, and iron oxide and phosphate coatings. Bioclasts are commonly abraded and cemented with fibrous calcite indicating submarine cementation. The deepening-upward trend below the hardground in these sections (Fig. 16D and E) and the shallowing-upward trends in time-equivalent strata of the southern platform sections (Fig. 16A–C) indicate that the initiation of the House Range Embayment may have slightly preceded the timing of erosion at the top of the Swasey Limestone. The abrupt increase in water depth at the Swasey-Wheeler contact is interpreted as recording a major uplift event that exposed the southern

platform (forming the lower sequence boundary) but drowned the carbonate platform in the basin.

Overlying the hardground, the lower Wheeler Formation in the House Range and Drum Mountains is dominated by dark gray/black shales, calcareous shale and parallel-laminated argillaceous lime mudstone, and rare wackestone (Fig. 16D and E). The Drum Mountains, which are in the northern part of the present outcrop belt, contains significantly more carbonate beds, indicating that the source of fine-grained carbonate was from the north (Fig. 14B; Rees, 1986; Elrick and Snider, 2002; Langenburg, 2003). Paleogeographic reconstructions indicate that Laurentia was astride the equator, and partly within the belt of northeast trade winds (Drewry et al., 1974; Scotese and McKerrow, 1990; Scotese and Barrett, 1990; Peng and Babcock, 2008) that would support transport of carbonate into the House Range Embayment from the northern ramp as opposed to the southern platform. In the House Range, the section is either condensed or its thickness is underestimated due to irrecoverable offsets caused by low-angle faults (Hintze and Robison, 1975), or both. The Marjum Pass section, in particular, contains faults in multiple positions (Babcock et al., 2004). In both sections, a major hardground above the FAD of *P. atavus* is expressed by strong mineralization (hematite crust and hematite-replaced pyrites) and condensation of agnostoid trilobites (Langenburg, 2003; Babcock et al., 2004, 2007). This hardground lies 31 m above the Swasey-Wheeler contact in the House Range (Marjum Pass section), and 72 m above the contact in the Drum Mountains (Stratotype Ridge section). Below this hardground, a subtle fining-upward trend is present in both sections. This trend starts slightly below the FAD of *P. atavus* and is characterized by the decrease of siliciclastic silt in shale and carbonates and an increase in dark grey, papery shale close to the hardground. Both sections contain bioclast-rich layers (trilobite-rich in the Drum Mountains and sponge spicule-rich in the House Range) associated with the hardground. The base of this

fining-upward trend is interpreted as time-equivalent to the upper sequence boundary on the southern platform, and the hardground is possibly correlative to the abrupt facies change above the sequence boundary (Fig. 16). The fining-upward trend expressed by the decrease of coarser-grained siliciclastic components and increase of organic carbon in the basin may be time-equivalent to the exposure and early transgression in the southern platform, during which silt and fine-grained sand were transported to the basin. Sea-level rise on the shelf resulted in retrogradation of the carbonate factory along the northern ramp and sediment starvation in the basin, depositing organic-rich shales and forming the submarine hardground.

Carbon isotope chemostratigraphy

Materials and methods

Samples for carbonate carbon isotope ($\delta^{13}C_{carb}$) analysis were collected to cover the upper *Ehmaniella* – lower *Bolaspidella* Biozone in a platform-to-basin transect. In platform sections, samples were collected every 0.5 to 1.5 m, but at narrower intervals across major facies changes. In the basinal sections, samples were collected from every available carbonate layer. In general, care was taken to avoid fractures, dissolution cavities, and breccias, but a selected set of slabs that contain different components (cements, intraclasts, and matrix) were also collected for the purpose of identifying the isotope alterations related to meteoric and burial diagenesis. Sample powders were microdrilled from polished slabs and reacted with orthophosphoric acid for 10 minutes at 70ºC in a Kiel-Device automatically connected to a Finnigan Delta Plus dual-inlet mass spectrometer. Most analyses were conducted at the UNLV LVIS Lab (Las Vegas Isotope Science Laboratory), but a small number of samples was analyzed at the stable isotope lab of INSTAAR (Institute of Arctic and Alpine Research) at the University of Colorado, Boulder. Isotopic results are reported as δ values with reference to the Vienna Peedee

belemnite standard (VPDB). Precision monitored by NBS-19 calcite and an internal standard is better than 0.05‰ for both C and O isotopes.

Results

The isotope data from the five measured sections are presented in Figs. 17-21 and in the supplementary appendix. In the Desert Range (Fig. 17), isotope measurements cover the lower Banded Mountain Member of the Bonanza King Formation. Below the upper sequence boundary, most $\delta^{13}C$ values are between -0.5‰ and -1‰. A negative shift from -0.3‰ to a minimum of -3.5‰ is present above the sequence boundary. Above an 8-m-thick shale interval, $\delta^{13}C$ values return to 0.5‰. No systematic $\delta^{13}C$ variation between lithologies is observed, but a few large slabs collected from karstic breccias below the upper sequence boundary show up to 6‰ variations between clasts and sparry calcite cements, suggesting significant alteration of $\delta^{13}C$ by meteoric diagenesis (Allan and Matthews, 1982; Theiling et al., 2007). This intrasample variation is consistent with the large variations in $\delta^{18}O$ below the sequence boundary, from which a strong covariation between $\delta^{13}C$ and $\delta^{18}O$ defines the diagenetic trend in this section. Above the upper sequence boundary, $\delta^{13}C$ values do not covary with $\delta^{18}O$.

In the Panaca Hills section (Fig. 18), $\delta^{13}C$ values of the upper Step Ridge Member increase upward from -1.5‰ to 0‰ and maintain at near 0‰ through the Condor Member. A negative $\delta^{13}C$ excursion with a minimum of -3‰ covers a 10-m-thick interval of the lower Meadow Valley Member above the upper sequence boundary. Thereafter $\delta^{13}C$ remains at values close to 0‰. No obvious lithology-dependent $\delta^{13}C$ variation has been observed, but when present, sparry calcite cements have lower $\delta^{13}C$ values compared to matrix. Most oxygen isotope values from the Step Ridge and Meadow Valley members range from -10‰ to -12‰, whereas $\delta^{18}O$ values from the Condor

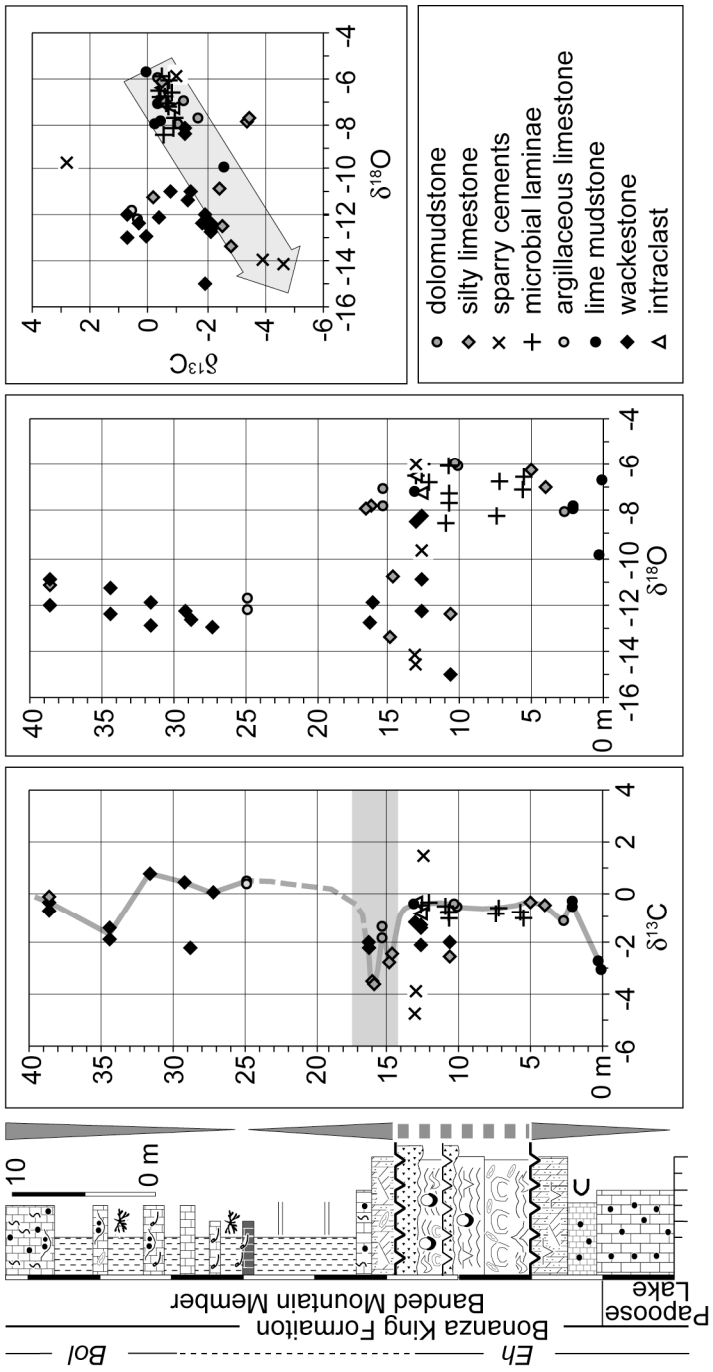

Figure 17. Integrated sequence and chemostratigraphy of the Desert Range section across the Ehmaniella and Bolaspidella transition in southern Nevada. A 3‰ negative shift in $\delta^{13}C$ is present above the upper sequence boundary (shaded region). The dashed line above represent an interval of no data. In the $\delta^{13}C$–$\delta^{18}O$ crossplot, the diagenetic trend (arrow) is derived from the matrix and sparry calcite cements of a large slab below the upper sequence boundary. See Figure 4 for lithologic legend.

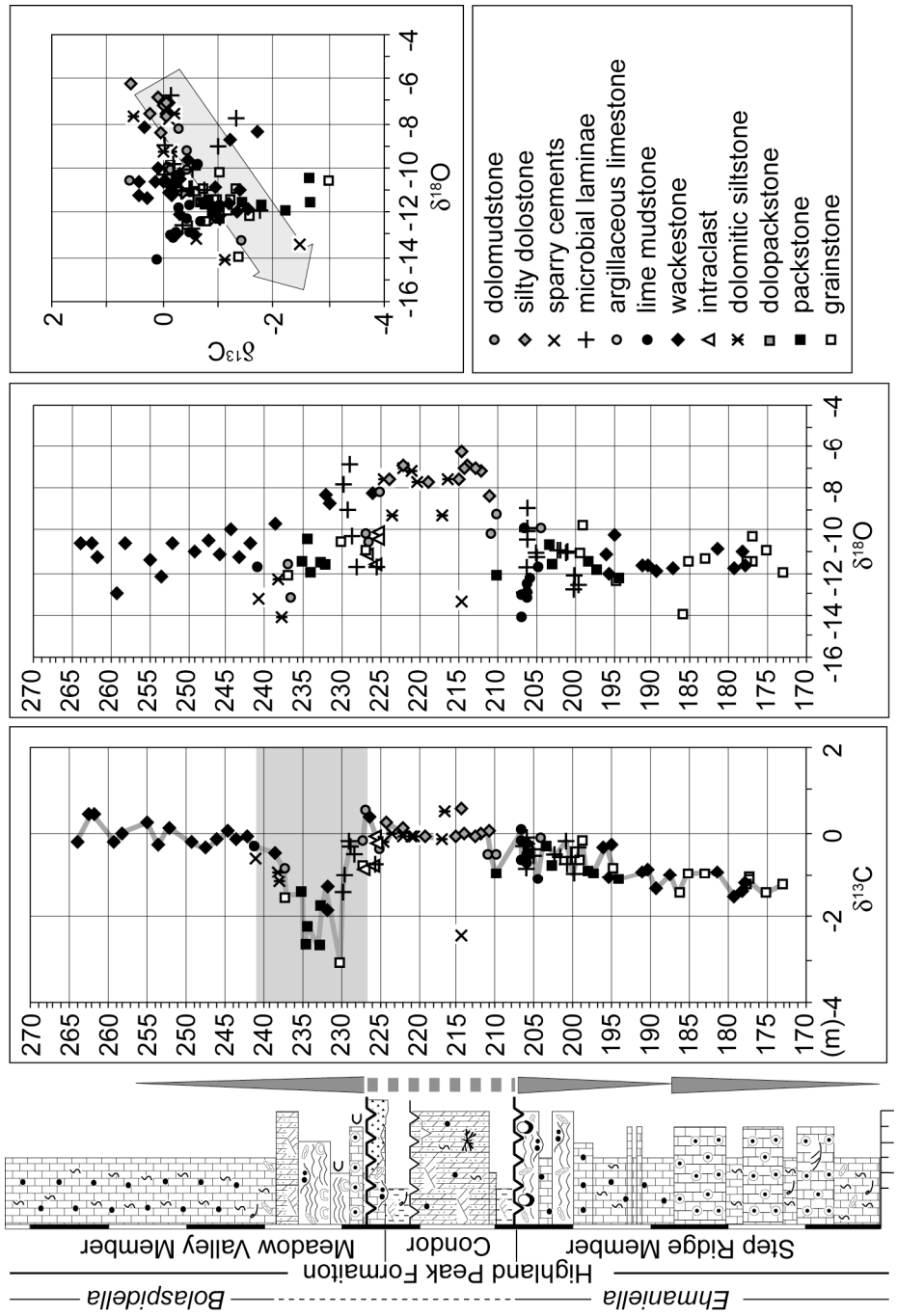

Figure 18. Integrated sequence and chemostratigraphy of the Panaca Hills section across the Ehmaniella and Bolaspidella transition in southern Nevada. A 3.6‰ negative $\delta^{13}C$ excursion is present above the upper sequence boundary. No obvious lithology-dependent isotope variation is observed. The diagenetic trend in the $\delta^{13}C$–$\delta^{18}O$ crossplot is defined by the isotope values of sparry calcite and micritic components of polished slabs.

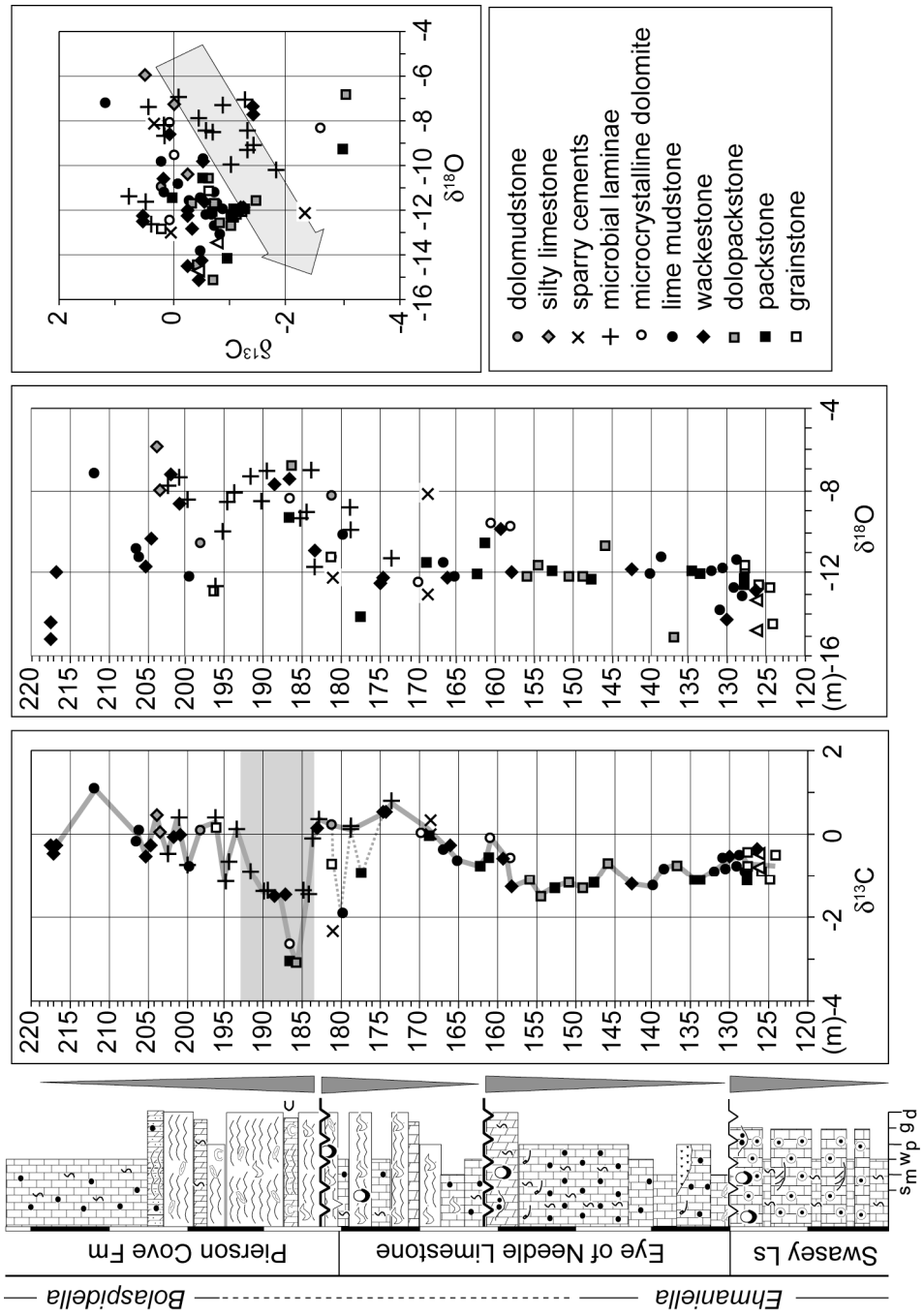

Figure 19. . Integrated sequence and chemostratigraphy of the Wah Wah Mountains section across the Ehmaniella and Bolaspidella transition in western Utah. A 3.5‰ negative $\delta^{13}C$ excursion is present above the upper sequence boundary, but note that significant $\delta^{13}C$ variations are present below the upper sequence boundary. The diagenetic trend in the $\delta^{13}C$–$\delta^{18}O$ crossplot is defined from samples immediately below the upper sequence boundary.

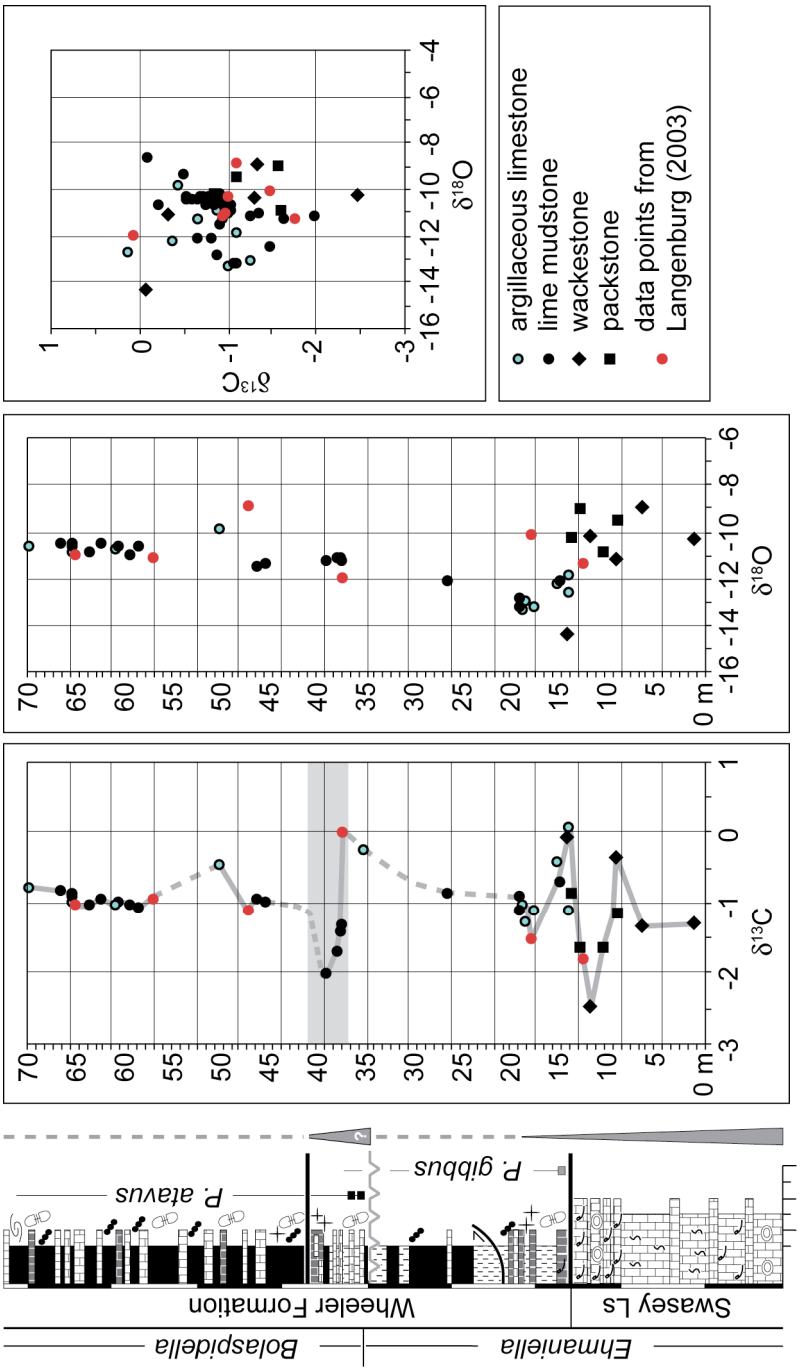

Figure 20. Carbon and oxygen isotope profiles and $\delta^{13}C$–$\delta^{18}O$ cross-plot of the House Range section in western Utah. A negative to positive shift in $\delta^{13}C$ is present at the Wheeler-Swasey boundary, but its regional significance needs further confirmation in adjacent sections. A 2‰ negative shift in $\delta^{13}C$ occurs 3 m above the FAD of P. atavus. No obvious $\delta^{13}C$–$\delta^{18}O$ covariation is observed.

Member are mostly between -7‰ and -9‰. A cross-plot of $\delta^{13}C$ and $\delta^{18}O$ values indicate that portion of the data points fall within the diagenetic trend defined from sparry calcite cements and matrix of the same slab, indicating partial alternation of isotope values by meteoric and/or burial diagenesis in this section (e.g., Kaufman and Knoll, 1995; Knauth and Kennedy, 2009).

The $\delta^{13}C$ trend from the Wah Wah Mountains section (Fig. 19) is similar to that from the Panaca Hills. The $\delta^{13}C$ values show a slight decrease from ~ -1‰ in the uppermost Swasey Limestone down to -1.5‰ in the lower Eye of Needle Limestone and an increase to ~0.4‰ at the base of the Pierson Cove Formation. A -3.5‰ negative $\delta^{13}C$ excursion is present in the lower Pierson Cove Formation (from 0.4‰ down to -3‰), above the upper sequence boundary. Below the sequence boundary, $\delta^{13}C$ values show large variations in vertically adjacent samples and between sparry calcite cements and matrix of the same polished slabs, indicating isotope alteration during meteoric diagenesis associated with the sequence boundary. Oxygen isotope values in this section are mostly clustered around -12‰ in the Eye of Needle Limestone but increase to -7‰ in the lower Pierson Cove Formation. The negative $\delta^{13}C$ excursion has the highest $\delta^{18}O$ values around -8‰ in this section, followed by scattered $\delta^{18}O$ values above the negative $\delta^{13}C$ excursion. Similar to the case seen in the Panaca Hills section, a portion of the data points fall on the diagenetic trend defined from $\delta^{13}C$ and $\delta^{18}O$ values of matrix and cements in large sample slabs.

The $\delta^{13}C$ values from the House Range (Fig. 20) show negative and positive shifts across the Swasey-Wheeler transition. The paucity of carbonate in the basal Wheeler Formation in the Marjum Pass section prevents a detailed $\delta^{13}C_{carb}$ isotope record, but available data show an increase of $\delta^{13}C$ from around -1‰ in the base to 0‰ slightly below the FAD of *P. atavus*. A negative $\delta^{13}C$ shift down to -2‰ follows slightly the FAD of *P. atavus* and $\delta^{13}C$ values return to near -1‰ above the hardground. Oxygen isotopes

are variable from –9‰ to -14‰ across the Swasey-Wheeler transition but vary little through the rest of the section, with values ranging between -10‰ and -12‰. No obvious $\delta^{13}C$–$\delta^{18}O$ covariation is observed in this section.

In the Drum Mountains (Fig. 21), $\delta^{13}C$ values show a positive shift from -1‰ to 1.3‰ across the Swasey-Wheeler transition. Below the FAD of *P. atavus* (the Drumian Stage GSSP) in the lower Wheeler Formation $\delta^{13}C$ values are close to 0‰. A negative shift in $\delta^{13}C$, from 0‰ to -2.5‰, occurs approximately 7 m above the FAD of *P. atavus* (GSSP), as shown in data summarized in Babcock et al. (2007). This negative shift covers only a 2-m-thick interval and values return back to ~0‰ slightly above the hardground. The $\delta^{18}O$ values in this section show a negative shift from about -10‰ to -14‰ at the Swasey-Wheeler contact and remain at -8‰ to -10‰ for the rest of the section. Apart from the shifted values associated with the Swasey-Wheeler contact (increased $\delta^{13}C$ with decreased $\delta^{18}O$), no $\delta^{13}C$–$\delta^{18}O$ covariation was observed in the section.

Data evaluation

The absolute $\delta^{13}C$ values from the five measured sections show considerable variation, particularly below the sequence boundaries in the southern platform sections (Figs. 17–19) and at the Swasey-Wheeler transition in the basinal sections (Figs. 20 and 21). Oxygen isotope values from all sections are lower than -8‰ and in the southern platform sections they show some degree of covariation with $\delta^{13}C$. These features indicate that absolute isotope values in the Great Basin may have been altered by diagenesis during subaerial exposure and post-depositional burial. However, aside from the Swasey-Wheeler transition in the basinal sections, which displays large variations in both $\delta^{13}C$ and $\delta^{18}O$, most $\delta^{13}C$ variations in equivalent strata across the transect are within 1‰ (Fig. 22). In addition, there is no lithology-dependent $\delta^{13}C$ variation in these sections. The lack of facies-dependent correlation of isotope values in the DICE, the

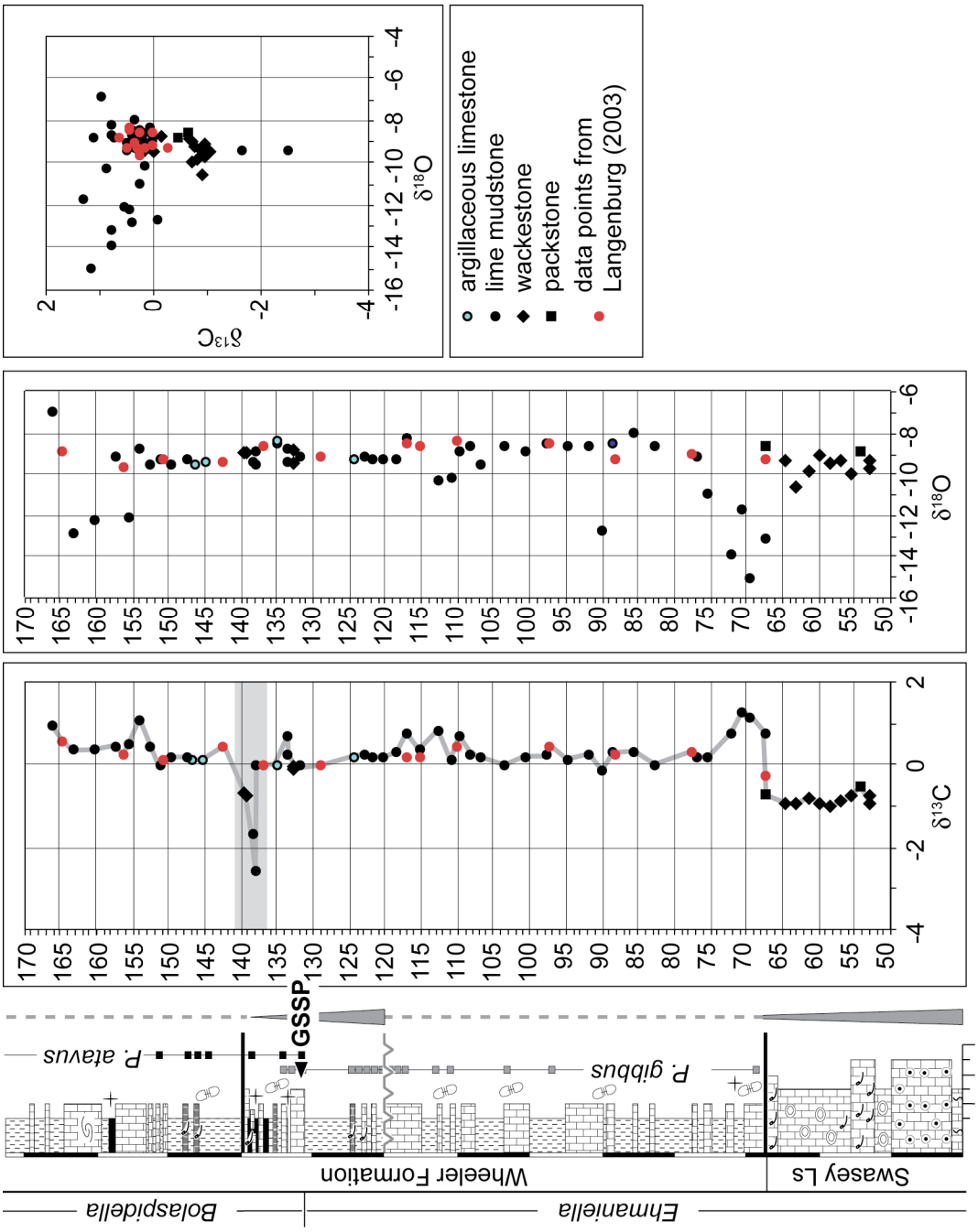

Figure 21. Carbon and oxygen isotope profiles and $\delta^{13}C$–$\delta^{18}O$ cross-plot of the Stratotype Ridge section in the Drum Mountains, western Utah. A 2.5‰ negative shift in $\delta^{13}C$ occurs 8 m above the GSSP. No obvious $\delta^{13}C$–$\delta^{18}O$ covariation is observed.

presence of a similar excursion in sections separated laterally by 10's of kilometers all indicate that the DICE is a real isotopic signal. Burial diagenesis would have affected the absolute values of all isotope values, including the DICE, and all of these values would have been shifted to more negative carbon and oxygen values by an equal amount within each section. Thus the laterally consistent, 2‰ – 3.6‰ negative $\delta^{13}C$ excursion above the upper sequence boundary may record a temporal change in seawater isotope composition, although the absolute $\delta^{13}C$ values may not represent that of the original calcite deposited in isotopic equilibrium with primary seawater. The positive $\delta^{13}C$ values at the Swasey-Wheeler transition in the basinal sections may record the isotope values of detrital carbonates shed from the exposed carbonate platform, but more detailed work in adjacent sections needs to be conducted to confirm the laterally consistency of this positive $\delta^{13}C$ shift.

Discussion

The DICE in the Great Basin

The DICE was defined as a negative $\delta^{13}C$ excursion nearly coinciding with the beginning of the Drumian Stage, in which the FAD of *P. atavus* occurs in the lower part, associated with a eustatic rise (Zhu et al., 2006). Although the onset of the excursion relative to the FAD of *P. atavus* is constrained, this position is not as well constrained from the standpoint of polymerid trilobite biostratigraphy. Also, because *P. atavus* first occurs in transgressive deposits overlying a significant eustatic lowstand, the first described appearance of *P. atavus* in all areas of the world may not be precisely the same (Fig. 13A; Zhu et al., 2006). Integrated sequence and chemostratigraphic profiles across the platform to basin in western Utah and Nevada (Fig. 22) indicate that the only candidate for the DICE in the Great Basin is the regionally consistent $\delta^{13}C$ excursion just above the Drumian base. In the House Range, the onset of the negative $\delta^{13}C$ excursion

is 3 m above the FAD of *P. atavus*, and in the Drum Mountains, it is 7 m above that horizon (Fig. 22D and E). In the southern platform sections (Fig. 22A-C), it occurs above a major sequence boundary. Other intervals with negative $\delta^{13}C$ values down to -1.5‰ to -2‰ are below the lower sequence boundary, but stratigraphically they are far below the base of the Drumian Stage and thus should not be candidates for the DICE. Considering that the Stratotype Ridge section in the Drum Mountains is the type section for the Drumian GSSP, the definition of the DICE should be refined to: "the negative $\delta^{13}C$ excursion slightly superjacent to the FAD of *P. atavus*; it is associated with transgressive deposits in shallow-water carbonate platforms and stratigraphic condensation in deep-water environments" (Fig. 22).

The sequence and chemostratigraphic profile across the platform-to-basin transect (Fig. 22) also provides information on the relationship between the FAD of *P. atavus*, sea-level change, and the DICE. Although it is difficult to identify the water-depth change across the Drumian boundary horizon in the deep-water sections, the fining-upward trend expressed by the decrease of silt-sized siliciclastic components and increase of organic-rich shales suggests that the stratigraphic interval below the Drumian base may be time-equivalent to the subaerial exposure and stratigraphic gap in shallow-water platforms (the "lowstand" deposits in sequence stratigraphic terms). Drumian sediments may first appear as part of the initial transgression that did not yet flood the shallow-water platforms in the Great Basin. However, the DICE follows slightly the position of the GSSP and may have developed in the later stage of transgression on the shallow-water platforms. Thus the DICE may have a wider geographic distribution than the FAD of *P. atavus*, which appears mostly in deep-water environments (Robison, 1982; Rowell et al., 1982; Geyer and Shergold, 2000; Peng and Robison, 2000; Peng et al., 2004). In this regard, the DICE is a useful for closely constraining the position of the Drumian base across shallow-water carbonate platforms where agnostoid trilobites are absent, even

though the precise horizon of the Drumian base may be associated with a subaerial hiatus in some successions.

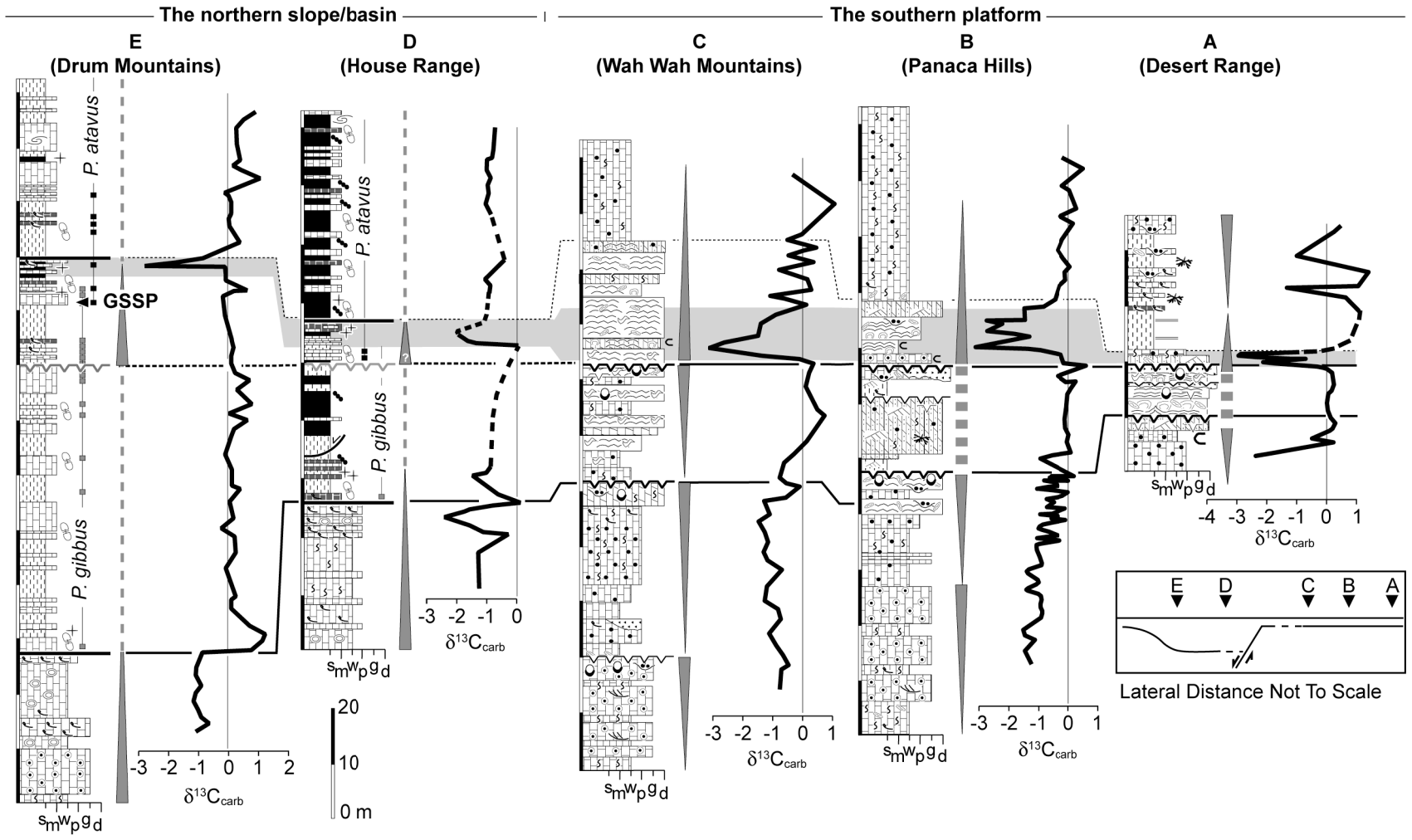
The northern slope/basin
The southern platform
E
(Drum Mountains)
D
(House Range)
C
(Wah Wah Mountains)
B
(Panaca Hills)
A
(Desert Range)
P. atavus
P. gibbus
GSSP
δ13Ccarb
smwpgd
20
10
0 m
E D C B A
Lateral Distance Not To Scale

Figure 22. Sequence and carbon isotope chemostratigraphic correlation across the platform-to-basin transect. The regionally consistent $\delta^{13}C$ excursion is at least an event of regional scale in the Great Basin.

Global correlation of the DICE

Although carbon isotope chemostratigraphy spanning Cambrian Series 3 has been conducted in many stratigraphic successions (e.g., Brasier and Sukhov, 1998; Montañez et al., 2000; Buggisch et at., 2003; Babcock et al., 2004, 2007; Zhu et al., 2004, 2006; Lindsay et al., 2005; Saltzman, 2005; Gomez et al., 2007; Álvaro et al., 2008; Kouchinsky et al., 2008; Ahlberg et al., 2009; Peng et al., 2009), existing data do not always illustrate a consistent expression of the DICE, and its global correlation at a detailed level remains questionable in some areas. This ambiguity is likely the result of the low resolution of data from published studies; in the present study of the Great Basin, the DICE covers a stratigraphic interval of less than 10 m (Fig. 22). This sharp excursion could easily be missed in stratigraphic studies aimed at obtaining a long-term isotope record for stratigraphic units that are hundreds of meters thick. In some studies (e.g., Saltzman, 2005; Gomez et al., 2007), positive shifts in $\delta^{13}C$ were preferred as a global correlation tool because most diagenetic fluids would shift $\delta^{13}C$ of carbonate rocks towards negative values. However, most Cambrian Series 3 $\delta^{13}C$ records do not show real "positive" $\delta^{13}C$ excursions. The absolute $\delta^{13}C$ values at those "positive" excursions are mostly from 0‰ to 1‰ (see review in Gomez et al., 2007), which is identical to the background values of the modern ocean seawater.

Another uncertainty in correlation, in some areas, is the biostratigraphic control on existing chemostratigraphic profiles. Although biostratigraphic control based on agnostoids tends to be precise, that based on polymerids are more variable in precision. For example, the composite $\delta^{13}C$ curve from the Great Basin (Montañez et al., 2000) contains two prominent negative $\delta^{13}C$ excursions, within the lower part of the *Ehmaniella* Biozone, with a minor negative excursion that straddles the *Ehmaniella-Bolaspidella* boundary (Fig. 23). Because the boundary between the *Bolaspidella* and *Ehmaniella* biozones is often difficult to identify in platform sections within the Great Basin, it is

uncertain whether the DICE should be correlated to the negative $\delta^{13}C$ excursion within the *Ehmaniella* Biozone or the much less prominent $\delta^{13}C$ shift within the basal *Bolaspidella* Biozone. The results from this study confirm that the DICE in the Great Basin is the negative excursion present across the *Ehmaniella-Bolaspidella* boundary in the Montañez et al. (2000) curve (Fig. 23). The South China succession (Fig. 23; Zhu et al., 2004) contains a large negative $\delta^{13}C$ excursion below the FAD of *P. atavus* and a minor negative shift just above that horizon. Because $\delta^{13}C$ values of the latter are positive (Fig. 23), the correlation of the DICE to the South China $\delta^{13}C$ profile is still questionable (Fig. 23; Zhu et al., 2004). Similarly, in time-equivalent strata of Sweden, only a minor negative $\delta^{13}C_{org}$ excursion is present within strata overlying the FAD of *P. atavus* (Ahlberg et al., 2009). Existing data raises two possibilities: (1) The DICE of the Great Basin is correlative to the $\delta^{13}C$ excursion below the first known appearance FAD of *P. atavus* in South China, but that horizon may differ slightly from the first appearance of the species in the Drum Mountains; and (2) the DICE is correlative with the small negative shift in $\delta^{13}C$ above the FAD of *P. atavus*, but absolute $\delta^{13}C$ values differ due to local environmental control on isotope values. More detailed biostratigraphic, sequence-stratigraphic, and chemostratigraphic research is required to clarify these uncertainties.

Local vs. global origin of the DICE

The FAD of *P. atavus* is present only in slope and basinal strata from the western United States, China, and Sweden, but in all sections this horizon is associated with the early stages of a transgressive event (Peng and Robison, 2000; Babcock et al., 2004; Peng et al., 2004; Zhu et al., 2004; 2006; Babcock et al., 2007; Ahlberg, 2009). The association of the DICE excursion with the FAD of *P. atavus* in the House Range Embayment and the correlation of the DICE to shallow-water facies on the southern platform further documents the association of the DICE with the early stages of

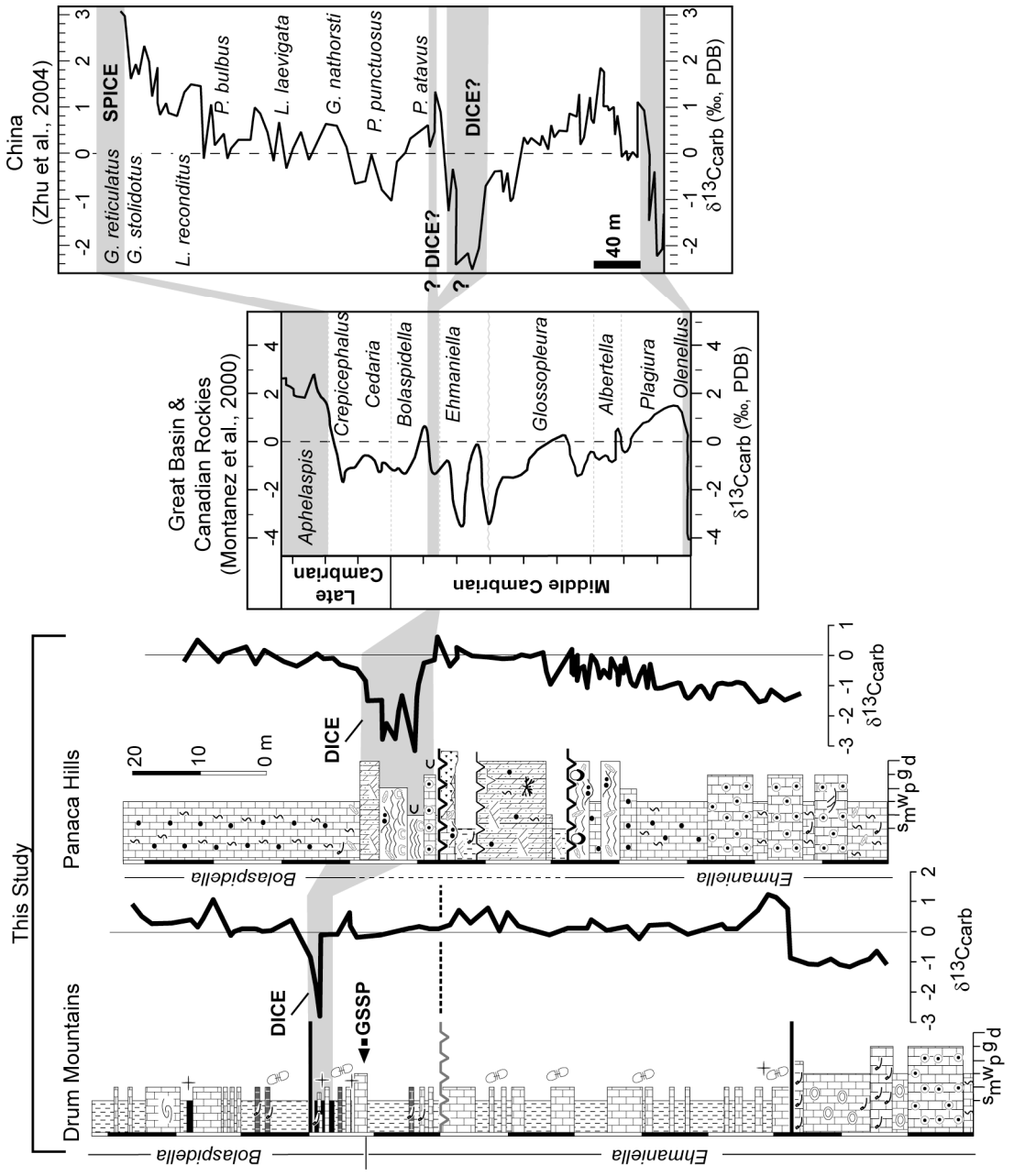

Figure 23. The DICE refined in this study and its potential correlation with existing $\delta^{13}C$ excursions from the Great Basin (Montañez et al., 2000) and South China (Zhu et al., 2004).

transgression. The most accepted theory regarding the cause of negative $\delta^{13}C$ excursions is that they form in conjunction with oxidation of organic matter during overturning of stratified water masses during transgression. These ^{13}C-depleted waters are transferred to slope and open-shelf environments resulting in carbonate sediments and cements with lower $\delta^{13}C$ values than those formed under normal open-marine conditions (Wilde and Berry, 1984; Derry et al., 1992; Kaufman and Knoll, 1995; Ahlberg et al., 2009). The Cambrian was a time period where the open ocean was likely stratified with poorly oxygenated bottom waters (Wilde and Berry, 1984; Weissert, 1989; Zhuralev and Wood, 1996; Glumac and Walker, 1998; Gaines et al., 2005; Saltzman, 2005; Hurtgen et al., 2009) and therefore the potential for a global overturning of ^{13}C-depleted water was high. Further documentation of the DICE excursion in other shallow-water regions outside of the western United States is needed to support this interpretation because the House Range Embayment was also likely stratified and therefore a similar mechanism at the local scale is also likely.

The small differences on a global scale of the DICE excursion compared to the first appearance of *P. atavus*, if confirmed in future studies, also raises the possibility of a local origin for the negative $\delta^{13}C$ excursion in the Great Basin (Fig. 22) and in other successions such as South China (Fig. 23). The $\delta^{13}C$ values of marine carbonates can diverge from "normal" seawater values by local carbon cycling in restricted basins and epeiric seas (Patterson and Walter, 1994; Holmden et al., 1998; Immenhauser et al., 2003; Panchuk et al., 2006) and by meteoric diagenesis (Allan and Matthews, 1982; Railsback et al., 2003; Theiling et al., 2007). As discussed earlier, significant diagenetic modification may have imprinted the absolute $\delta^{13}C$ values, particularly for stratigraphic intervals immediately below the sequence boundaries. However, the consistent $\delta^{13}C$ anomaly across the platform-to-basin transect, above a sequence boundary, favors an

origin related to a change in the isotopic composition of seawater at least at a regional scale.

If the DICE is determined to be a local seawater signature in the Great Basin, potential mechanisms for the negative $\delta^{13}C$ excursion may include respiration and mineralization of organic matter or increased fresh-water input (Patterson and Walter, 1994; Panchuk et al., 2006). The House Range Embayment was stratified during the time of deposition of the lower Wheeler Formation (Rees, 1986; Gaines and Droser, 2003; Gaines et al., 2005). Like the model for a globally stratified ocean, in a local stratified basin respiration and mineralization of organic matter could add isotopically light carbon into the surface water, leading to ^{13}C depletion in carbonates (Patterson and Walter, 1994; Panchuk et al., 2006). Respiration and mineralization could be enhanced during seawater transgression due to the upwelling of deep-water and the potential increase of sulfate supply from weathering input. The DICE, as present in the Great Basin, is closely associated with the initiation of the House Range Embayment (Fig. 22). Uplift and exposure of the platform may have resulted in increased fresh-water input, lowering the $\delta^{13}C$ values in shelf environments (Patterson and Walter, 1994; Immenhauser et al., 2002, 2003; Panchuk et al., 2006).

Conclusion

An integrated sequence and chemostratigraphic study of Cambrian Series 3 strata in the Great Basin reveals a regionally consistent, 2‰ – 3.6‰ negative $\delta^{13}C$ excursion referred to as the Drumian Carbon isotope Excursion (DICE). The DICE in the Great Basin slightly follows the FAD of *P. atavus* in deep-water environments and occurs above a major sequence boundary on the adjacent shallow-water carbonate platform. Considering the ambiguity in expression of the DICE in the literature and the fact that the Stratotype Ridge section in the Drum Mountains, Utah, hosts the GSSP for the base of

the Drumian Stage, we suggest that the definition of the DICE should be refined to “the negative $\delta^{13}C$ excursion slightly superjacent to the FAD of *P. atavus*; it is associated with retrogradation of shallow-water carbonate platforms and stratigraphic condensation in deep-water environments”. Although regionally consistent in the Great Basin, the DICE is difficult to firmly correlate on the basis of published $\delta^{13}C$ curves from some sections on other continents. This is possibly due to the relatively low resolution of published chemostratigraphic data and the lack of reliable biostratigraphic control in some successions. The integrated sequence and chemostratigraphic study from the Great Basin thus provides a guide for future studies in other successions. Alternatively, the DICE from the Great Basin may be a localized isotopic anomaly formed by respiration and mineralization of organic matter in a restricted basin and/or by increased fresh water input during the initiation of the House Range Embayment.

CHAPTER 3

CARBON ISOTOPE VARIABILITY BETWEEN PLATFORM AND BASIN SECTIONS OF THE MIDDLE CAMBRIAN HOUSE RANGE EMBAYMENT

Abstract

Strata of the middle Cambrian House Range Embayment host exceptionally well-preserved burgess-shale type (BST) fossils and are considered to have been deposited under anoxic bottom-water conditions. In anoxic basins, local carbon cycling through remineralization of organic matter would be an expected process resulting in a potentially large vertical carbon isotope gradient similar to that of the modern Black Sea. In this study, $\delta^{13}C_{carb}$ profiles were analyzed from a shallow-water carbonate platform section adjacent to the House Range Embayment, and from a deep-water basinal section from the axis of the House Range Embayment. A comparison of platform and basin profiles does not reveal significant isotopic variability that can be attributed solely to local carbon cycling in an anoxic basin. The 1‰ platform-to-basin isotopic gradient present in a portion of the Wheeler Formation interval can be attributed to either localized basin anoxia or burial diagenesis. In most of the interval investigated however, $\delta^{13}C_{carb}$ values from the platform section (-2‰ to 0‰) are consistently more negative than those from the coeval basinal section (mostly 0‰ to 2‰). This trend, and the fact that most basinal values are positive, is not expected for sediments of an anoxic basin. Negative values on the platform most likely resulted from diagenetic alteration of $\delta^{13}C_{carb}$ values on the platform due to episodic exposure and karstification of shallow-water carbonate sediments. Several negative carbon isotope shifts are present in both platform and basinal sections, but only two of them can be correlated with confidence within the sequence stratigraphic framework. The results indicate that chemostratigraphic correlation in poorly dated successions deposited from significantly different paleoenvironments should be approached with caution.

Introduction

Facies-dependant variations in $\delta^{13}C_{carb}$ are common in modern (Patterson and Walter, 1994; Swart and Eberli, 2005; Swart, 2008) and ancient marine basins (Holmden et al., 1998; Immenhauser et al., 2002, 2003; Panchuk et al., 2006; Jiang et al., 2007, 2008) due to local carbon cycling in restricted basins, and diagenetic alteration (Irwin et al., 1977; Allan and Matthews, 1982; Railsback et al., 2003; Theiling et al., 2007). In anoxic basins in particular, local carbon cycling through remineralization of organic matter may generate a large surface-to-deep water carbon isotope gradient that may be significantly larger than in the modern ocean (~2‰). In the Black Sea (surface = -3.4‰ to 0.8‰; basin = -6.8‰) and the Framvaren Fjord (surface = estimated to be 0‰; basin = -19.5‰), a ≥ 7‰ carbon isotope gradient has been observed (e.g., Deuser, 1970; Volkov, 2000). Similar vertical isotopic gradients may have also existed in ancient basins (Surge et al., 1997; Hotinski et al., 2004; Jiang et al., 2007; 2008), although the magnitude and aerial distribution of such gradients vary from case to case.

The middle Cambrian House Range Embayment of western Utah, USA was a syndepositional fault-controlled deep-water basin and strata deposited in this restricted basin contain exceptionally well-preserved burgess-shale type fossils. It has long been inferred that anoxic conditions during the early stages of basin evolution contributed to the exceptional preservation of organisms (e.g., Gaines and Droser, 2005; Gaines et al., 2005). If the House Range Embayment was a restricted, anoxic basin, a surface-to-deep carbon isotopic gradient larger than that of the modern ocean (~2‰) would be expected. To test this hypothesis and to explore the possibility of using carbon isotope excursions for regional/global stratigraphic correlation, in this chapter I examined the $\delta^{13}C_{carb}$ profiles across platform-to-basin transect of the House Range Embayment. The sequence stratigraphic framework proposed in Chapter 1 provides an opportunity to compare both long- and short-term isotopic events recorded in stratigraphic profiles between platform

and basinal sections, and to determine whether any isotopic events are useful for regional and global correlation of this interval.

Stratigraphy and depositional environments

Cambrian strata of western North America were deposited on a passive continental margin that was developed over the rift associated with the breakup of the supercontinent Rodinia during the late Neoproterozoic (Bond and Kominz, 1984; Levy and Christie-Blick, 1991; Burchfiel et al., 1992; Poole et al., 1992). By Cambrian Series 3, a northwest-facing carbonate platform covered most of present day Utah, Nevada, and southeastern California. Fine-grained terrigenous sediments accumulated in deep-water to the west of the carbonate platform and in shallow-water to the east (Palmer, 1971). Syndepositional fault activity within the House Range Embayment is inferred to have started during the latest *Ehmaniella* Zone (Fig. 24; Rees, 1986). This basin extended for more than 400 km and controlled the distribution of depositional facies through the Early Ordovician (Rees, 1986; Miller et al., 2003). On the northern (downthrown) side of the fault, deep-water shale and fine-grained carbonates span most of the Cambrian Series 3, with the depocenter close to the present day Marjum Pass region of the House Range in western Utah. Further north, a gentle carbonate ramp with perhaps <1° topographic gradient was developed towards the basin during the latest *Ehmaniella* zone and earliest *Bolaspidella* zone (Fig. 24b; Rees, 1986; Elrick and Snider, 2002), although detailed documentation of shallow ramp facies is lacking due to the limited availability of outcrop. On the southern side of the inferred normal fault, however, shallow-water carbonate deposition continued through the Cambrian Epoch 3 and the Furongian Epoch (Palmer, 1971; Kepper, 1972, 1976; Rees, 1986; Montañez and Osleger, 1993).

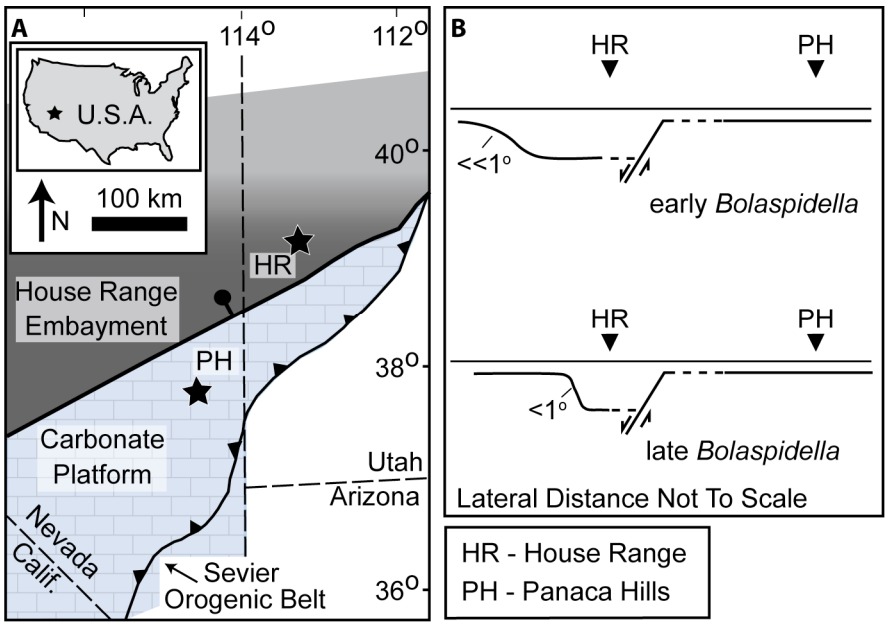

Figure 24. (A) Location map illustrating the geographic extent of the House Range Embayment during the early *Bolaspidella* zone (modified from Rees, 1986). (B) Cross-sectional representation of the House Range Embayment (modified from Elrick and Snider, 2002).

Stratigraphic units, biostratigraphic control, and sequence stratigraphic data associated with House Range Embayment and adjacent carbonate platform strata are summarized in Figure 25. Detailed documentation of the sequence stratigraphic framework is presented in Chapters 1 and 2. Basinal strata are dominated by fine-grained carbonate mudstone/calcisiltite, and calcareous and non-calcareous shale, with sedimentary features indicating deposition below storm wave base. Platform strata are dominated by burrow-mottled wackestone/packstone and laminated and/or fenestral microbial laminites, with abundant dolomitized beds, indicating deposition under environments ranging from quiet shallow-subtidal lagoons to extensive frequently exposed tidal flats.

Biostratigraphic zonation is based on open-shelf polymerid trilobites that are useful for regional correlation, and cosmopolitan agnostoid trilobites that are useful for global correlation. Only the basinal section contains both types of fossils. Biostratigraphic data from the carbonate platform is poor and biozone boundaries can only be approximately defined or inferred due to the paucity of fossils and the facies-dependant distribution of polymerid trilobites (Robison, 1976; Palmer, 1977; Robison et al., 1977; Rowell et al., 1982; Geyer and Shergold, 2000). Detailed documentation of the *Ehmaniella-Bolaspidella* boundary is presented in Chapter 2.

Chemostratigraphy

Materials and methods

For this study, 462 samples were collected for $\delta^{13}C_{carb}$ and $\delta^{18}O$ analysis from one shallow-water carbonate platform section and one deep-water basinal section. Platform samples were collected from the southern Panaca Hills region in eastern Nevada and basinal samples were collected from the Marjum Pass area of the House Range in western Utah. Care was taken to sample only the finest grained portion of a sample although that was not always possible with platform samples where coarser grained textures were unavoidable in certain horizons. Sample powders were microdrilled from polished slabs or fresh surfaces and reacted with orthophosphoric acid for 10 minutes at 70ºC in a Kiel-Device automatically connected to a Finnigan Delta Plus dual-inlet mass spectrometer. The majority of analyses were conducted at the LVIS Lab (Las Vegas Isotope Science Laboratory) at the University of Nevada Las Vegas, but a portion of samples from the Panaca Hills section were analyzed at the stable isotope lab of INSTAAR (Institute of Arctic and Alpine Research) at the University of Colorado, Boulder. Isotopic results are reported as δ values with reference to the Vienna Peedee

belemnite standard (VPDB). Precision monitored by NBS-19 calcite and an internal standard is better than 0.1‰ for both C and O isotopes.

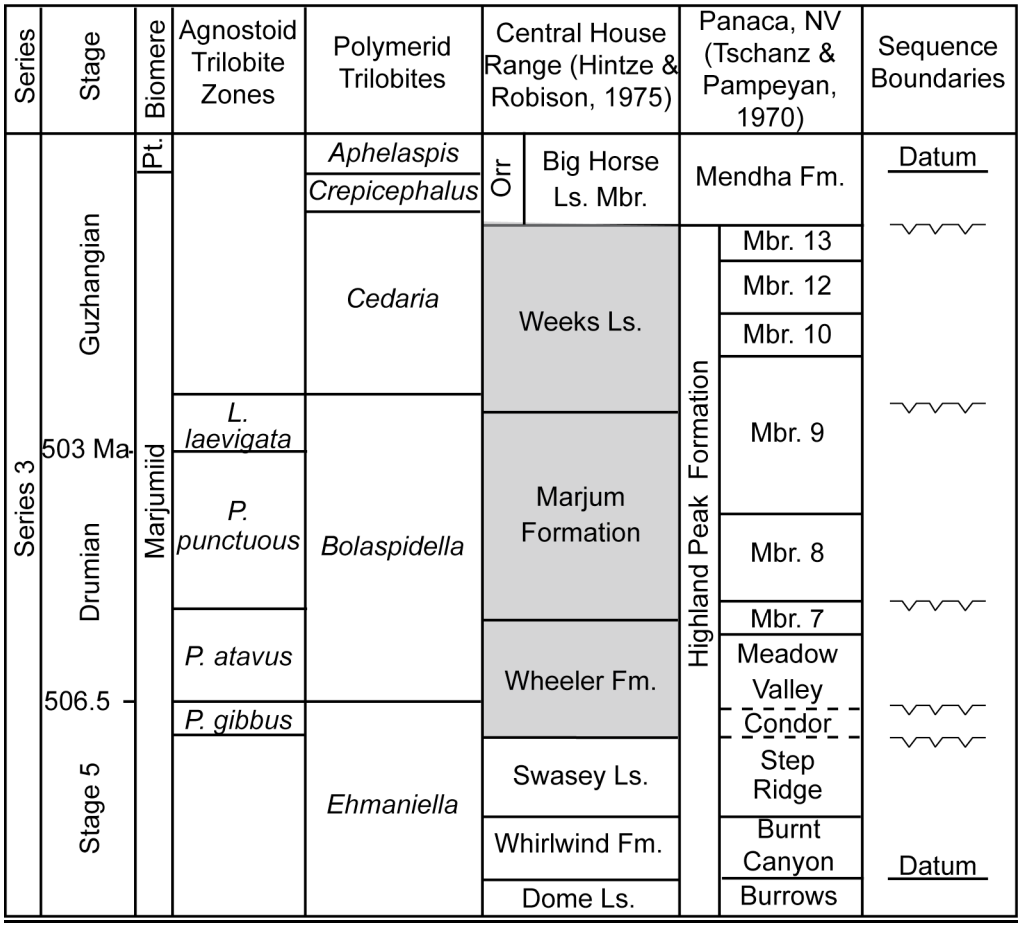

Figure 25. Correlation chart for the stratigraphic, biostratigraphic and chronostratigraphic units of interest in this paper. The shaded region represents strata deposited within the House Range Embayment. Trilobite zones are from Robison (1976), Babcock et al. (2007), and Geyer and Shergold (2000). Chronostratigraphic data is from Gradstein et al., (2004) and Ogg et al. (2008).

Results

Platform section

Isotope data from the Highland Peak Formation platform section in the Panaca Hills reveal median $\delta^{13}C_{carb}$ values of -0.6‰ that fall between -3.0 and 0.7‰, and widely variable $\delta^{18}O$ values that range between -14.0 and -6.2‰ (Fig. 26). Values at the base of the section within the Step Ridge Member form a vertical trend with values between -1‰ and 0‰. This trend shifts to negative $\delta^{13}C_{carb}$ values around -1.5‰ that cover a 100-m-thick interval dominated by oolitic grainstone. $\delta^{13}C_{carb}$ values increase upward from the top of the Step Ridge Member and reach the maximum value of ~0.5‰ at the top of the Condor Member. A significant negative $\delta^{13}C_{carb}$ excursion with a minimum of -3‰ is present at the base of the Meadow Valley Member and is associated with transgressive strata that overlie a karstic unconformity. This negative excursion is time-equivalent to the Drumian Carbon Isotope Excursion (DICE) at the base of the Drumian Stage (Chapter 2; Howley and Jiang, 2010). Above this excursion, $\delta^{13}C_{carb}$ values remain near 0‰ through the lower half of the Meadow Valley Member and are only broken up by a sharp 1‰ negative shift around 289 m. From 300 to 443 m, $\delta^{13}C_{carb}$ values are mostly negative with a minimum of -2.2‰ at the base of Member 8. Several small negative shifts in $\delta^{13}C_{carb}$ occur within the microbial-laminite beds that dominate Member 7, but their magnitudes are less than 1‰. At 443 m the overall negative trend shifts to positive, with a peak up to 0.7‰ around 549 m at the base of Member 9. Overlying this positive shift, $\delta^{13}C_{carb}$ values fluctuate between -1‰ and 1‰ through the top of Member 9, with several sharp shifts present, but no long-term trend is identified. At the transition between Member 9 and Member 10, $\delta^{13}C_{carb}$ values shift to -1.7‰ and remain at values between -1‰ and -0.5‰ through Member 13.

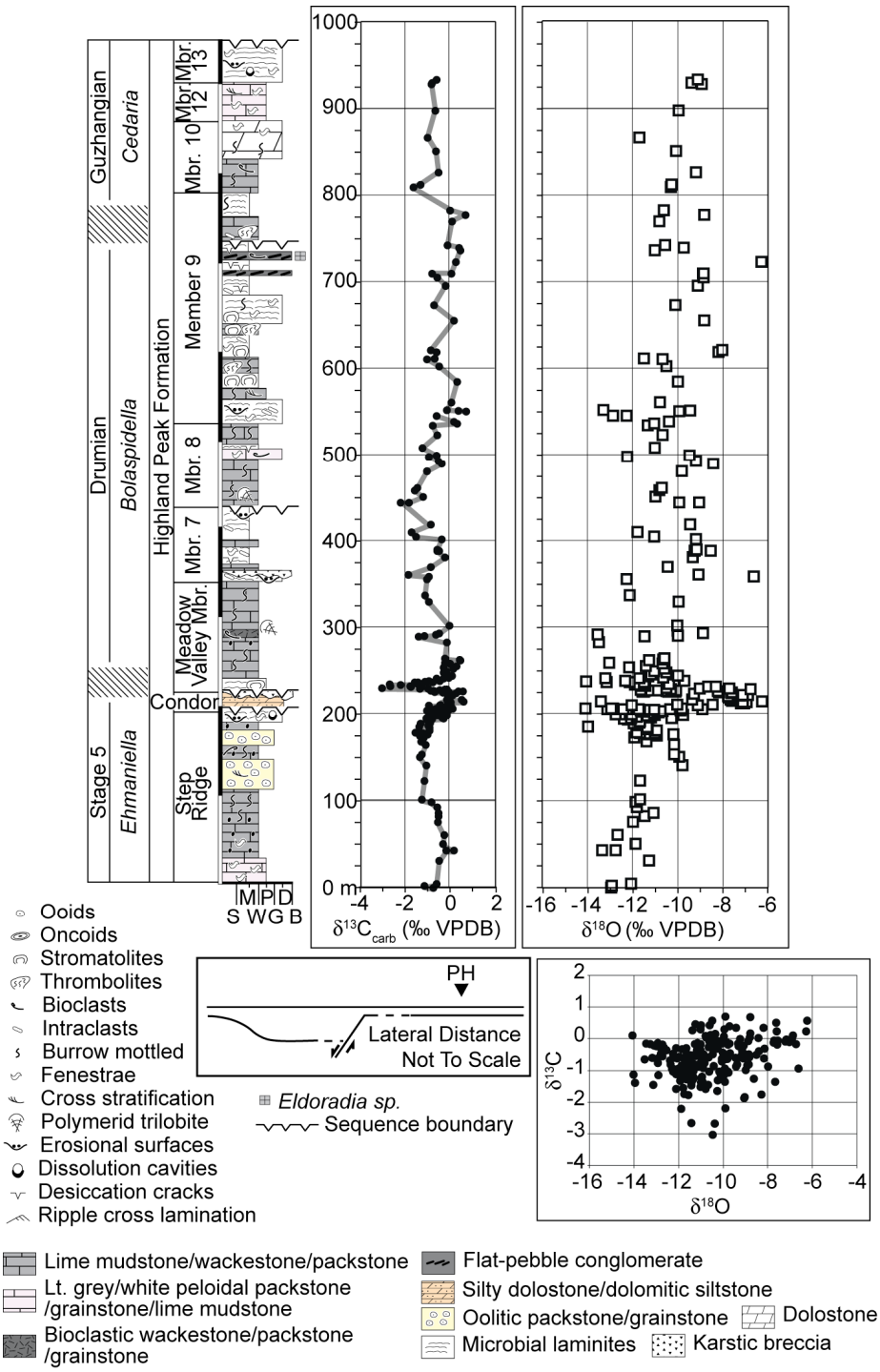

Figure 26. Carbon and oxygen isotope data from the shallow-water platform section in the Panaca Hills, Nevada.

Oxygen isotope values of the Highland Peak Formation vary from -14‰ to -6‰, but most values fall between -12‰ and -8‰. Except for one sharp positive shift (from -14‰ to -6‰) associated with the dolomitic and siliciclastic-rich Condor Member, most $\delta^{18}O$ values are scattered and do not show a clear trend. The $\delta^{13}C$– $\delta^{18}O$ cross-plot indicates that most isotope values fall in the range typical of Phanerozoic carbonates that have experienced alteration during meteoric and burial diagenesis (Knauth and Kennedy, 2009). No covariation between lithology and isotope values was observed except that silty dolostone and dolomitic siltstone samples tend to have higher $\delta^{18}O$ values than the majority of carbonate lithofacies (Fig. 27A).

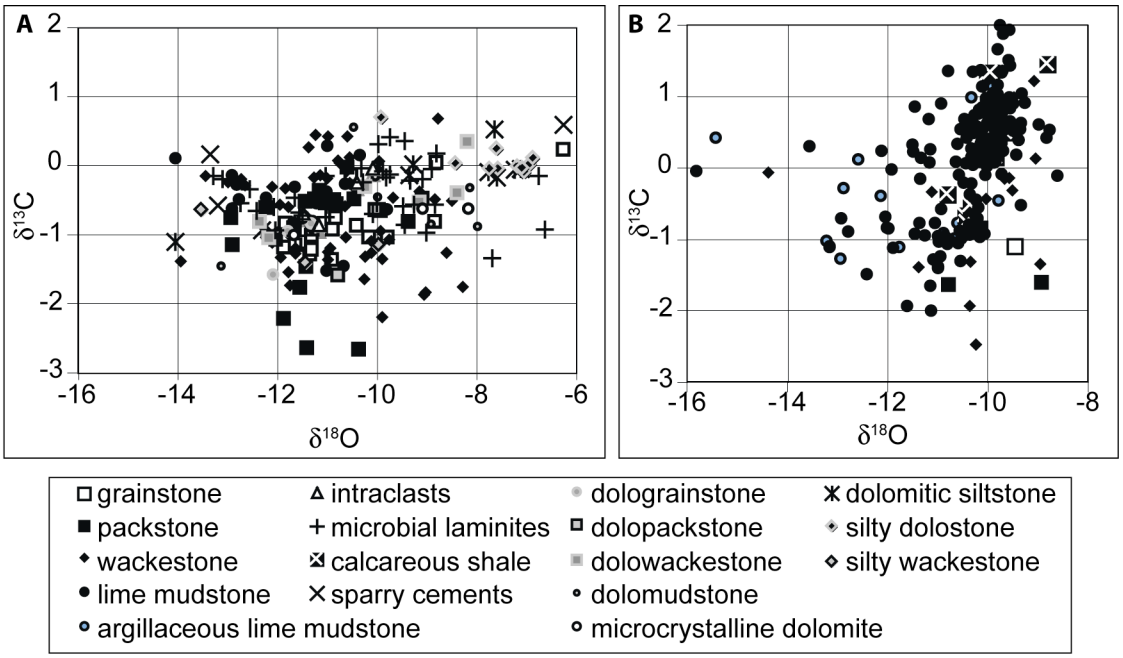

Figure 27. Cross-plots of carbon and oxygen isotopes based on lithology. (A) Platform section. (B) Basin section.

Basinal section

The basin section from the Marjum Pass region of the House Range has median $\delta^{13}C_{carb}$ values of -0.3‰ and range from -2.5‰ to 2.0‰. $\delta^{18}O$ values range from -15‰ to -8‰, with an average of -10‰ (Fig. 28). $\delta^{13}C_{carb}$ values at the transition between the Swasey Limestone and Wheeler Formation are highly variable from -2.5‰ to 1‰, with variations of ~1‰ occurring from bed to bed. The limited amount of carbonate material available for analysis in the basal Wheeler Formation precludes identification of detailed isotopic trends through the interval below the first appearance of *Ptychagnostus atavus*. However, analyzed samples have $\delta^{13}C_{carb}$ values around -0.8‰. Above this interval is a sharp negative $\delta^{13}C_{carb}$ shift down to -2‰ between 40 and 45 m. This negative shift is interpreted as the DICE at the base of the Drumian Stage and has been described in detail in Chapter 2. For the rest of the Wheeler Formation, most $\delta^{13}C$ values are around -1‰, with a few down to -1.5‰ and up to 0.5‰. A negative shift down to -2‰ occurs in the basal Marjum Formation. This shift is associated with the appearance of limestone-dominated rhythmites with bioturbation features, bioclastic material, and benthic infauna indicating oxygenated conditions and increased input of detrital carbonate from the adjacent carbonate platform. Overlying this negative shift, $\delta^{13}C_{carb}$ values shift to positive values of ~0.6‰. This positive shift is significant considering that $\delta^{13}C_{carb}$ values in the Wheeler Formation are negative with a median value of -0.9‰. For the remainder of the Marjum Formation up to 510 m, $\delta^{13}C_{carb}$ values are mostly positive and shift between 0‰ and 0.5‰, with a few values down to -1‰ and up to 1.5‰. No persistent trend was identified in this data. A major negative $\delta^{13}C_{carb}$ shift from 2‰ to -1.3‰ is present at the top of the section.

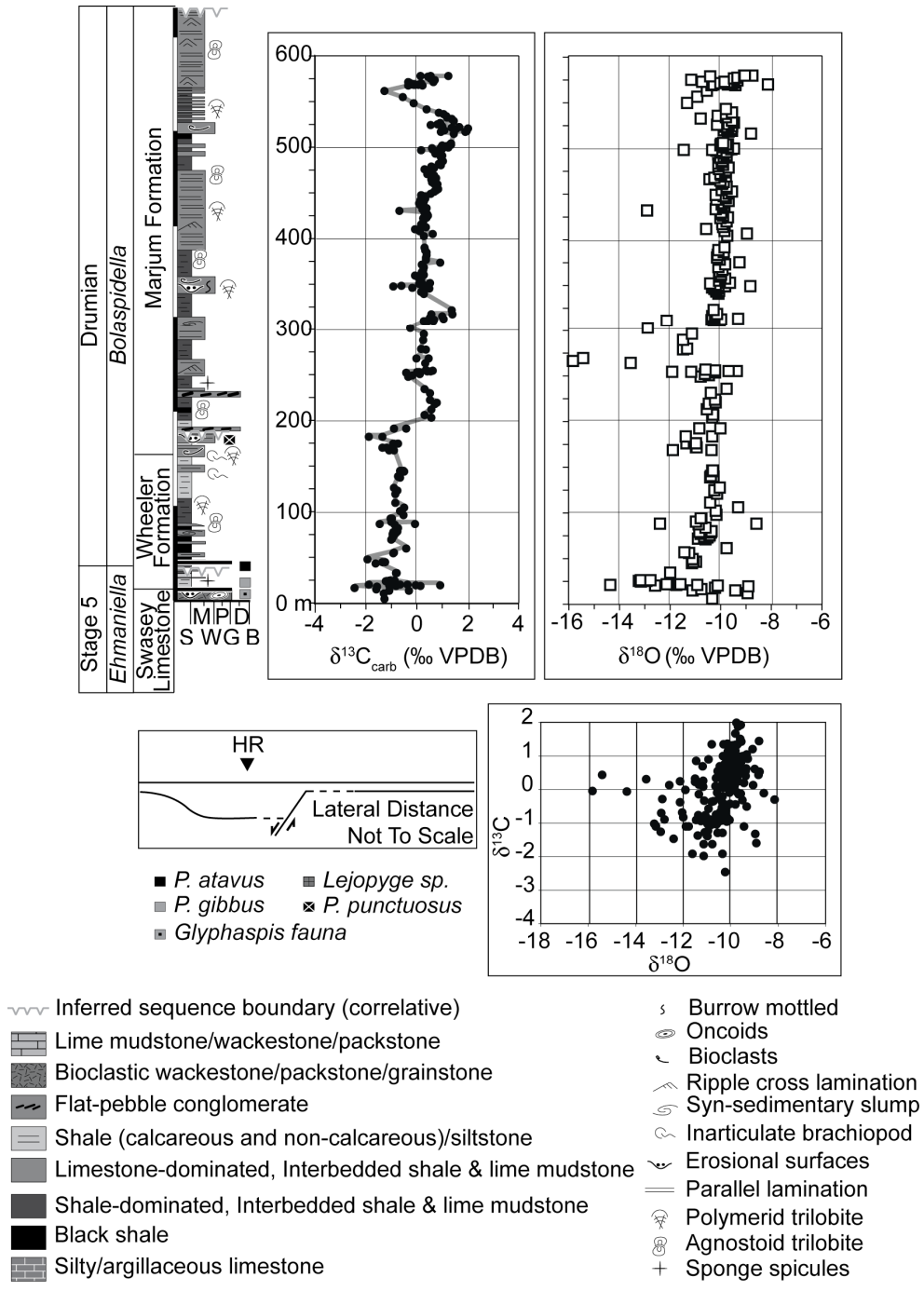

Figure 28. Carbon and oxygen isotope data from the deep-water basinal section in the House Range, Utah.

Oxygen isotope values from this section are mostly clustered between -12‰ and -10‰, but small portions of the sampled interval have values down to -14‰ and up to -9‰. No obvious trend in $\delta^{18}O$ is observed. Cross-plot of $\delta^{13}C$ and $\delta^{18}O$ (Fig. 28) does not reveal any obvious covariation between $\delta^{13}C_{carb}$ and $\delta^{18}O$, but most data points values fall within the normal range for Phanerozoic carbonates that have been interpreted as diagenetically modified (Knauth and Kennedy, 2009). There is no observable covariation between lithology and isotope values (Fig. 27B).

Discussion

Facies-dependant isotope variations

Comparison of the platform and basin carbon isotope profiles (Fig. 29) does not reveal systematically more negative $\delta^{13}C_{carb}$ values in the basinal section, as would be expected in anoxic and stratified basins, except in a short interval immediately overlying the DICE. The interval above the DICE in the basin section has fairly stable $\delta^{13}C_{carb}$ values around -1‰ through the top of the Wheeler Formation. In the platform section, the interval above the DICE has stable $\delta^{13}C$ values that are ~1‰ higher than in the basin. The facies from this interval in the basin are representative of sediments deposited under intermittent dysoxic and anoxic conditions (Gaines and Droser, 2005). These interbedded black shale and very thinly bedded lime mudstone and argillaceous lime mudstone layers represent deposition below storm wave base and below the photic zone. The 1‰ difference in $\delta^{13}C_{carb}$ between the platform and basin, with more positive values on the platform, may be the result of early cementation of platform-derived detrital carbonate under low oxygen conditions in the House Range Embayment, which resulted in lower $\delta^{13}C$ values in basin strata. A similar isotopic gradient is present in modern oceans where well-oxygenated surface waters are enriched in ^{13}C relative to poorly oxygenated deep waters that are enriched in ^{12}C due to an increase in the amount of

CO_2 released from decaying organic matter (Kroopnick, 1974). Surge et al. (1997) documented a ~0.5‰ gradient in the Cambrian Ajax Formation in Australia and argued that this was evidence of an ancient seawater isotopic gradient. The ~ 1‰ shift identified in this study may indicate localized anoxia in the HRE during deposition of the Wheeler Formation. This gradient however is significantly smaller than gradients documented in modern environments (>3‰) and is within the spread of values observed in oxygenated surfaces waters in the modern open ocean (~2‰). During the middle Cambrian, however, atmospheric CO_2 levels may have been significantly higher than today (Berner, 2003). Under high atmospheric CO_2, the ocean dissolved inorganic carbon (DIC) reservoir may have been larger than modern and therefore a smaller isotope gradient would be expected due to the diminishing effect of a biological pump at elevated seawater DIC concentration (Hotinski et al., 2004).

An alternative to the anoxic gradient hypothesis is that the 1‰ gradient recorded diagenetic alteration of basin sediments during burial. The lower Wheeler Formation is predominately composed of black shales, and carbonate sediments that are buried with these organic-rich rocks can easily incorporate ^{12}C-enriched organic carbon into carbonate carbon through precipitation of carbonate cements during burial (Irwin et al., 1977).

In contrast to the minor isotopic gradient that potentially existed during deposition of the Wheeler Formation, the isotopic difference between the platform and basin during deposition of the Marjum Formation is reversed: $\delta^{13}C_{carb}$ values from the basin section are isotopically higher than those from the coeval platform section (Fig. 29). The most reasonable interpretation of this difference is that strata from the shallow-water carbonate platform were affected by meteoric diagenesis during periods of subaerial exposure. The interval in the Marjum Formation above 200 m has fairly stable $\delta^{13}C_{carb}$

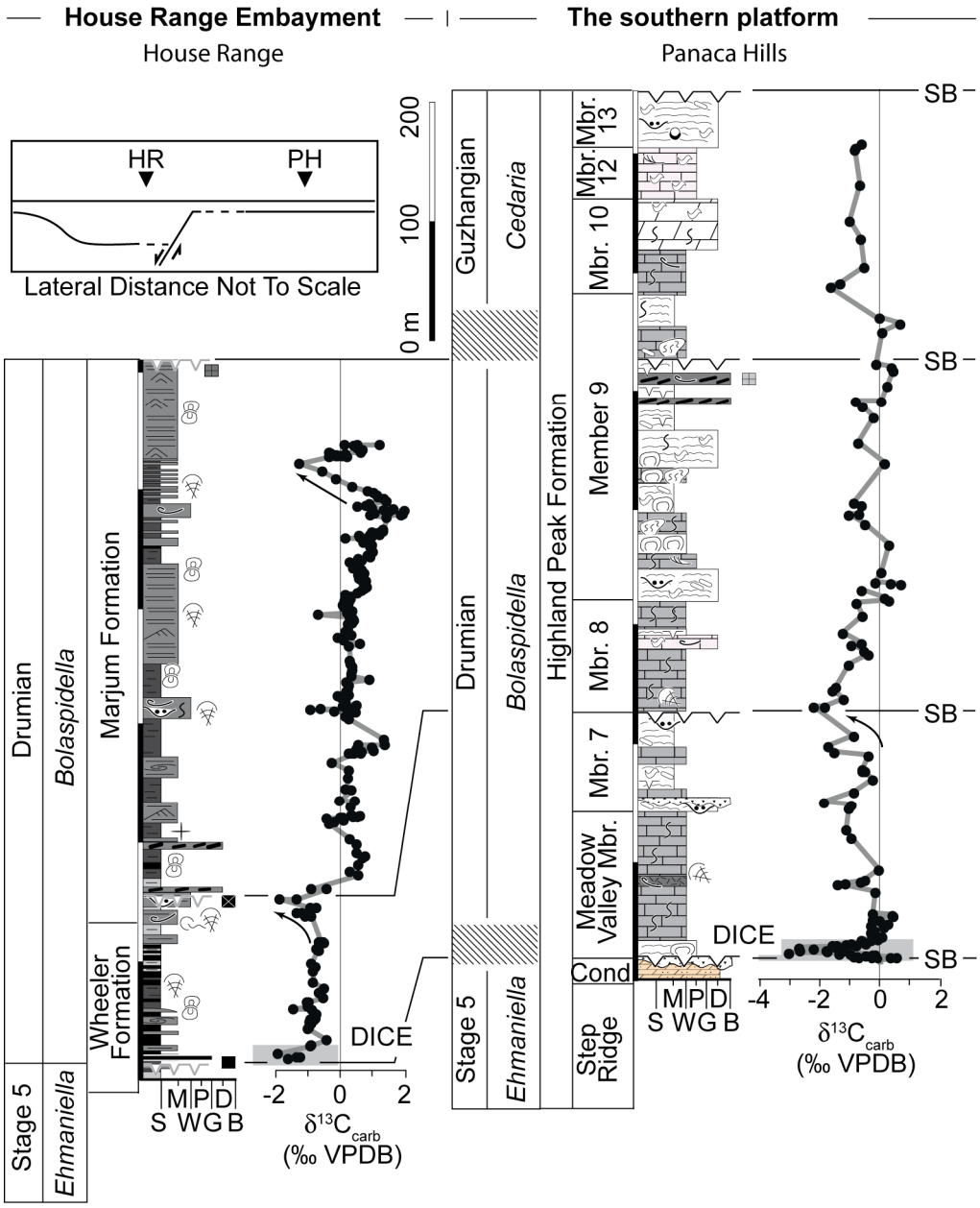

Figure 29. Correlation of the shallow-water platform section and the deep-water basin section carbon isotope profiles. Shaded interval at base is the DICE excursion. Arrows above the DICE indicate the negative trend of values below the sequence boundary.

values around 0.42‰ whereas the platform section has $\delta^{13}C_{carb}$ values that fluctuate around -0.9‰. In addition, basinal values are more stable than correlative platform values. Associated with these more negative $\delta^{13}C_{carb}$ values on the platform are abundant subaerial exposure surfaces indicating that the more negative $\delta^{13}C$ values in platform strata resulted from diagenetic alteration of isotope values by meteoric fluids. Dissolution of carbonate sediments by meteoric fluids and precipitation of carbonate cements from these ^{12}C-enriched fluids results in $\delta^{13}C_{carb}$ values that are lower than the values of the original sediment. In modern and ancient carbonates that have been affected by meteoric diagenesis, the $\delta^{13}C_{carb}$ values progressively increase up section towards the exposure surface (Allan and Matthews, 1982; Railsback et al., 2003; Theiling et al., 2007). The zig-zag appearance of $\delta^{13}C_{carb}$ values, and the general correspondence of negative shifts near exposure surfaces, indicates that episodic diagenetic alteration of sediments on the platform top was commonplace and had a not insignificant affect on the isotopic values preserved in the stratigraphic record.

An additional observation is that if meteoric diagenesis was responsible for the more negative $\delta^{13}C_{carb}$ values of the platform section, it may imply that during the middle Cambrian land may have had a primitive plant cover because most of the carbon in meteoric fluids comes from soil respiration. Although definitive plant fossils did not appear until the late Ordovician or Silurian, negative $\delta^{13}C$ values at karstic surfaces indicate that a primitive plant cover may have existed as early as the Ediacaran (Horodyski and Knauth, 1994; Strother et al., 1996; Knauth and Kennedy, 2009).

Implications for anoxic conditions of the House Range Embayment

Conditions necessary for exceptional fossil preservation include but are not limited to high sedimentation rates (constant or episodic), anoxic or dysoxic conditions, absence of bioturbation or scavenging, low to zero current activity on the seafloor, and geographic

restriction of deposits that provided protection from post-depositional tectonic and metamorphic modification or destruction (Bottjer et al., 2002). These conditions were met in varying degrees throughout deposition in and preservation of the House Range Embayment.

The exceptional preservation of organisms and the abundance of organic-rich shale in the Wheeler Formation of the House Range Embayment have led to the hypothesis that basinal waters in the House Range Embayment were at least periodically anoxic. Whether anoxic conditions in the basin persisted through the entire Wheeler Formation or were episodic and lasting for only short periods of time has been debated and results of bed-by-bed analysis of fossil preservation and degree of bioturbation by Gaines et al. (2005) and Gaines and Droser (2005) indicate that anoxic conditions were periodic and excellent fossil preservation resulted from either the expansion of these anoxic waters over the low-angle ramp where organisms lived under more oxygenated conditions, or when organisms were transported the short distance down-slope to anoxic waters. In addition, their research illustrated that benthic trilobites in the Wheeler (*Elrathia kingii* and associated fauna) lived in the exaerobic zone at the boundary between anoxic and dysoxic bottom waters, and most likely used sulfur bacteria as their food source. No non-mineralized fossils (BST) are associated with these benthic faunas except for algae. BST fossils are restricted to shale beds that include disseminated pyrite and a complete lack of bioturbation. Results from comparison of the Wheeler Formation above the DICE to those of the platform reveal a slight (~1‰) isotopic gradient that could be the result of at least periodic anoxia during deposition of the Wheeler. The results from this study in the Wheeler Formation appear to be consistent with the results of Gaines et al. (2005) and Gaines and Droser (2005).

The lack of a systematic carbon isotope difference between the platform and basin during deposition of the Marjum Formation implies that the House Range Embayment

did not contain anoxic basinal waters during the remainder of time represented by the *Bolaspidella* biozone. In contrast to deposition of the Wheeler Formation, which was primarily by pelagic sedimentation of fine-grained siliciclastic and carbonate mud, sediments that comprise the Marjum Formation were derived primarily from periplatform sedimentation. This type of sedimentation is a mixture of both pelagic sources of fine-grained carbonate and siliciclastic mud, and of fine-grained detrital carbonate transported down-slope from the carbonate platform by turbidity currents. Pelagic sedimentation of siliciclastic mud was diluted by the abundance of carbonate material during highstand shedding of the carbonate platform. Modern rates of periplatform sedimentation are high (2.5 – 15 m per 1000 years) on the Great Bahama Bank and Florida Shelf and have led to rapid progradation into the adjacent basins (Eberli and Ginsburg, 1987; Wilson and Roberts, 1992; Schlager et al., 1994). During deposition of the Marjum Formation, frequent rapid sedimentation events not only transported fauna down-slope, but also rapidly buried them. When present, bioturbation features are dominated by surface tracks and traces. Vertical bioturbation was limited to only a few horizons. This indicates that while oxygen was present, it was not in high enough amounts to support significant infaunal populations. Rapid burial of benthic organisms would have therefore provided the optimal conditions for preservation of both mineralized and non-mineralized (BST) organisms, without the need for local upwelling or expansion of an anoxic water mass. Rapid sedimentation resulted in 'smothering' of organisms living on the seafloor. This 'sediment smothering model' for preservation of BST fossils was common in the Cambrian (Babcock et al., 2001) and has been suggested for deposits such as the Spence Shale in Utah (Liddell et al., 1997).

Chemostratigraphic correlation

Much discussion has surrounded the use of $\delta^{13}C_{carb}$ curves for correlation of poorly dated carbonate successions (Brasier, 1993; Montañez et al., 2000; Glumac and Spivak-

Birndorf, 2002; Peng et al., 2004; Glumac and Mutti, 2007). In Chapter 2 (and Howley and Jiang, 2010), results from a platform-wide region supported correlation of a negative excursion at the base of the Drumian Stage as the DICE, however a combination of moderate to high-resolution biostratigraphy and sequence stratigraphy was required. On a larger scale, in this chapter a test of the applicability of chemostratigraphic correlation was performed using one platform and one basin isotopic section, using the sequence stratigraphic framework documented in Chapter 1, and the correlation of the Drumian Carbon Isotope Excursion (DICE) documented in Chapter 2. The significance of this opportunity is two-fold. First, the platform section at Panaca Hills, Nevada is correlative to similar platform sections in southern Nevada and the Canadian Rockies used by Montañez et al. (2000) to create the composite curve for the middle Cambrian that is currently used for global correlation (Zhu et al., 2004; 2006; Gomez et al., 2007). The new Panaca Hills $\delta^{13}C_{carb}$ curve will now be the highest resolution curve for the middle Cambrian in the western U.S. Second, the $\delta^{13}C_{carb}$ curve for the House Range, Utah House Range Embayment section will now be the highest resolution curve for the Wheeler and Marjum formations and will provide high-resolution correlation to the platform section and also to other global slope and basin curves. Each platform and basin section shows significant temporal variation in $\delta^{13}C_{carb}$, but only two isotopic shifts can be correlated within the available sequence and biostratigraphic data (Fig. 29) and in fact the sequence stratigraphic data is crucial for the correlation. The first isotopic shift is the DICE and is located at the base of the Wheeler Formation – Meadow Valley Member (of the Highland Peak Formation) interval, and the second isotopic shift is present at the base of the Marjum Formation and top of Member 7 (of the Highland Peak Formation) interval. The negative excursion (DICE) that overlies the lowermost sequence boundary is associated with the early part of transgression and corresponds with increased black shale deposition in the basin. The DICE is also recognized globally

within the early part of a transgressive event (Babcock et al., 2004; Zhu et al., 2004, 2006; Babcock et al., 2007; Álvaro et al., 2008; Howley and Jiang, 2010).

The second isotopic shift is a negative excursion at the base of the Marjum Formation and top of Member 7 of the Highland Peak Formation. This shift underlies a major sequence boundary and has a similar magnitude shift (~2‰) in both the platform and basin sections. The correspondence of this negative shift with a sequence boundary calls into question its usefulness as a correlation tool because the possibility for altered values due to meteoric diagenesis on the platform is high. However, if the basin values of this negative shift represent those of the coeval platform (detrital carbonate transported from the carbonate platform to the basin may still record platform values), then correlation may be at least regional in nature. Further documentation of this shift across the House Range Embayment, carbonate platform, and in other non-regional locations would be needed to support the use of this shift as a correlation marker.

The remainder of isotopic shifts and trends in both sections are difficult to correlate within the present resolution of biostratigraphic and sequence stratigraphic data. The fluctuations in $\delta^{13}C_{carb}$ values in Members 8 and 9 of the Highland Peak Formation are likely due to diagenetic alteration during frequent subaerial exposure of the carbonate platform as indicated by the zig-zag nature of negative isotopic shifts and the scatter in $\delta^{18}O$, but higher resolution sampling of platform strata are needed to truly support this hypothesis. A particular point that needs to be mentioned is the negative $\delta^{13}C_{carb}$ shift near the top of the Marjum Formation between 533 and 575 m. This 2.7‰ negative shift is associated with a thick interval of interbedded calcareous shale and lime mudstone/calcisiltite above a thick interval of limestone-dominated rhythmites, but is not obvious in the platform section. It is possible that the low-resolution sampling in the platform has missed the equivalent strata of this $\delta^{13}C$ excursion.

Conclusions

Carbon isotope profiles from shallow- and deep-water sections across the middle Cambrian House Range Embayment do not show systematic $\delta^{13}C$ changes that would be expected if local carbon cycling in a prolonged anoxic basin dominated the isotopic record. Results from the Wheeler Formation interval indicate either a history of periodic basin water anoxia or alternatively the effects of burial diagenesis of organic-rich sediments on the $\delta^{13}C_{carb}$ values of basin carbonate strata. Results from the Marjum Formation interval reveals a pattern opposite of that expected for an anoxic basin. The majority of platform section $\delta^{13}C_{carb}$ values are more negative than coeval strata in the basin. This phenomenon is explained by meteoric diagenesis of platform carbonates in response to frequent exposure and karstification. Exceptional fossil preservation in the Marjum Formation is explained by rapid burial and 'smothering' of organisms living on the seafloor during sedimentation of detrital carbonate that was transported from the adjacent carbonate platform during highstand shedding. In addition to isotopic gradients, a number of $\delta^{13}C_{carb}$ shifts are present in both platform and basinal sections, however only two of them can be correlated with confidence within the sequence stratigraphic framework. Although higher resolution sampling is needed to discuss the pattern of $\delta^{13}C_{carb}$ values between platform and basin during deposition of the Marjum Formation and coeval strata, the isotope data from this study indicate that $\delta^{13}C_{carb}$ values from the middle Cambrian platform sections may have a significant diagenetic overprint that calls attention to using $\delta^{13}C$ chemostratigraphy for blind dating of stratigraphic successions of limited age control.

APPENDIX 1

STRATIGRAPHIC COLUMNS

Stratigraphic Columns - Legend

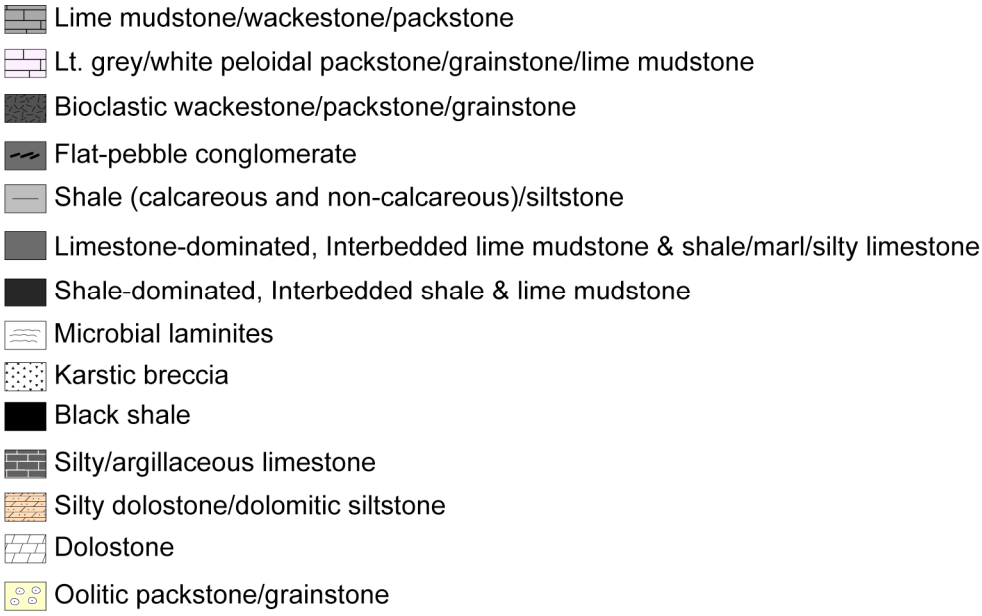

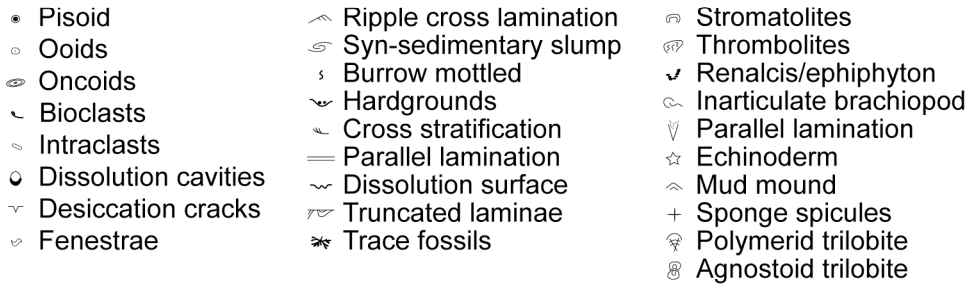

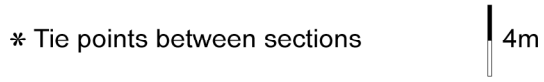

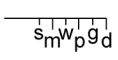

s = shale/siltstone, m = lime mudstone, w = wackestone, p = packstone, g = grainstone, d = dolomite

Note:
Detailed stratigraphic columns for the Panaca Hills section are located in Howley (2002). Other stratigraphy used in the text was from published material.

Desert Range, Nevada

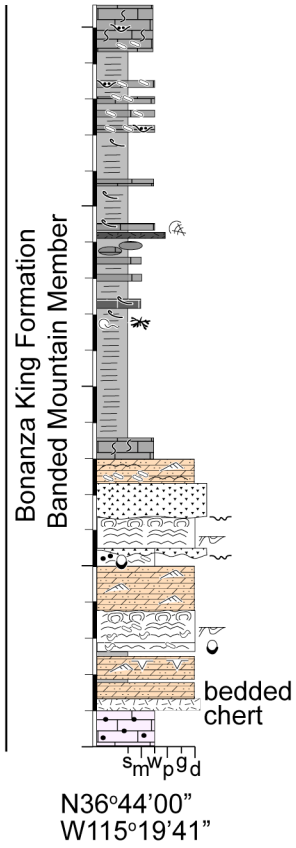

N36°44’00”
W115°19’41”

Wah Wah Mountains - Howell through Eye of Needle

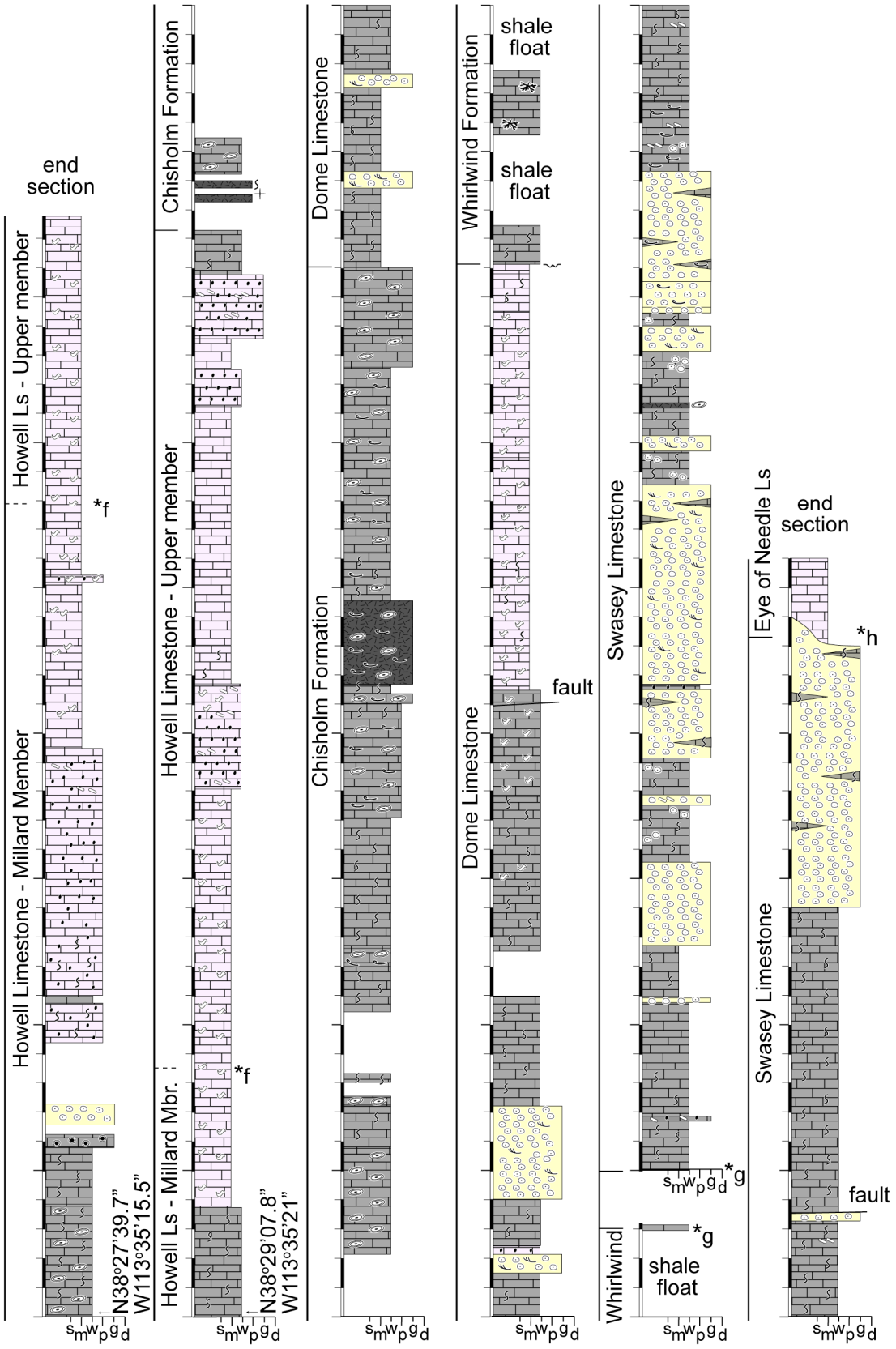

Wah Wah Mountains - Eye of Needle through lower Trippe

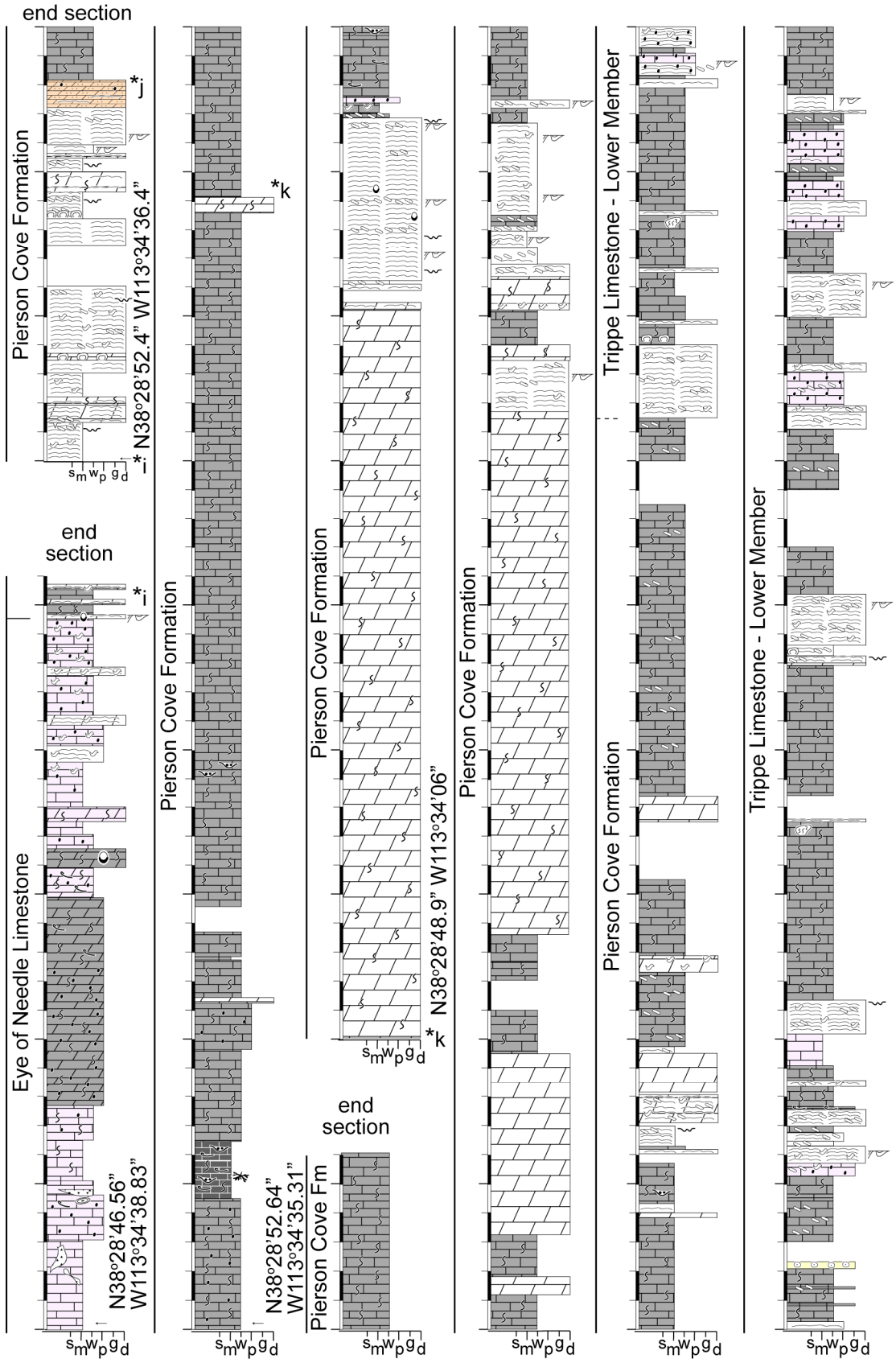

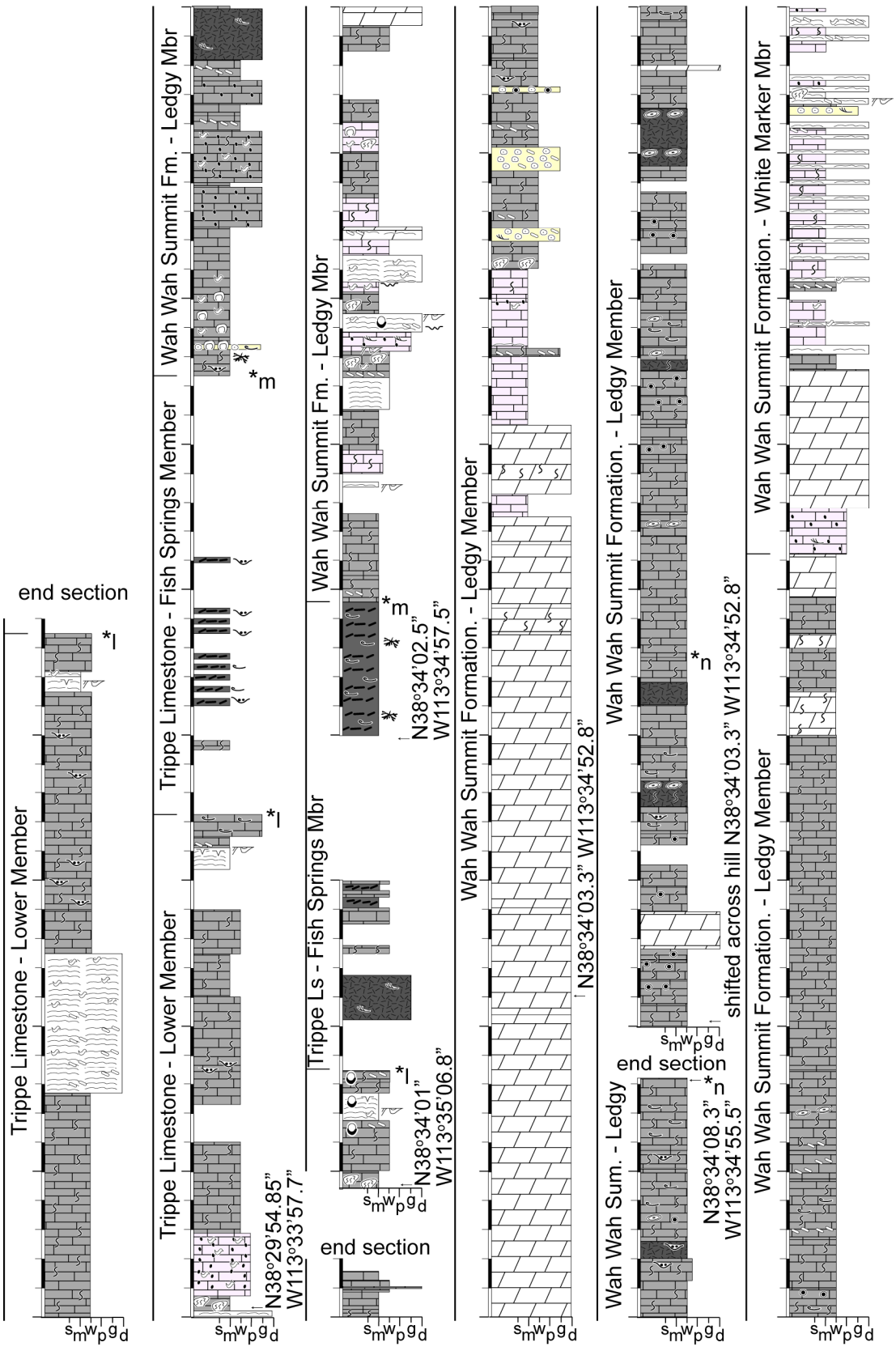
Trippe Limestone - Lower Member
end section
*l
Trippe Limestone - Lower Member
Trippe Limestone - Fish Springs Member
Wah Wah Summit Fm. - Ledgy Mbr
*m
*l
N38°29'54.85"
W113°33'57.7"
Trippe Ls - Fish Springs Mbr
Wah Wah Summit Fm. - Ledgy Mbr
*m
N38°34'02.5"
W113°34'57.5"
*l
N38°34'01"
W113°35'06.8"
end section
Wah Wah Summit Formation. - Ledgy Member
N38°34'03.3" W113°34'52.8"
Wah Wah Sum. - Ledgy
Wah Wah Summit Formation. - Ledgy Member
*n
end section
*n
N38°34'08.3"
W113°34'55.5"
shifted across hill N38°34'03.3" W113°34'52.8"
Wah Wah Summit Formation. - Ledgy Member
Wah Wah Summit Formation. - White Marker Mbr
s m w p g d

end section

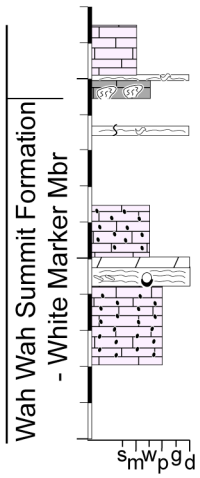

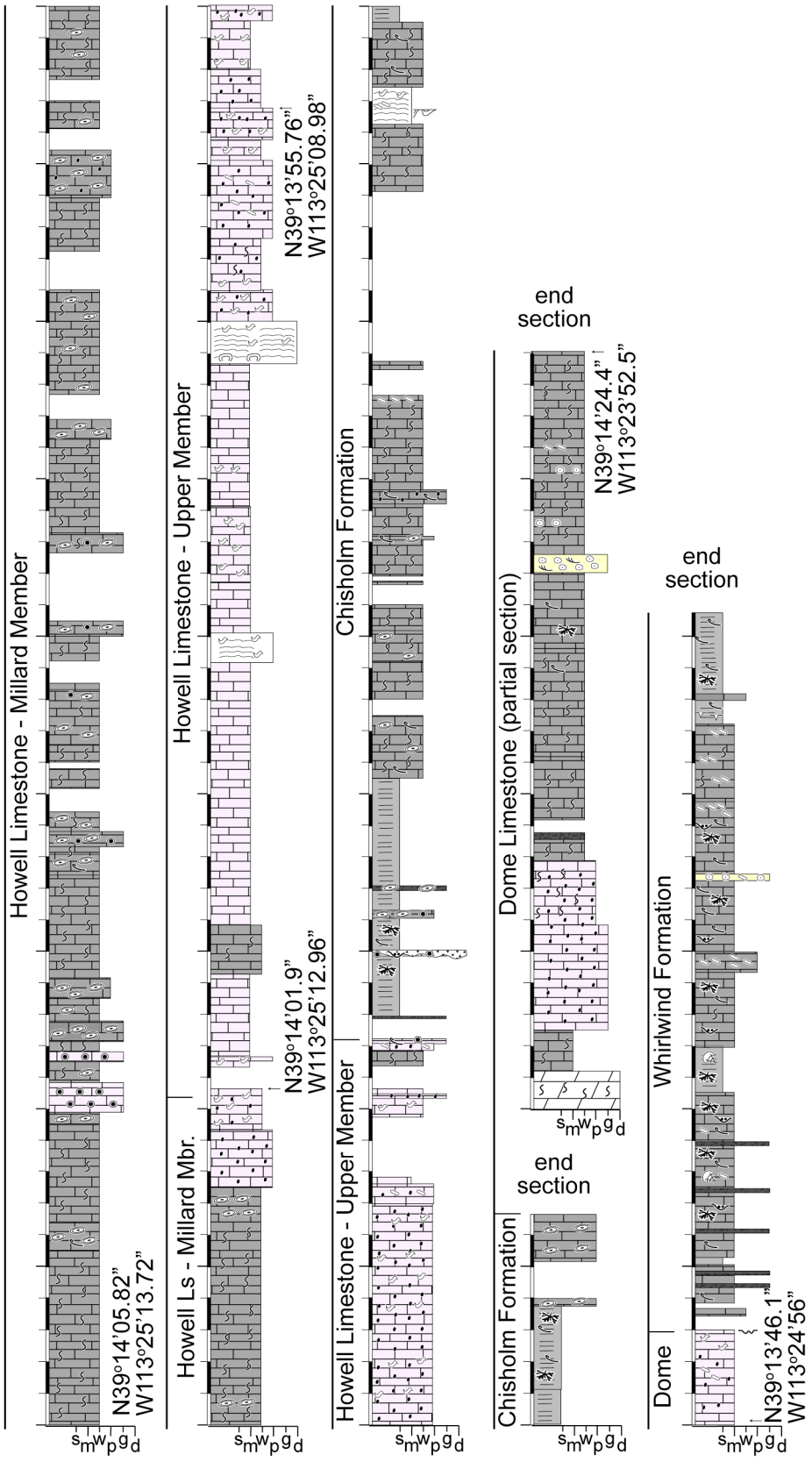
Howell Limestone - Millard Member
N39°14'05.82"
W113°25'13.72"
Howell Ls - Millard Mbr.
Howell Limestone - Upper Member
N39°14'01.9"
W113°25'12.96"
N39°13'55.76"
W113°25'08.98"
Chisholm Formation
Howell Limestone - Upper Member
Dome Limestone (partial section)
end section
N39°14'24.4"
W113°23'52.5"
Chisholm Formation
end section
Dome
Whirlwind Formation
end section
N39°13'46.1"
W113°24'56"
s m w p g d

House Range - Swasey through lower Marjum

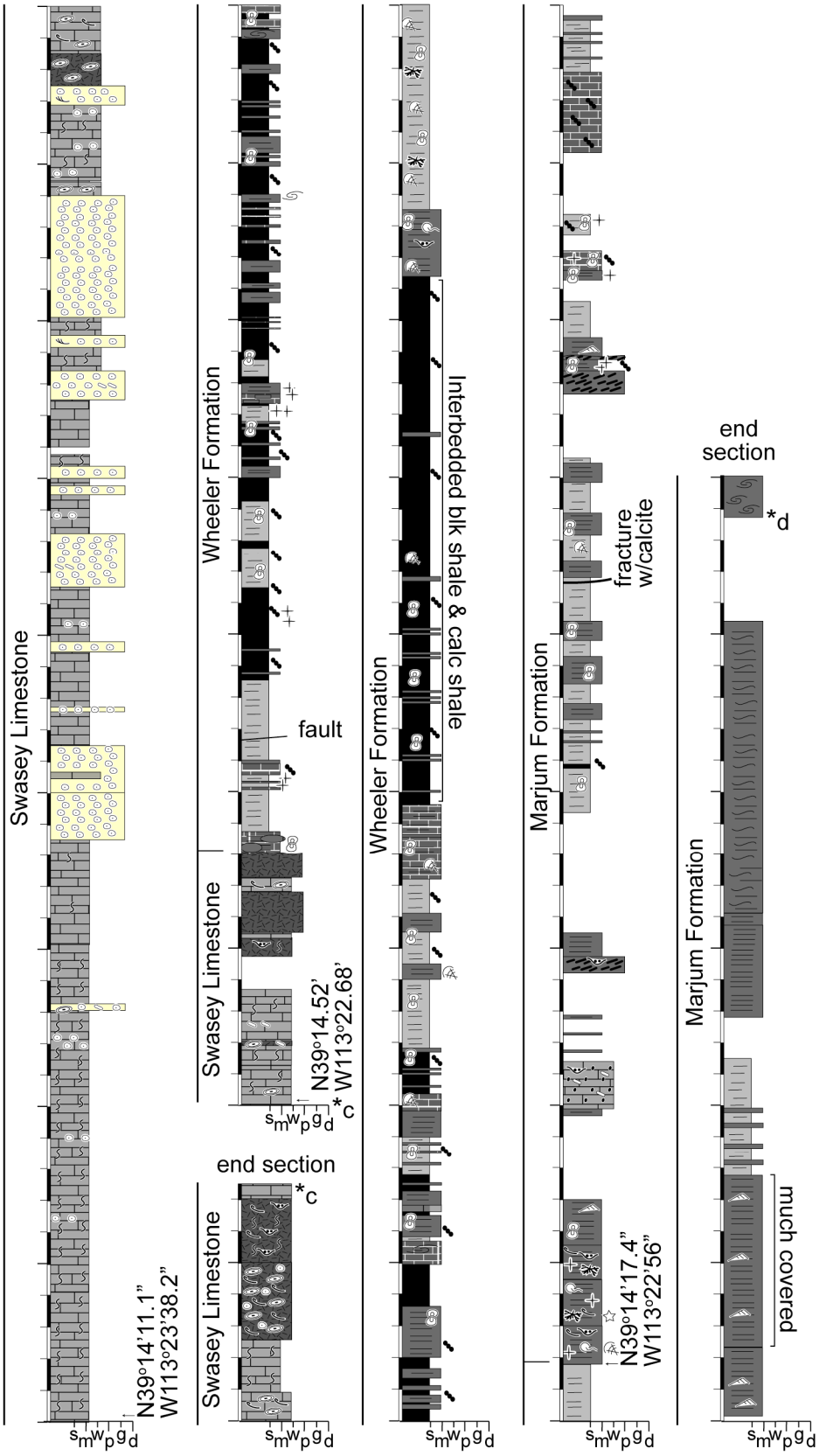

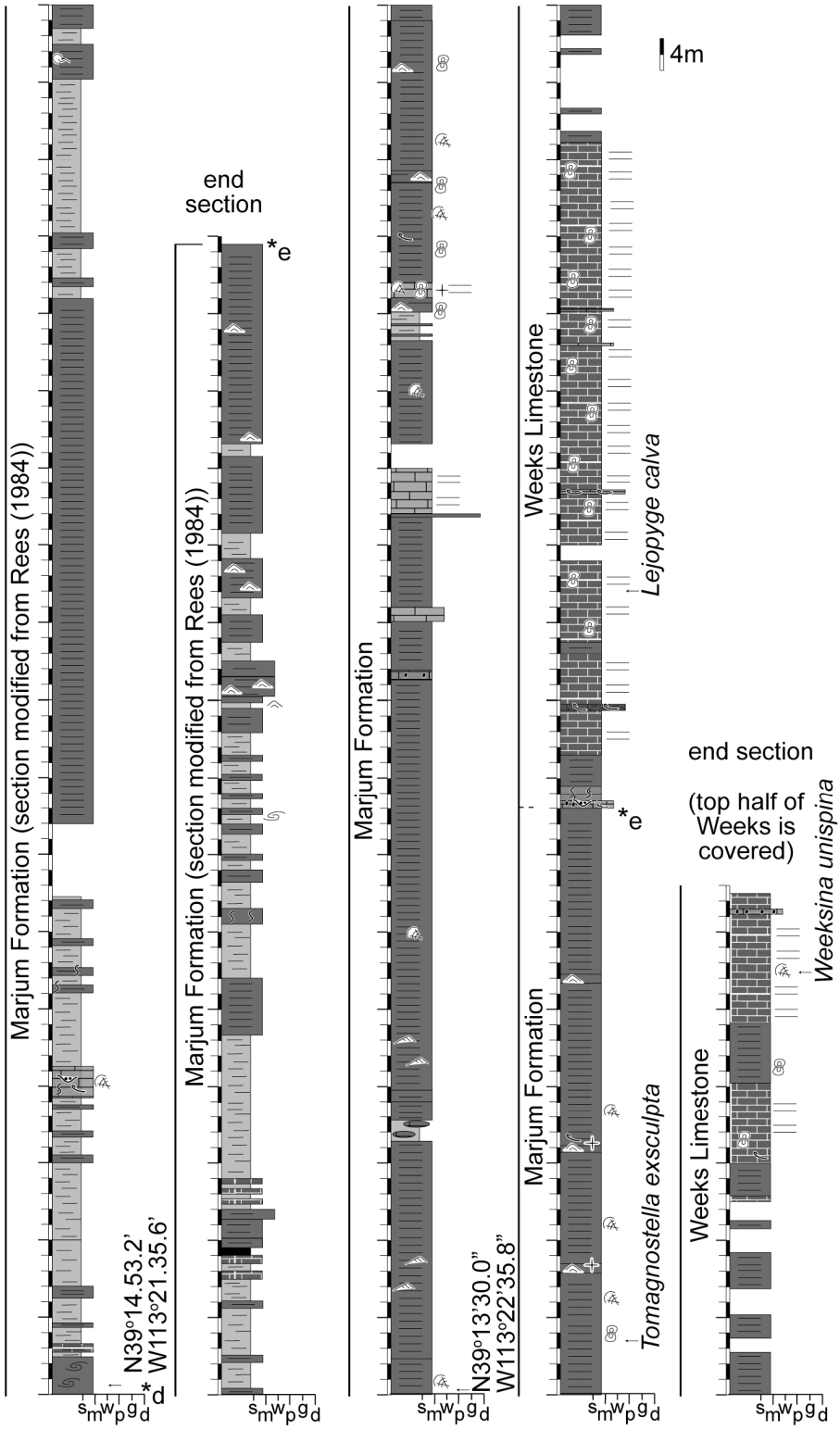
Marjum Formation (section modified from Rees (1984))
N39°14.53.2'
W113°21.35.6'
*d
Marjum Formation (section modified from Rees (1984))
end section
*e
Marjum Formation
N39°13'30.0"
W113°22'35.8"
Weeks Limestone
Marjum Formation
Tomagnostella exsculpta
Lejopyge calva
*e
4m
end section
(top half of Weeks is covered)
Weeks Limestone
Weeksina unispina
s m w p g d

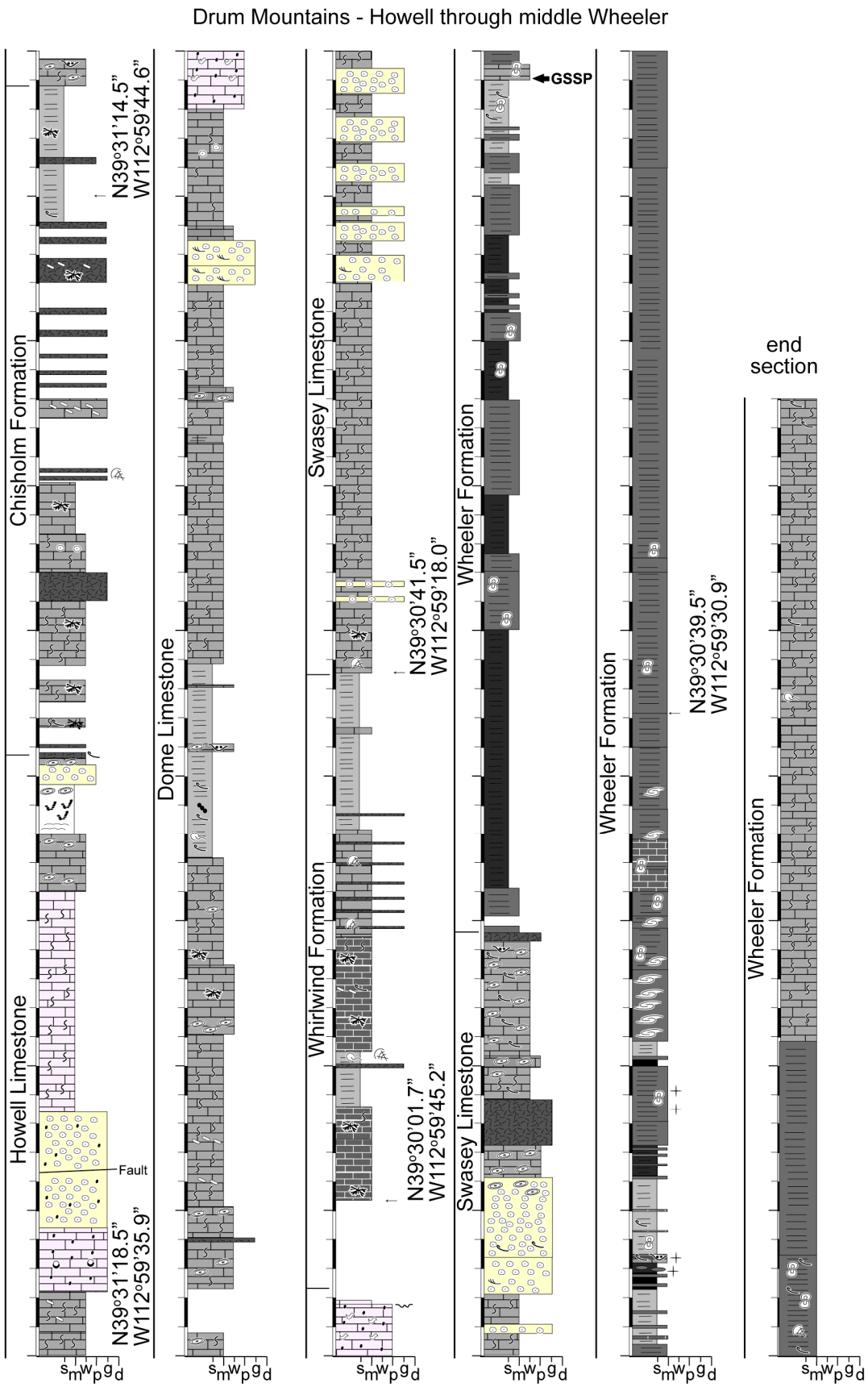
Drum Mountains - Howell through middle Wheeler
Howell Limestone
Chisholm Formation
Dome Limestone
Whirlwind Formation
Swasey Limestone
Swasey Limestone
Wheeler Formation
Wheeler Formation
Wheeler Formation
end section
GSSP
Fault
N39°31'18.5"
W112°59'35.9"
N39°31'14.5"
W112°59'44.6"
N39°30'01.7"
W112°59'45.2"
N39°30'41.5"
W112°59'18.0"
N39°30'39.5"
W112°59'30.9"
s m w p g d

Drum Mountains - middle Wheeler through lower Trippe

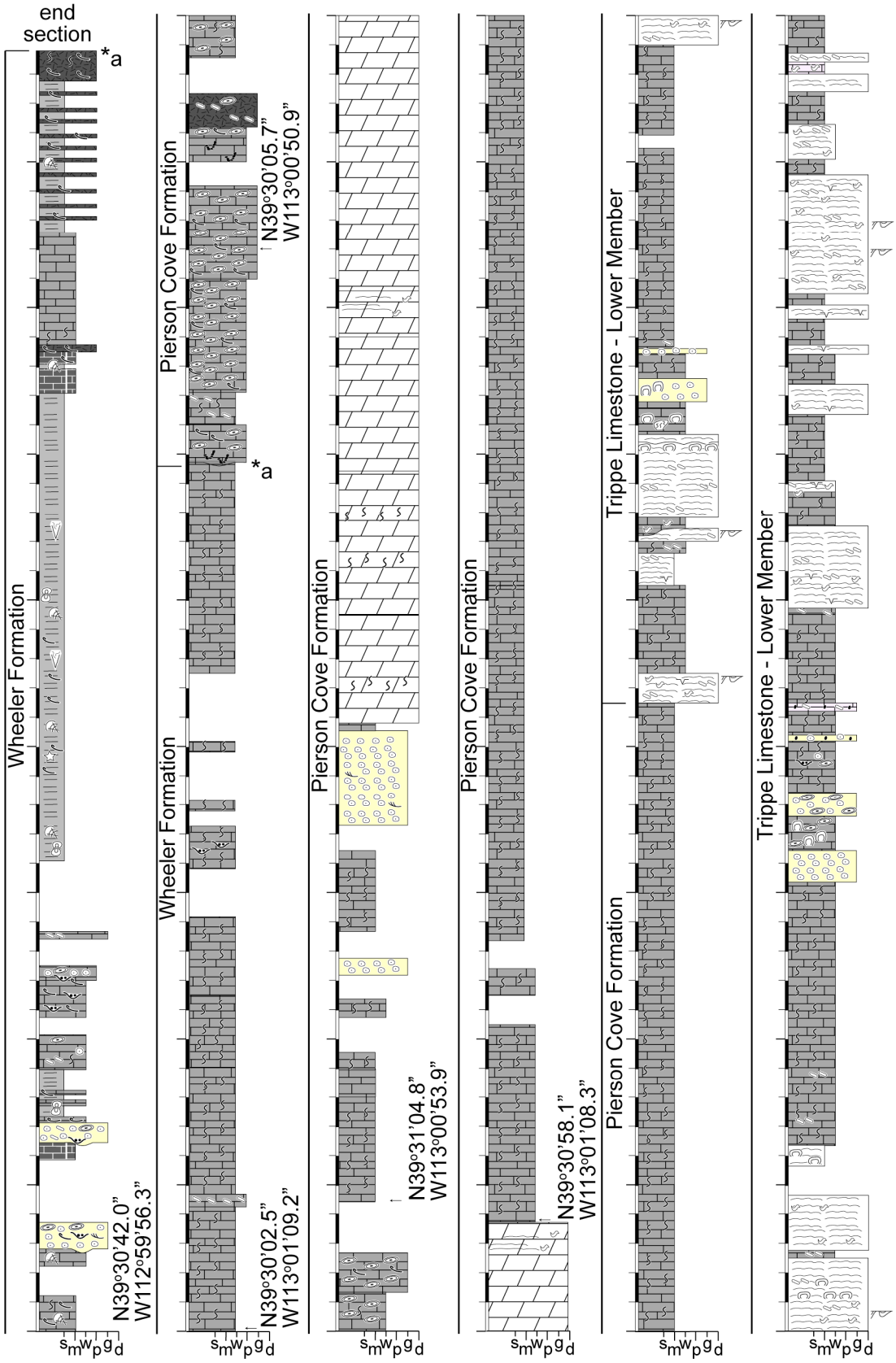

Drum Mountains - Trippe through Lamb

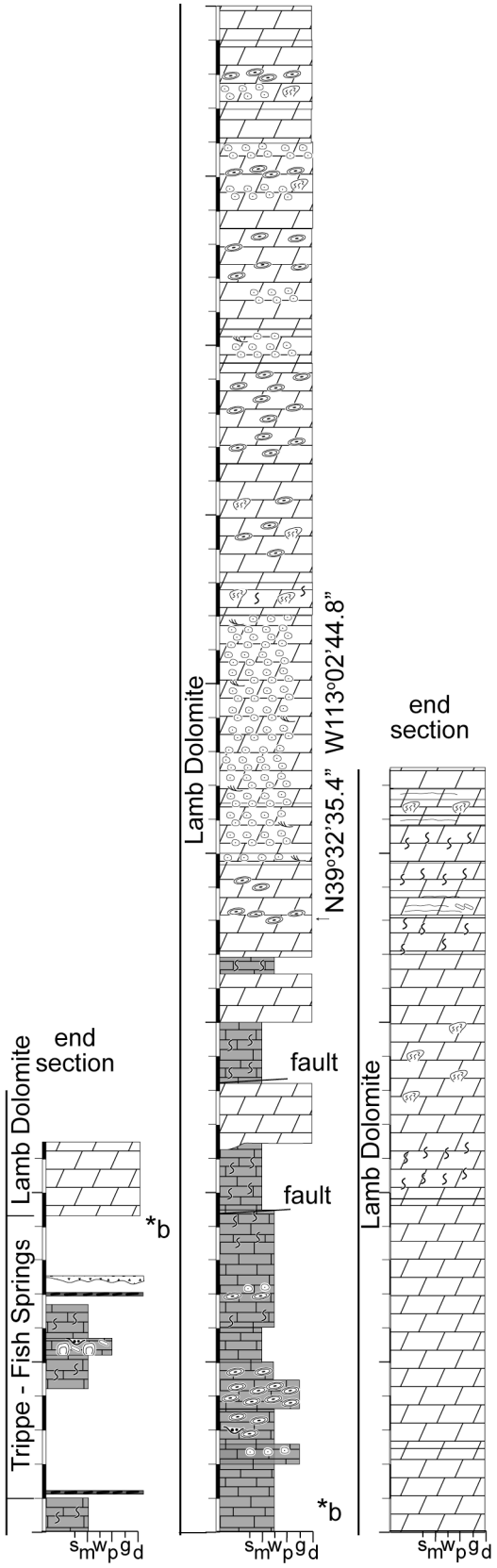

APPENDIX 2

ISOTOPE DATA

Desert Range, Nevada

Formation	Sample	Strat. Height	Lithology	$\delta^{13}C$	$\delta^{18}O$
Bonanza King Fm.	07-1000	0	lime mudstone	-3.0	-6.6
Bonanza King Fm.	07-1001	0.2	lime mudstone	-2.6	-9.8
Bonanza King Fm.	07-1002x	2	lime mudstone	-0.5	-7.7
Bonanza King Fm.	07-1002	2.1	lime mudstone	-0.3	-7.9
Bonanza King Fm.	07-1004	2.55	dolomudstone	-1.0	-7.9
Bonanza King Fm.	07-1005	4.1	silty dolostone	-0.5	-7.0
Bonanza King Fm.	07-1006	5.1	silty dolostone	-0.4	-6.2
Bonanza King Fm.	07-1007	5.36	microbial lamina	-0.9	-6.5
Bonanza King Fm.	07-1008	5.61	microbial lamina	-0.7	-7.0
Bonanza King Fm.	07-1009x	7.3	microbial lamina	-0.5	-5.9
Bonanza King Fm.	07-1009	7.4	microbial lamina	-0.4	-6.5
Bonanza King Fm.	07-1010x	10.1	dolomudstone	-0.5	-6.0
Bonanza King Fm.	07-1011	10.25	dolomudstone	-0.3	-5.9
Bonanza King Fm.	07-1013B	10.6	wackestone	-1.9	-14.9
Bonanza King Fm.	07-1013A	10.6	silty wackestone	-2.5	-12.4
Bonanza King Fm.	07-1012x-2	10.62	microbial lamina	-1.0	-7.6
Bonanza King Fm.	07-1012	10.65	microbial lamina	-0.8	-7.2
Bonanza King Fm.	07-1012x-1	10.67	microbial lamina	-0.8	-6.0
Bonanza King Fm.	07-1014	10.87	microbial lamina	-0.5	-8.5
Bonanza King Fm.	07-1015	12.1	microbial lamina	-0.4	-6.8
Bonanza King Fm.	07-1016A	12.7	wackestone	-1.4	-11.0
Bonanza King Fm.	07-1016x-1	12.7	wackestone	-2.1	-12.3
Bonanza King Fm.	07-1016x-2	12.7	wackestone	-1.2	-8.2
Bonanza King Fm.	07-1016C	12.7	sparry calcite cement	2.8	-9.7
Bonanza King Fm.	07-1016B	12.7	microbial lamina	-0.6	-6.8
Bonanza King Fm.	07-1016x-3	12.7	intraclast	-0.8	-7.3
Bonanza King Fm.	07-1017x-1	13.15	wackestone	-1.2	-8.4
Bonanza King Fm.	07-1017x-4	13.15	sparry calcite cement	-1.0	-5.9
Bonanza King Fm.	07-1017B	13.15	sparry calcite cement	-3.9	-14.3
Bonanza King Fm.	07-1017x-5	13.15	sparry calcite cement	-4.7	-14.1
Bonanza King Fm.	07-1017A	13.15	microbial lamina	-0.8	-8.2
Bonanza King Fm.	07-1017x-3	13.15	lime mudstone	-0.3	-7.1
Bonanza King Fm.	07-1017x-2	13.15	intraclast	-0.4	-6.5
Bonanza King Fm.	07-1018x	14.75	silty limestone	-2.4	-10.8
Bonanza King Fm.	07-1018	14.8	silty limestone	-2.8	-13.4
Bonanza King Fm.	07-1019x	15.2	dolomudstone	-1.7	-7.7
Bonanza King Fm.	07-1019	15.3	dolomudstone	-1.3	-7.0
Bonanza King Fm.	07-1020	15.8	silty limestone	-3.5	-7.7
Bonanza King Fm.	07-1020x	15.9	silty limestone	-3.5	-7.8
Bonanza King Fm.	07-1021x	16.15	wackestone	-1.9	-11.9
Bonanza King Fm.	07-1021	16.2	wackestone	-2.2	-12.8
Bonanza King Fm.	07-1024x	24.69	argillaceous limestone	0.5	-11.7
Bonanza King Fm.	07-1024	24.7	argillaceous limestone	0.4	-12.1
Bonanza King Fm.	07-1025	27.1	wackestone	0.0	-12.8
Bonanza King Fm.	07-1026	28.7	wackestone	-2.2	-12.6

Formation	Sample	Strat. Height	Lithology	$\delta^{13}C$	$\delta^{18}O$
Bonanza King Fm.	07-1027	29.1	wackestone	0.3	-12.3
Bonanza King Fm.	07-1028x	31.58	wackestone	0.7	-11.9
Bonanza King Fm.	07-1028	31.6	wackestone	0.7	-12.9
Bonanza King Fm.	07-1029x	34.33	wackestone	-1.8	-12.4
Bonanza King Fm.	07-1029	34.35	wackestone	-1.4	-11.3
Bonanza King Fm.	07-1030	38.6	wackestone	-0.7	-10.9
Bonanza King Fm.	07-1030x-1	38.66	wackestone	-0.3	-12.1
Bonanza King Fm.	07-1030x-2	38.68	silty lime mudstone	-0.1	-11.2

Formation	Sample	Strat. Height	Lithology	$\delta^{13}C$	$\delta^{18}O$
HPF (Step Ridge Mbr.)	HSR00-1	1	packstone	-0.8	-12.9
HPF (Step Ridge Mbr.)	HSR00-4	3	packstone	-1.2	-12.9
HPF (Step Ridge Mbr.)	HSR00-5	5	microbial laminite	-0.6	-12.1
HPF (Step Ridge Mbr.)	HSR00-6	31.5	packstone	-0.5	-11.3
HPF (Step Ridge Mbr.)	HSR00-24A	43.5	microbial mud	-0.2	-12.7
HPF (Step Ridge Mbr.)	HSR00-24B	43.5	cement	0.1	-13.3
HPF (Step Ridge Mbr.)	HSR00-10	51	microbial mud	-0.3	-11.8
HPF (Step Ridge Mbr.)	HSR00-9	61.5	microbial mud	-0.3	-12.7
HPF (Step Ridge Mbr.)	HSR00-11	76.5	microbial mud	-0.6	-12.0
HPF (Step Ridge Mbr.)	HSR00-13	83	packstone	-0.5	-11.4
HPF (Step Ridge Mbr.)	HSR00-14	86.5	packstone	-0.5	-11.0
HPF (Step Ridge Mbr.)	HSR00-16	93	microbial mud	-0.6	-11.8
HPF (Step Ridge Mbr.)	HSR00-20	99	grainstone	-0.8	-11.9
HPF (Step Ridge Mbr.)	HSR00-21A	102	pink mudstone	-4.4	-12.6
HPF (Step Ridge Mbr.)	HSR00-21B	102	microbial mud	-1.3	-11.7
HPF (Step Ridge Mbr.)	HSR00-1A	123.5	grainstone	-1.2	-11.7
HPF (Step Ridge Mbr.)	HSR00-4A	141	wackestone	-1.1	-9.8
HPF (Step Ridge Mbr.)	HSR00-26	151	wackestone	-1.4	-9.9
HPF (Step Ridge Mbr.)	HSR00-5A	154	wackestone	-1.3	-10.1
HPF (Step Ridge Mbr.)	HSR00-27	165	wackestone	-1.1	-10.1
HPF (Step Ridge Mbr.)	HSR00-28	169	grainstone	-1.3	-11.4
HPF (Step Ridge Mbr.)	07-1050-1	173	grainstone	-1.2	-11.9
HPF (Step Ridge Mbr.)	07-1050-2	175	grainstone	-1.4	-10.9
HPF (Step Ridge Mbr.)	HSR00-7A1	177	grainstone	-1.0	-10.2
HPF (Step Ridge Mbr.)	07-1050-3	177	grainstone	-1.0	-11.3
HPF (Step Ridge Mbr.)	07-1050-4	177.6	grainstone	-1.2	-11.3
HPF (Step Ridge Mbr.)	HSR00-31	178	wackestone	-1.2	-11.6
HPF (Step Ridge Mbr.)	07-1050-5	178.1	wackestone	-1.4	-11.0
HPF (Step Ridge Mbr.)	07-1050-6	179.2	wackestone	-1.5	-11.8
HPF (Step Ridge Mbr.)	07-1051-2	181.5	wackestone	-0.9	-10.9
HPF (Step Ridge Mbr.)	07-1051-3	183	grainstone	-0.9	-11.3
HPF (Step Ridge Mbr.)	HSR00-30	185	grainstone	-0.9	-11.3
HPF (Step Ridge Mbr.)	07-1051-4	186	grainstone	-1.4	-13.9
HPF (Step Ridge Mbr.)	07-1051-5	187.4	wackestone	-1.0	-11.8
HPF (Step Ridge Mbr.)	07-1051-6	189.3	wackestone	-1.3	-11.9
HPF (Step Ridge Mbr.)	07-1051-7	190.5	wackestone	-0.9	-11.7
HPF (Step Ridge Mbr.)	07-1051-8	191.3	wackestone	-0.9	-11.7
HPF (Step Ridge Mbr.)	07-1051-9	194	packstone	-1.0	-12.2
HPF (Step Ridge Mbr.)	07-1051-10	194.6	grainstone	-0.8	-12.4
HPF (Step Ridge Mbr.)	HSR00-33	195	dolowackestone	-0.3	-10.3
HPF (Step Ridge Mbr.)	07-1052-1	195.4	dolowackestone	-1.1	-12.0
HPF (Step Ridge Mbr.)	07-1052-2	196	dolowackestone	-0.4	-11.2
HPF (Step Ridge Mbr.)	07-1052-3	197.1	packstone	-1.0	-11.8
HPF (Step Ridge Mbr.)	HSR00-34	198	packstone	-0.8	-11.3
HPF (Step Ridge Mbr.)	07-1052-4	198.7	dolograinstone	-0.2	-9.7

Formation	Sample	Strat. Height	Lithology	$\delta^{13}C$	$\delta^{18}O$
HPF (Step Ridge Mbr.)	07-1052-5	199	dolograinstone	-0.6	-11.0
HPF (Step Ridge Mbr.)	HSR00-35	199.5	microbial laminite	-0.4	-12.5
HPF (Step Ridge Mbr.)	07-1052-6	199.8	microbial laminite	-1.0	-12.0
HPF (Step Ridge Mbr.)	07-1052-7	200	microbial laminite	-0.6	-12.7
HPF (Step Ridge Mbr.)	07-1052-8	200.9	microbial laminite	-0.2	-11.0
HPF (Step Ridge Mbr.)	HSR00-36B	201	microbial laminite	-0.8	-11.0
HPF (Step Ridge Mbr.)	07-1052-9	201.7	microbial laminite	-0.6	-10.8
HPF (Step Ridge Mbr.)	07-1052-10	202.1	microbial laminite	-0.5	-10.9
HPF (Step Ridge Mbr.)	07-1053-1	202.6	packstone	-0.8	-11.5
HPF (Step Ridge Mbr.)	07-1053-2	203.2	packstone	-0.3	-10.6
HPF (Step Ridge Mbr.)	07-1053-3	204	microbial laminite	-0.1	-9.9
HPF (Step Ridge Mbr.)	07-1053-4	204.5	lime mudstone	-1.0	-11.6
HPF (Step Ridge Mbr.)	07-1053-5	205	microbial laminite	-0.4	-11.0
HPF (Step Ridge Mbr.)	HSR00-41	205	microbial laminite	-0.5	-11.2
HPF (Step Ridge Mbr.)	HSR00-43	205.5	lime mudstone	-0.5	-12.2
HPF (Step Ridge Mbr.)	07-1053-6	205.8	lime mudstone	-0.5	-12.8
HPF (Step Ridge Mbr.)	07-1053-7	205.82	lime mudstone	-0.2	-13.1
HPF (Step Ridge Mbr.)	07-1053-8	205.88	lime mudstone	-0.7	-12.4
HPF (Step Ridge Mbr.)	07-1053-11	205.89	microbial laminite	-0.1	-8.9
HPF (Step Ridge Mbr.)	07-1053-12	205.89	microbial laminite	-0.1	-10.3
HPF (Step Ridge Mbr.)	07-1053-9	205.95	microbial laminite	-0.6	-10.0
HPF (Step Ridge Mbr.)	07-1053-10	205.96	microbial laminite	-0.2	-9.8
HPF (Step Ridge Mbr.)	07-1053-13	206	microbial laminite	-0.8	-11.7
HPF (Step Ridge Mbr.)	07-1053-14	206.24	microbial laminite	-0.3	-12.8
HPF (Step Ridge Mbr.)	07-1053-15	206.45	lime mudstone	-0.6	-9.8
HPF (Step Ridge Mbr.)	HSR00-44	206.5	lime mudstone	-0.1	-12.9
HPF (Step Ridge Mbr.)	07-1053-16	206.7	lime mudstone	-0.6	-12.9
HPF (Step Ridge Mbr.)	07-1053-17	206.7	lime mudstone	0.1	-14.1
HPF (Condor Mbr.)	HC00-46	209.85	packstone	-1.0	-12.0
HPF (Condor Mbr.)	07-1054-1	209.9	dolomudstone	-0.5	-9.1
HPF (Condor Mbr.)	07-1054-2	210.75	dolomudstone	-0.5	-10.0
HPF (Condor Mbr.)	07-1054-3	211	silty dolostone	0.0	-8.4
HPF (Condor Mbr.)	07-1054-4	212	silty dolostone	0.0	-7.2
HPF (Condor Mbr.)	07-1054-5	212.7	silty dolostone	-0.1	-7.0
HPF (Condor Mbr.)	HC00-50	214	silty dolostone	0.0	-6.9
HPF (Condor Mbr.)	07-1054-6	214.1	silty dolostone	0.0	-7.1
HPF (Condor Mbr.)	07-1054-7B	214.5	sparry dolomite cement	-2.5	-13.4
HPF (Condor Mbr.)	07-1054-7A	214.5	silty dolostone	0.6	-6.2
HPF (Condor Mbr.)	07-1054-8	215	silty dolostone	-0.1	-7.6
HPF (Condor Mbr.)	07-1054-9	216.5	dolomitic siltstone	0.5	-7.6
HPF (Condor Mbr.)	07-1054-10	217.1	dolomitic siltstone	-0.2	-9.3
HPF (Condor Mbr.)	HC00-56	219	silty dolostone	-0.1	-7.7
HPF (Condor Mbr.)	07-1054-11	220.5	dolomitic siltstone	-0.1	-7.7
HPF (Condor Mbr.)	07-1054-12	221	dolomitic siltstone	-0.1	-7.2
HPF (Condor Mbr.)	HC00-53	222	silty dolostone	0.1	-6.9
HPF (Condor Mbr.)	07-1054-13	222	dolomitic siltstone	-0.1	-7.1

Formation	Sample	Strat. Height	Lithology	$\delta^{13}C$	$\delta^{18}O$
HPF (Condor Mbr.)	07-1054-14	223.5	dolomitic siltstone	0.0	-9.2
HPF (Condor Mbr.)	HC00-62	224	silty dolostone	0.2	-7.6
HPF (Condor Mbr.)	07-1054-15	224.6	dolomitic siltstone	-0.2	-7.6
HPF (Condor Mbr.)	06-c3	224.99	dolomudstone	-0.3	-8.1
HPF (Meadow Valley)	07-1055-1	225.3	intraclasts	-0.3	-10.4
HPF (Meadow Valley)	07-1055-2	225.4	microbial laminite	-0.7	-11.5
HPF (Meadow Valley)	HMV00-64	225.5	intraclasts	-0.1	-10.1
HPF (Meadow Valley)	07-1055-3	225.5	intraclasts	-0.7	-11.5
HPF (Meadow Valley)	07-1055-4	226.1	dolowackestone	0.3	-8.2
HPF (Meadow Valley)	07-1055-5	226.5	dolomudstone	0.6	-10.5
HPF (Meadow Valley)	07-1055-6	227	intraclasts	-0.9	-11.2
HPF (Meadow Valley)	MV-1	227	grainstone	-0.8	-10.8
HPF (Meadow Valley)	07-1055-7	227	dolomudstone	-0.2	-10.0
HPF (Meadow Valley)	07-1055-8	228	microbial laminite	-0.5	-11.6
HPF (Meadow Valley)	07-1055-9	228.6	microbial laminite	-0.3	-10.3
HPF (Meadow Valley)	07-1055-10	228.9	microbial laminite	-0.2	-6.7
HPF (Meadow Valley)	HMV00-66	229.5	microbial laminite	-1.0	-9.0
HPF (Meadow Valley)	07-1055-11	229.6	microbial laminite	-1.4	-7.7
HPF (Meadow Valley)	07-1055-12A	229.9	grainstone	-3.0	-10.5
HPF (Meadow Valley)	HMV00-67	231.5	wackestone	-1.3	-8.6
HPF (Meadow Valley)	07-1055-13	231.7	wackestone	-1.8	-8.3
HPF (Meadow Valley)	07-1055-14	232.3	packstone	-1.8	-11.6
HPF (Meadow Valley)	07-1055-15	232.6	packstone	-2.7	-11.4
HPF (Meadow Valley)	07-1055-16	234	packstone	-2.2	-11.9
HPF (Meadow Valley)	07-1055-17	234.4	packstone	-2.7	-10.4
HPF (Meadow Valley)	07-1055-18	235	packstone	-1.5	-11.4
HPF (Meadow Valley)	07-1055-19	236.7	dolomudstone	-1.5	-13.1
HPF (Meadow Valley)	07-1055-20	237	dolomudstone	-0.8	-11.5
HPF (Meadow Valley)	HMV00-69	237	dolograinstone	-1.6	-12.1
HPF (Meadow Valley)	HMV00-71	237.7	dolomitic siltstone	-1.1	-14.0
HPF (Meadow Valley)	07-1055-21	238.2	dolomitic siltstone	-1.0	-12.3
HPF (Meadow Valley)	07-1055-22	238.6	wackestone	-0.5	-9.7
HPF (Meadow Valley)	07-1055-23C	241	sparry calcite cement	-0.6	-13.2
HPF (Meadow Valley)	07-1055-23A	241	lime mudstone	-0.3	-11.7
HPF (Meadow Valley)	07-1055-24	242	wackestone	-0.1	-10.6
HPF (Meadow Valley)	07-1055-25	243.4	wackestone	-0.2	-11.3
HPF (Meadow Valley)	HMV00-73	244.5	wackestone	0.1	-10.0
HPF (Meadow Valley)	07-1055-26	246	wackestone	-0.1	-11.1
HPF (Meadow Valley)	07-1055-27	247.5	wackestone	-0.3	-10.5
HPF (Meadow Valley)	07-1055-28	249.1	wackestone	-0.2	-11.0
HPF (Meadow Valley)	07-1055-29	252	wackestone	0.1	-10.6
HPF (Meadow Valley)	07-1055-30	253.5	wackestone	-0.3	-12.1
HPF (Meadow Valley)	07-1055-31	255	wackestone	0.3	-11.4
HPF (Meadow Valley)	07-1055-32	258	wackestone	0.0	-10.6
HPF (Meadow Valley)	07-1055-33	259.3	wackestone	-0.2	-13.0
HPF (Meadow Valley)	07-1055-34	261.6	wackestone	0.5	-11.2

Formation	Sample	Strat. Height	Lithology	$\delta^{13}C$	$\delta^{18}O$
HPF (Meadow Valley)	07-1055-35	262.5	wackestone	0.4	-10.6
HPF (Meadow Valley)	00-74	264	wackestone	-0.2	-10.6
HPF (Meadow Valley)	00-75	283	wackestone	-0.2	-13.5
HPF (Meadow Valley)	00-76	289	silty wackestone	-1.4	-11.4
HPF (Meadow Valley)	00-77	290	silty wackestone	-1.2	-10.0
HPF (Meadow Valley)	00-78	291.2	silty wackestone	-0.7	-13.5
HPF (Meadow Valley)	HMV00-81	293	wackestone	-0.5	-8.9
HPF (Meadow Valley)	HMV00-83	302	wackestone	-0.1	-10.0
HPF (Meadow Valley)	HMV00-85	329.5	wackestone	-1.0	-9.9
HPF (Meadow Valley)	00-84	337	wackestone	-1.1	-12.1
HPF (Meadow Valley)	HMV00-91	355	wackestone	-1.0	-12.2
HPF (Mbr. 7)	H700-94A	358	microbial laminite	-1.0	-6.6
HPF (Mbr. 7)	RH05-M7-1	360.5	wackestone	-1.9	-9.1
HPF (Mbr. 7)	H700-97	369.5	grainstone	-0.9	-10.4
HPF (Mbr. 7)	H700-98	380.5	microbial laminite	-0.2	-9.3
HPF (Mbr. 7)	H700-99	388	microbial laminite	-0.6	-9.2
HPF (Mbr. 7)	H700-100	388	wackestone	-0.5	-8.5
HPF (Mbr. 7)	H700-101	389.5	wackestone	-0.6	-9.1
HPF (Mbr. 7)	H700-102	401	wackestone	-0.4	-9.2
HPF (Mbr. 7)	00-103	404	lime mudstone	-1.5	-11.0
HPF (Mbr. 7)	H700-104A	409	wackestone	-1.7	-11.8
HPF (Mbr. 7)	00-105	418	microbial laminite	-0.9	-9.4
HPF (Mbr. 8)	H800-106	443	wackestone	-2.2	-9.9
HPF (Mbr. 8)	H800-107	443.5	wackestone	-1.8	-9.0
HPF (Mbr. 8)	H800-108	449.5	wackestone	-1.2	-11.0
HPF (Mbr. 8)	H800-110	457	dolomitic packstone	-1.6	-10.8
HPF (Mbr. 8)	H800-111	460.5	lime mudstone	-1.5	-10.7
HPF (Mbr. 8)	H800-113	479.5	grainstone	-1.0	-9.8
HPF (Mbr. 8)	H800-114	488.6	dolomitic wackestone	-0.4	-8.4
HPF (Mbr. 8)	H800-115	491.5	dolomitic grainstone	-0.5	-9.2
HPF (Mbr. 8)	H800-116	496.6	wackestone	-1.0	-12.2
HPF (Mbr. 8)	H800-117	498	microbial laminite	-0.6	-9.5
HPF (Mbr. 8)	H800-119	506.8	wackestone	-1.3	-11.0
HPF (Mbr. 8)	H800-121	521.3	wackestone	-0.6	-10.7
HPF (Mbr. 8)	M8-1	533	lime mudstone	-0.8	-11.3
HPF (Mbr. 8)	H900-1A	535	lime mudstone	0.3	-11.0
HPF (Mbr. 8)	H800-125	537	lime mudstone	0.2	-10.4
HPF (Mbr. 8)	H800-126	543.5	packstone	-0.6	-12.2
HPF (Mbr. 9)	H900-127	544	microbial laminite	3.0	-12.8
HPF (Mbr. 9)	H900-129	550	microbial laminite	0.3	-9.4
HPF (Mbr. 9)	H900-8A2	549	silty dolomudstone	0.7	-9.9
HPF (Mbr. 9)	H900-130	550.6	microbial laminite	-0.2	-13.3
HPF (Mbr. 9)	H900-133	559.4	wackestone	0.0	-10.8
HPF (Mbr. 9)	H900-136	583	stromatolite	0.3	-10.0
HPF (Mbr. 9)	H900-137	600.6	packstone	-0.5	-10.5
HPF (Mbr. 9)	00-139	609	wackestone	-1.0	-10.6

Formation	Sample	Strat. Height	Lithology	$\delta^{13}C$	$\delta^{18}O$
HPF (Mbr. 9)	00-140	609.8	wackestone	-0.7	-11.5
HPF (Mbr. 9)	H900-141	617	dolomite	-0.6	-8.2
HPF (Mbr. 9)	00-142	619.5	dolomudstone	-0.9	-8.0
HPF (Mbr. 9)	H900-145	653	microbial laminite	0.2	-8.8
HPF (Mbr. 9)	H900-149A	670.9	microbial laminite	-0.7	-10.1
HPF (Mbr. 9)	H900-154	693	microbial laminite	-0.2	-9.1
HPF (Mbr. 9)	H900-156	703	microbial laminite	-0.6	-8.8
HPF (Mbr. 9)	H900-157A	707.2	grainstone	-0.8	-8.8
HPF (Mbr. 9)	H900-157B	707.2	grainstone	0.0	-8.8
HPF (Mbr. 9)	H900-158	721	grainstone	0.2	-6.3
HPF (Mbr. 9)	H900-161	734.3	wackestone	0.4	-11.0
HPF (Mbr. 9)	H900-162	736.8	microbial laminite	0.4	-9.7
HPF (Mbr. 9)	H900-163A	740	grainstone	-0.1	-10.5
HPF (Mbr. 9)	00-163B	767	wackestone	0.1	-10.8
HPF (Mbr. 9)	H900-165	775	wackestone	0.7	-8.8
HPF (Mbr. 9)	H900-167	779.7	packstone	0.0	-10.6
HPF (Mbr. 10)	H1000-169	806.5	wackstone	-1.7	-10.3
HPF (Mbr. 10)	RH01-10-9	809.7	wackstone	-1.3	-10.3
HPF (Mbr. 10)	H1000-173	823.5	dolowackstone	-0.5	-9.2
HPF (Mbr. 10)	H1000-176	848.1	dolomitic packstone	-0.6	-10.1
HPF (Mbr. 12)	H1200-179	863.8	dololaminite	-1.0	-11.7
HPF (Mbr. 12)	H1200-181	894.5	packstone	-0.7	-9.9
HPF (Mbr. 13)	H1300-187	925	dolomudstone	-0.9	-8.9
HPF (Mbr. 13)	H1300-188	926.5	packstone	-0.8	-9.4
HPF (Mbr. 13)	H1300-189	930	dololaminite	-0.6	-9.1

Formation	Sample	Strat. Height	Lithology	$\delta^{13}C$	$\delta^{18}O$
Swasey Ls.	07-SMP68	123.8	oolitic grainstone	-0.5	-14.4
Swasey Ls.	07-SMP69	124.5	oolitic grainstone	-1.1	-12.6
Swasey Ls.	07-SMP71	125.6	oolitic grainstone	-0.8	-12.4
Swasey Ls.	07-SMP78-1	126	intraclasts	-0.8	-13.3
Swasey Ls.	07-SMP78-2	126	intraclasts	-0.5	-14.8
Swasey Ls.	06-353	127.5	packstone	-1.1	-12.6
Swasey Ls.	06-354	127.5	ooltic grainstone	-0.7	-11.6
Swasey Ls.	07-SMP72	127.7	ooltic grainstone	-0.4	-11.6
Eye of Needle Ls.	07-SMP75	128	lime mudstone	-0.9	-13.1
Eye of Needle Ls.	07-SMP73	128.5	lime mudstone	-0.5	-11.3
Eye of Needle Ls.	07-SMP80	129	lime mudstone	-0.8	-12.7
Eye of Needle Ls.	07-SMP76	130	wackestone	-0.5	-14.3
Eye of Needle Ls.	07-SMP81	130.5	lime mudstone	-0.8	-11.6
Eye of Needle Ls.	07-SMP77	130.9	lime mudstone	-0.5	-13.8
Eye of Needle Ls.	07-SMP82	132	lime mudstone	-0.9	-11.9
Eye of Needle Ls.	07-SMP83	133.5	peloidal packstone	-1.1	-12.0
Eye of Needle Ls.	07-SMP84	134.5	peloidal packstone	-1.1	-11.9
Eye of Needle Ls.	07-SMP87	137	dolopackstone	-0.7	-15.1
Eye of Needle Ls.	07-SMP89	138.5	lime mudstone	-0.8	-11.1
Eye of Needle Ls.	07-SMP90	139.7	lime mudstone	-1.2	-12.0
Eye of Needle Ls.	07-SMP92	142.5	wackestone	-1.2	-11.8
Eye of Needle Ls.	07-SMP93	145.5	dolopackstone	-0.7	-10.5
Eye of Needle Ls.	07-SMP94	147.3	dolopackstone	-1.1	-12.2
Eye of Needle Ls.	07-SMP95	148.7	dolopackstone	-1.3	-12.1
Eye of Needle Ls.	07-SMP96	150.4	dolopackstone	-1.1	-12.1
Eye of Needle Ls.	07-SMP97	152.5	peloidal packstone	-1.3	-11.8
Eye of Needle Ls.	07-SMP98	154.3	dolopackstone	-1.5	-11.5
Eye of Needle Ls.	07-SMP99	155.6	dolopackstone	-1.1	-12.1
Eye of Needle Ls.	07-SMP100-1	158	wackestone	-1.2	-11.9
Eye of Needle Ls.	07-SMP100-2	158	microcrystalline dolomite	-0.6	-9.7
Eye of Needle Ls.	07-SMP101	159	wackestone	-0.5	-9.7
Eye of Needle Ls.	07-SMP102	160.5	dolomudstone	-0.1	-9.5
Eye of Needle Ls.	07-SMP103	161	dolomudstone	-0.6	-10.5
Eye of Needle Ls.	07-SMP104	162.2	dolomudstone	-0.7	-12.0
Eye of Needle Ls.	07-SMP105	165	lime mudstone	-0.6	-12.1
Eye of Needle Ls.	07-SMP106	166.2	wackestone	-0.3	-12.3
Eye of Needle Ls.	07-SMP107	166.7	lime mudstone	-0.3	-11.5
Eye of Needle Ls.	07-SMP108-3	168.7	sparry calcite cement	0.0	-13.0
Eye of Needle Ls.	07-SMP108-2	168.7	radiaxial fibrous calcite	0.3	-8.2
Eye of Needle Ls.	07-SMP108-1	168.7	packstone	0.0	-11.4
Eye of Needle Ls.	07-SMP109	169.7	microcrystalline dolomite	0.0	-12.3
Eye of Needle Ls.	07-SMP111	173.5	microbial laminae	0.8	-11.3
Eye of Needle Ls.	07-SMP112-1	174.4	wackestone	0.5	-12.3
Eye of Needle Ls.	07-SMP113	174.7	wackestone	0.5	-12.4
Eye of Needle Ls.	07-SMP114	177.5	packstone	-1.0	-14.1

Formation	Sample	Strat. Height	Lithology	$\delta^{13}C$	$\delta^{18}O$
Pierson Cove Fm.	07-SMP115	178.5	lime mudstone	0.2	-9.8
Pierson Cove Fm.	06-382	178.6	microbial laminae	0.1	-8.7
Pierson Cove Fm.	07-SMP128	179.6	microbial laminae	-1.9	-10.1
Pierson Cove Fm.	07-SMP122-1	181	sparry calcite cement	-2.3	-12.2
Pierson Cove Fm.	07-SMP122-3	181	grainstone	-0.6	-11.2
Pierson Cove Fm.	07-SMP122-2	181	dolomudstone	0.3	-8.1
Pierson Cove Fm.	06-383	182.8	dolowackestone	0.2	-10.8
Pierson Cove Fm.	07-SMP130	183	microbial laminae	0.4	-11.7
Pierson Cove Fm.	07-SMP131	183.6	microbial laminae	-0.1	-6.9
Pierson Cove Fm.	06-384	184.2	microbial laminae	-1.4	-9.0
Pierson Cove Fm.	07-SMP132	184.9	microbial laminae	-1.3	-9.2
Pierson Cove Fm.	06-385	186	dolopackstone	-3.1	-6.7
Pierson Cove Fm.	06-386	186.4	packstone	-3.0	-9.2
Pierson Cove Fm.	07-SMP134	186.4	microcrystalline dolomite	-2.6	-8.3
Pierson Cove Fm.	07-SMP136	186.5	wackestone	-1.4	-7.4
Pierson Cove Fm.	07-SMP137	187.9	wackestone	-1.4	-7.7
Pierson Cove Fm.	07-SMP138	189.3	microbial laminae	-1.3	-7.0
Pierson Cove Fm.	06-387	189.9	microbial laminae	-1.3	-8.4
Pierson Cove Fm.	07-SMP140	191.5	microbial laminae	-0.9	-7.3
Pierson Cove Fm.	07-SMP141	193.5	microbial laminae	0.1	-8.1
Pierson Cove Fm.	07-SMP142	194.3	microbial laminae	-0.6	-8.4
Pierson Cove Fm.	07-SMP143	195	microbial laminae	-1.0	-9.9
Pierson Cove Fm.	06-388	196	grainstone	0.2	-12.8
Pierson Cove Fm.	06-389	196.2	microbial laminae	0.4	-12.7
Pierson Cove Fm.	06-390	198	dolomudstone	0.1	-10.5
Pierson Cove Fm.	06-391	199.4	lime mudstone	-0.7	-12.1
Pierson Cove Fm.	06-392	199.7	microbial laminae	-0.7	-8.4
Pierson Cove Fm.	06-393	200.5	wackestone	0.0	-8.5
Pierson Cove Fm.	07-SMP147	200.8	microbial laminae	0.4	-7.4
Pierson Cove Fm.	07-SMP148	201.8	wackestone	-0.1	-7.2
Pierson Cove Fm.	07-SMP149	202.4	microbial laminae	-0.4	-7.8
Pierson Cove Fm.	07-SMP154	203.2	silty limestone	0.0	-7.9
Pierson Cove Fm.	07-SMP155	203.9	silty limestone	0.5	-5.8
Pierson Cove Fm.	07-SMP157	204.5	wackestone	-0.2	-10.4
Pierson Cove Fm.	07-SMP151	205.3	wackestone	-0.6	-11.7
Pierson Cove Fm.	07-SMP152	205.9	lime mudstone	0.1	-11.2
Pierson Cove Fm.	07-SMP153	206.4	lime mudstone	-0.1	-10.8
Pierson Cove Fm.	06-470	210.8	wackestone	-3.5	-16.0
Pierson Cove Fm.	06-471	211.7	lime mudstone	1.2	-7.1
Pierson Cove Fm.	06-475	216.6	wackestone	-0.3	-12.0
Pierson Cove Fm.	06-474	217.3	wackestone	-0.5	-15.2
Pierson Cove Fm.	06-472	217.4	wackestone	-0.3	-14.4

Formation	Sample	Strat. Height	Lithology	$\delta^{13}C$	$\delta^{18}O$
Swasey Ls.	06-100	1.5	wackestone	-1.3	-10.3
Swasey Ls.	06-101	7.5	wackestone	-1.3	-9.0
Swasey Ls.	06-103	10.35	bioclastic grainstone	-1.1	-9.4
Swasey Ls.	06-102	10.4	wackestone	-0.3	-11.1
Swasey Ls.	06-104	12	bioclastic packstone	-1.6	-10.8
Swasey Ls.	06-105	13.7	wackestone	-2.5	-10.2
Swasey Ls.	06-106	14.7	bioclastic packstone	-1.6	-8.9
Swasey Ls.	06-107	15.8	bioclastic packstone	-0.8	-10.1
Wheeler Fm.	06-108	16.1	argillaceous limestone	0.1	-12.6
Wheeler Fm.	06-109	16.15	argillaceous limestone	-1.1	-11.8
Wheeler Fm.	06-110	16.2	wackestone	-0.1	-14.4
Wheeler Fm.	06-112	17.1	lime mudstone	-1.9	-11.6
Wheeler Fm.	06-113	17.16	lime mudstone	-0.7	-12.1
Wheeler Fm.	06-114	17.3	argillaceous limestone	-0.4	-12.1
Wheeler Fm.	06-116	20.1	argillaceous limestone	-1.1	-13.2
Wheeler Fm.	06-118	20.5	calcite cement	-0.2	-10.6
Wheeler Fm.	07-MP53	21.1	argillaceous limestone	-1.3	-12.9
Wheeler Fm.	06-119	21.3	argillaceous limestone	-1.0	-13.2
Wheeler Fm.	06-120	21.9	lime mudstone	-1.1	-13.2
Wheeler Fm.	07-MP54	21.9	lime mudstone	-0.9	-12.8
Wheeler Fm.	06-122	30.29	lime mudstone	-0.8	-12.0
Wheeler Fm.	06-122x	30.30	lime mudstone	-0.8	-12.0
Wheeler Fm.	06-126	40.5	argillaceous limestone	-0.2	-11.6
Wheeler Fm.	06-128x	43.1	lime mudstone	-1.4	-11.0
Wheeler Fm.	06-128	43.2	lime mudstone	-1.3	-11.1
Wheeler Fm.	06-125	43.5	lime mudstone	-1.6	-11.1
Wheeler Fm.	06-130	45	lime mudstone	-2.0	-11.1
Wheeler Fm.	06-133	51.6	lime mudstone	-0.9	-11.3
Wheeler Fm.	06-134	52.6	lime mudstone	-0.9	-11.5
Wheeler Fm.	07-MP55	57.2	argillaceous limestone	-0.4	-9.8
Wheeler Fm.	06-136	66.6	lime mudstone	-1.0	-10.6
Wheeler Fm.	06-137	67.6	lime mudstone	-1.0	-10.9
Wheeler Fm.	06-138	69	lime mudstone	-1.0	-10.5
Wheeler Fm.	07-MP56	69.3	argillaceous limestone	-1.0	-10.7
Wheeler Fm.	07-MP57	71	lime mudstone	-0.9	-10.5
Wheeler Fm.	07-MP58	72.5	lime mudstone	-1.0	-10.8
Wheeler Fm.	06-139	74.5	lime mudstone	-0.8	-10.4
Wheeler Fm.	06-140	74.5	lime mudstone	-0.9	-10.6
Wheeler Fm.	06-141	74.5	lime mudstone	-0.9	-10.5
Wheeler Fm.	07-MP59	74.6	argillaceous limestone	-1.0	-10.9
Wheeler Fm.	07-MP60	76	lime mudstone	-0.8	-10.4
Wheeler Fm.	07-MP61	79.5	argillaceous limestone	-0.8	-10.6
Wheeler Fm.	07-MP62	83	argill. lime mudstone	-0.9	-10.9
Wheeler Fm.	06-146	83.7	lime mudstone	-0.1	-8.6
Wheeler Fm.	06-147	83.8	lime mudstone	-1.5	-12.4

Formation	Sample	Strat. Height	Lithology	$\delta^{13}C$	$\delta^{18}O$
Wheeler Fm.	07-MP63	86.5	argill. lime mudstone	-1.0	-11.0
Wheeler Fm.	06-149	89.7	lime mudstone	-1.0	-10.8
Wheeler Fm.	07-MP64	90	lime mudstone	-1.1	-10.8
Wheeler Fm.	06-150	93.6	lime mudstone	-0.5	-10.2
Wheeler Fm.	06-152	98.5	lime mudstone	-0.7	-10.2
Wheeler Fm.	06-154	102.2	lime mudstone	-0.5	-9.3
Wheeler Fm.	06-156	107.2	lime mudstone	-0.9	-10.4
Wheeler Fm.	06-157	116.7	lime mudstone	-0.9	-10.2
Wheeler Fm.	06-158	120.3	lime mudstone	-0.8	-10.3
Wheeler Fm.	06-159	123.8	lime mudstone	-0.9	-10.1
Wheeler Fm.	06-161	135.5	argill. lime mudstone	-0.7	-10.3
Wheeler Fm.	06-162	134.9	calcareous shale	-0.7	-10.4
Wheeler Fm.	06-163	136.6	calcareous shale	-0.8	-10.4
Wheeler Fm.	06-164	141.9	calcareous shale	-0.5	-10.3
Wheeler Fm.	06-165	142.2	argill. lime mudstone	-0.5	-10.4
Wheeler Fm.	06-166	142.2	argill. lime mudstone	-0.7	-10.3
Wheeler Fm.	06-167	142.6	argill. lime mudstone	-0.6	-10.3
Wheeler Fm.	06-168	165	lime mudstone	-0.9	-10.4
Marjum Fm.	06-171	165	lime mudstone	-1.1	-11.9
Marjum Fm.	06-172	168	lime mudstone	-1.4	-11.0
Marjum Fm.	06-172x	168.01	lime mudstone	-1.2	-11.0
Marjum Fm.	06-173	172.1	lime mudstone	-0.8	-11.4
Marjum Fm.	06-174x	172.18	lime mudstone	-0.8	-11.1
Marjum Fm.	06-174	172.2	lime mudstone	-0.9	-11.0
Marjum Fm.	06-175	179.9	wackestone	-1.9	-10.4
Marjum Fm.	06-175x	179.91	wackestone	-1.4	-11.4
Marjum Fm.	06-176x	188.77	wackestone	-0.4	-10.0
Marjum Fm.	06-176	188.8	wackestone	-0.9	-10.9
Marjum Fm.	06-177	200.7	lime mudstone	0.6	-10.3
Marjum Fm.	06-178	203.6	lime mudstone	0.3	-10.3
Marjum Fm.	06-179	210	lime mudstone	0.5	-10.6
Marjum Fm.	06-180	215.9	lime mudstone	0.7	-10.5
Marjum Fm.	06-181	217.2	lime mudstone	0.8	-10.2
Marjum Fm.	06-183	220.1	lime mudstone	0.5	-10.2
Marjum Fm.	06-186	227.8	lime mudstone	0.5	-10.4
Marjum Fm.	06-187	232.5	lime mudstone	0.3	-9.8
Marjum Fm.	06-188	246	calc shale	-0.4	-10.8
Marjum Fm.	06-189	247.5	lime mudstone	-0.2	-10.5
Marjum Fm.	06-190	248.7	lime mudstone	0.1	-10.6
Marjum Fm.	06-191	250.5	lime mudstone	-0.4	-10.2
Marjum Fm.	06-192A	251.3	lime mudstone	0.1	-11.2
Marjum Fm.	06-192B	251.3	lime mudstone	0.0	-11.9
Marjum Fm.	06-193	251.9	lime mudstone	0.4	-9.4
Marjum Fm.	06-194	252.1	lime mudstone	0.6	-10.2
Marjum Fm.	06-195	251.6	lime mudstone	0.5	-9.7
Marjum Fm.	06-196	253.2	lime mudstone	0.3	-10.6

Formation	Sample Name	Meters	Lithology	$\delta^{13}C$	$\delta^{18}O$
Marjum Fm.	06-197	261	lime mudstone	0.3	-13.6
Marjum Fm.	06-198	266	lime mudstone	0.4	-15.4
Marjum Fm.	06-198x	266.10	lime mudstone	0.0	-15.8
Marjum Fm.	06-200	269.65	calc shale	-2.1	-13.8
Marjum Fm.	06-199	269.7	calc shale	-2.6	-12.9
Marjum Fm.	06-201	275.5	lime mudstone	0.3	-11.5
Marjum Fm.	06-202	276.6	lime mudstone	0.1	-11.3
Marjum Fm.	06-204	286.2	lime mudstone	0.2	-11.5
Marjum Fm.	06-205	292.8	lime mudstone	0.3	-11.2
Marjum Fm.	06-206	299.9	lime mudstone	-0.3	-12.9
Marjum Fm.	07-1056	307.5	lime mudstone	0.4	-10.0
Marjum Fm.	06-207	307.7	lime mudstone	0.2	-12.1
Marjum Fm.	06-208	308	lime mudstone	0.6	-10.3
Marjum Fm.	07-1057	308.07	lime mudstone	0.3	-10.1
Marjum Fm.	07-1058	308.64	lime mudstone	0.5	-10.4
Marjum Fm.	07-1059	309.21	lime mudstone	0.7	-10.0
Marjum Fm.	07-1060	309.78	lime mudstone	0.6	-10.3
Marjum Fm.	07-1061	310.35	lime mudstone	1.0	-9.3
Marjum Fm.	07-1062	310.92	lime mudstone	0.5	-10.4
Marjum Fm.	07-1063	311.49	lime mudstone	0.5	-10.3
Marjum Fm.	07-1064	313.11	lime mudstone	1.0	-10.3
Marjum Fm.	07-1065	315.11	lime mudstone	0.5	-10.2
Marjum Fm.	07-1066	315.11	lime mudstone	1.4	-10.2
Marjum Fm.	07-1067	320.11	lime mudstone	1.3	-10.3
Marjum Fm.	07-1068	338.11	lime mudstone	0.3	-10.1
Marjum Fm.	07-1069	340.11	lime mudstone	0.1	-10.2
Marjum Fm.	07-1070	341.01	lime mudstone	0.2	-10.1
Marjum Fm.	07-1071	342.01	lime mudstone	0.3	-10.2
Marjum Fm.	07-1072	343.01	lime mudstone	0.2	-10.3
Marjum Fm.	07-1073	343.91	lime mudstone	0.5	-10.1
Marjum Fm.	07-1074	344.81	lime mudstone	-0.2	-10.3
Marjum Fm.	07-1075-1	345.81	lime mudstone	0.4	-8.8
Marjum Fm.	07-1075-A	345.81	lime mudstone	-1.0	-10.2
Marjum Fm.	07-1075-B	345.81	calcite cement	0.3	-9.8
Marjum Fm.	07-1076-A	346.81	lime mudstone	-0.6	-10.3
Marjum Fm.	07-1076-B	346.81	calcite cement	0.4	-10.1
Marjum Fm.	07-1077	347.71	lime mudstone	0.2	-10.2
Marjum Fm.	07-1078	348.71	lime mudstone	0.1	-10.4
Marjum Fm.	07-1079	349.61	lime mudstone	0.2	-9.8
Marjum Fm.	07-1080	350	calc shale	0.5	-9.6
Marjum Fm.	07-1081	352.1	calc shale	0.1	-10.1
Marjum Fm.	07-1082	354.2	calc shale	0.1	-9.8
Marjum Fm.	07-1083	356.3	lime mudstone	0.0	-10.0
Marjum Fm.	07-1084	358.4	lime mudstone	-0.1	-10.0
Marjum Fm.	07-1085	358.8	lime mudstone	0.1	-10.1
Marjum Fm.	07-1086	359	lime mudstone	0.3	-10.0

Formation	Sample Name	Meters	Lithology	$\delta^{13}C$	$\delta^{18}O$
Marjum Fm.	07-1087	361.7	lime mudstone	0.2	-10.0
Marjum Fm.	07-1088	364.4	lime mudstone	0.2	-9.9
Marjum Fm.	07-1089	367.1	lime mudstone	0.3	-10.1
Marjum Fm.	07-1090	369.8	lime mudstone	0.2	-9.8
Marjum Fm.	07-1091	372.5	lime mudstone	0.9	-9.3
Marjum Fm.	07-1092	375.2	lime mudstone	0.3	-10.0
Marjum Fm.	07-1093	377.9	lime mudstone	0.3	-10.1
Marjum Fm.	07-1094	380.6	lime mudstone	0.4	-10.1
Marjum Fm.	07-1095	383.3	lime mudstone	0.4	-9.9
Marjum Fm.	07-1096	386	lime mudstone	0.3	-10.1
Marjum Fm.	07-1097	388.7	lime mudstone	0.3	-9.9
Marjum Fm.	07-1103	401.5	lime mudstone	0.3	-9.8
Marjum Fm.	07-1104	404	lime mudstone	0.6	-9.0
Marjum Fm.	07-1105	406.5	lime mudstone	0.1	-9.9
Marjum Fm.	07-1106	409	lime mudstone	-0.1	-10.6
Marjum Fm.	07-1107	411.5	lime mudstone	0.3	-9.9
Marjum Fm.	07-1108	414	lime mudstone	0.2	-9.9
Marjum Fm.	07-1109	417.6	argill. lime mudstone	0.2	-9.8
Marjum Fm.	07-1110	421.3	lime mudstone	0.2	-10.0
Marjum Fm.	07-1111	422	lime mudstone	0.3	-9.7
Marjum Fm.	07-1112	423.75	lime mudstone	0.4	-9.9
Marjum Fm.	07-1113	425.5	lime mudstone	0.4	-10.0
Marjum Fm.	07-1114	427.25	lime mudstone	0.3	-10.0
Marjum Fm.	07-1115	429	lime mudstone	-0.7	-12.9
Marjum Fm.	07-1116	430.75	lime mudstone	0.2	-10.2
Marjum Fm.	07-1117	432.5	lime mudstone	0.4	-9.9
Marjum Fm.	07-1118	434.25	lime mudstone	0.3	-9.9
Marjum Fm.	07-1119	436	lime mudstone	0.1	-10.0
Marjum Fm.	07-1120	437.75	lime mudstone	0.1	-9.9
Marjum Fm.	07-1121	439.5	lime mudstone	0.2	-9.7
Marjum Fm.	07-1122	441.25	lime mudstone	0.1	-10.2
Marjum Fm.	07-1123	443	lime mudstone	0.3	-9.8
Marjum Fm.	07-1124	444.75	wackestone	0.3	-9.9
Marjum Fm.	07-1125	446.5	lime mudstone	0.2	-10.2
Marjum Fm.	07-1126	448.25	lime mudstone	0.5	-9.7
Marjum Fm.	07-1127	450	lime mudstone	0.7	-9.6
Marjum Fm.	07-1128	451.75	lime mudstone	0.7	-10.0
Marjum Fm.	07-1129	453.5	lime mudstone	0.8	-9.8
Marjum Fm.	07-1130	455.25	lime mudstone	0.7	-9.8
Marjum Fm.	07-1132	458.75	lime mudstone	0.8	-10.0
Marjum Fm.	07-1133	459	lime mudstone	0.7	-9.9
Marjum Fm.	07-1134	460.56	lime mudstone	0.6	-9.9
Marjum Fm.	07-1135	462.12	lime mudstone	0.6	-10.0
Marjum Fm.	07-1136	463.68	lime mudstone	0.5	-10.4
Marjum Fm.	07-1137	465.24	lime mudstone	0.7	-10.3
Marjum Fm.	07-1138	466.8	lime mudstone	0.5	-9.8

Formation	Sample Name	Meters	Lithology	$\delta^{13}C$	$\delta^{18}O$
Marjum Fm.	07-1139	468.36	lime mudstone	0.7	-10.0
Marjum Fm.	07-1140	469.92	lime mudstone	0.4	-10.0
Marjum Fm.	07-1141	471.48	lime mudstone	0.5	-9.8
Marjum Fm.	07-1142	473.04	lime mudstone	0.5	-9.8
Marjum Fm.	07-1143	474.6	lime mudstone	0.3	-10.1
Marjum Fm.	07-1144	476.16	lime mudstone	0.7	-9.7
Marjum Fm.	07-1145	477.72	lime mudstone	0.6	-10.1
Marjum Fm.	07-1146	479.28	lime mudstone	0.9	-9.9
Marjum Fm.	07-1147	480.84	lime mudstone	0.8	-10.1
Marjum Fm.	07-1148	482.4	lime mudstone	1.0	-10.0
Marjum Fm.	07-1149	483.96	lime mudstone	1.0	-9.9
Marjum Fm.	07-1151	487.08	lime mudstone	0.9	-10.0
Marjum Fm.	07-1152	487.5	argill. lime mudstone	1.0	-10.0
Marjum Fm.	07-1153	488.58	argill. lime mudstone	0.9	-9.9
Marjum Fm.	07-1154	489.66	argill. lime mudstone	1.0	-9.8
Marjum Fm.	07-1156	491.82	lime mudstone	0.7	-9.9
Marjum Fm.	07-1157	492.9	lime mudstone	0.8	-10.0
Marjum Fm.	07-1158	493.98	lime mudstone	0.7	-9.8
Marjum Fm.	07-1159	495	lime mudstone	0.8	-10.2
Marjum Fm.	07-1160	495.6	lime mudstone	0.9	-11.5
Marjum Fm.	07-1161	496.2	lime mudstone	0.2	-10.3
Marjum Fm.	07-1162	496.8	wackestone	0.6	-9.6
Marjum Fm.	07-1163	497.4	wackestone	1.0	-9.5
Marjum Fm.	07-1164	498	argill. lime mudstone	0.6	-9.8
Marjum Fm.	07-1165	498.6	argill. lime mudstone	0.9	-9.7
Marjum Fm.	07-1166	499.2	argill. lime mudstone	1.2	-9.9
Marjum Fm.	07-1167	499.8	argill. lime mudstone	1.2	-9.9
Marjum Fm.	07-1168	500.4	argill. lime mudstone	1.1	-9.9
Marjum Fm.	07-1169	501	argill. lime mudstone	1.0	-10.0
Marjum Fm.	07-1170	501.6	lime mudstone	1.3	-9.7
Marjum Fm.	07-1171	502.2	argill. lime mudstone	1.3	-9.8
Marjum Fm.	07-1172	502.8	calc shale	1.3	-10.0
Marjum Fm.	07-1173	503	calc shale	1.3	-9.9
Marjum Fm.	07-1174	514	calc shale	1.4	-8.8
Marjum Fm.	07-1175	516	lime mudstone	0.9	-9.7
Marjum Fm.	07-1176	516	lime mudstone	1.9	-9.7
Marjum Fm.	07-1177	517	lime mudstone	1.9	-9.6
Marjum Fm.	07-1178	517.9	lime mudstone	1.0	-9.9
Marjum Fm.	07-1179	518.8	lime mudstone	1.5	-9.6
Marjum Fm.	07-1180	519.7	lime mudstone	2.0	-9.8
Marjum Fm.	07-1181	520.6	lime mudstone	1.4	-9.7
Marjum Fm.	07-1182	521.5	lime mudstone	1.7	-9.8
Marjum Fm.	07-1183	522.4	lime mudstone	1.0	-9.6
Marjum Fm.	07-1184	523.3	lime mudstone	0.5	-10.2
Marjum Fm.	07-1185	524	lime mudstone	0.8	-9.7
Marjum Fm.	07-1186	526	lime mudstone	0.9	-9.5

Formation	Sample Name	Meters	Lithology	$\delta^{13}C$	$\delta^{18}O$
Marjum Fm.	07-1187	528	lime mudstone	1.4	-9.6
Marjum Fm.	07-1188	530	lime mudstone	1.4	-10.8
Marjum Fm.	07-1189	532	lime mudstone	1.2	-9.8
Marjum Fm.	07-1190	533.5	lime mudstone	1.1	-10.1
Marjum Fm.	07-1191	535.38	lime mudstone	1.0	-9.8
Marjum Fm.	07-1192	537.26	lime mudstone	0.8	-9.6
Marjum Fm.	07-1193	541	lime mudstone	0.4	-9.8
Marjum Fm.	07-1194	547.6	lime mudstone	-0.1	-11.3
Marjum Fm.	07-1195	554.2	lime mudstone	-0.6	-10.9
Marjum Fm.	07-1196	560.8	lime mudstone	-1.3	-10.5
Marjum Fm.	07-1197	567	lime mudstone	-0.4	-10.4
Marjum Fm.	07-1198	567.4	lime mudstone	0.2	-9.4
Marjum Fm.	07-1199	568.1	lime mudstone	0.0	-10.3
Marjum Fm.	07-1199-1A	568.1	lime mudstone	-0.1	-9.7
Marjum Fm.	07-1199-1B	568.1	calcite cement	-4.0	-8.5
Marjum Fm.	07-1199-2A	568.1	wackestone	-0.1	-9.6
Marjum Fm.	07-1199-2B	568.1	calcite cement	-0.3	-8.1
Marjum Fm.	07-1200	568.8	wackestone	-0.1	-9.7
Marjum Fm.	07-1201	569.5	wackestone	0.1	-10.0
Marjum Fm.	07-1202	570.2	wackestone	-0.3	-9.5
Marjum Fm.	07-1203	570.9	calcite cement	-0.4	-10.7
Marjum Fm.	07-1204	571	lime mudstone	0.6	-9.9
Marjum Fm.	07-1205	572.1	lime mudstone	0.6	-9.3
Marjum Fm.	07-1206	573.2	lime mudstone	0.7	-11.2
Marjum Fm.	07-1207	574.3	lime mudstone	0.5	-9.5
Marjum Fm.	07-1208	575.4	lime mudstone	0.5	-9.4
Marjum Fm.	07-1209	576.5	lime mudstone	0.4	-10.4
Marjum Fm.	07-1210	577.6	lime mudstone	0.5	-8.8
Marjum Fm.	07-1210-A	577.6	wackestone	1.2	-9.1
Marjum Fm.	07-1210-1	577.6	wackestone	0.1	-9.0

Formation	Sample	Strat. Height	Lithology	$\delta^{13}C$	$\delta^{18}O$
Swasey Ls.	07-D7-1	52.8	wackestone	-0.9	-9.7
Swasey Ls.	07-D7-2	52.8	wackstone	-0.8	-9.2
Swasey Ls.	07-D8	54	bioclastic packstone	-0.5	-8.8
Swasey Ls.	07-D9	55.5	bioclastic wackestone	-0.7	-9.9
Swasey Ls.	07-D10	57	bioclastic wackestone	-0.9	-9.3
Swasey Ls.	07-D11	58.5	bioclastic wackestone	-1.0	-9.4
Swasey Ls.	07-D12	60	wackestone	-1.0	-9.1
Swasey Ls.	07-D13	61.5	wackestone	-0.8	-9.8
Swasey Ls.	07-D14	63	wackestone	-0.9	-10.5
Swasey Ls.	07-D15	64.5	wackestone	-0.9	-9.3
Swasey Ls.	07-D16	67	bioclastic packstone	-0.7	-8.5
Wheeler Fm.	07-D17	67.2	lime mudstone	0.8	-13.0
Wheeler Fm.	07-D18	69.2	lime mudstone	1.2	-15.0
Wheeler Fm.	07-D19	70.5	lime mudstone	1.3	-11.6
Wheeler Fm.	07-D20	71.9	lime mudstone	0.8	-13.8
Wheeler Fm.	07-D22	75.1	lime mudstone	0.2	-10.9
Wheeler Fm.	07-D23	76.5	lime mudstone	0.2	-9.1
Wheeler Fm.	07-D25	82.5	lime mudstone	0.0	-8.5
Wheeler Fm.	07-D27	85.5	lime mudstone	0.3	-7.9
Wheeler Fm.	07-D29	88.5	argillaceous limestone	0.4	-8.4
Wheeler Fm.	07-D30	90	lime mudstone	-0.1	-12.6
Wheeler Fm.	07-D31	91.5	lime mudstone	0.3	-8.5
Wheeler Fm.	07-D33	94.5	lime mudstone	0.2	-8.5
Wheeler Fm.	07-D35	97.6	lime mudstone	0.2	-8.4
Wheeler Fm.	07-D37	100.5	lime mudstone	0.2	-8.8
Wheeler Fm.	07-D39	103.5	lime mudstone	0.0	-8.5
Wheeler Fm.	07-D41	106.5	lime mudstone	0.2	-9.4
Wheeler Fm.	07-D42	108	lime mudstone	0.3	-8.6
Wheeler Fm.	07-D43	109.6	lime mudstone	0.7	-8.7
Wheeler Fm.	07-D44	110.6	lime mudstone	0.1	-10.1
Wheeler Fm.	07-D45	112.5	lime mudstone	0.9	-10.1
Wheeler Fm.	07-D46	115	lime mudstone	0.4	-8.6
Wheeler Fm.	07-D47	117	lime mudstone	0.8	-8.1
Wheeler Fm.	07-D48	118.5	lime mudstone	0.3	-9.2
Wheeler Fm.	07-D49	120	lime mudstone	0.2	-9.2
Wheeler Fm.	07-D50	121.7	lime mudstone	0.2	-9.2
Wheeler Fm.	07-D51	122.8	lime mudstone	0.3	-9.0
Wheeler Fm.	07-D52	124.3	argillaceous limestone	0.2	-9.1
Wheeler Fm.	07-D53	132	argillaceous limestone	0.0	-9.0
Wheeler Fm.	07-D54	133	wackestone	-0.1	-8.7
Wheeler Fm.	07-D54x	133.1	wackestone	0.0	-9.4
Wheeler Fm.	07-D55x	133.8	lime mudstone	0.3	-9.3
Wheeler Fm.	07-D55	134	lime mudstone	0.7	-8.6
Wheeler Fm.	07-D56x	135	argillaceous limestone	0.1	-8.4
Wheeler Fm.	07-D56	135	argillaceous limestone	0.0	-8.2

Formation	Sample	Strat. Height	Lithology	$\delta^{13}C$	$\delta^{18}O$
Wheeler Fm.	07-D57x1	137.9	lime mudstone	0.0	-8.8
Wheeler Fm.	07-D57	138	lime mudstone	-2.5	-9.4
Wheeler Fm.	07-D57x2	138.1	lime mudstone	-1.7	-9.3
Wheeler Fm.	07-D58x	138.8	wackestone	-0.7	-9.0
Wheeler Fm.	07-D58	139	wackestone	-0.7	-8.9
Wheeler Fm.	07-D59	145.2	argillaceous limestone	0.2	-9.2
Wheeler Fm.	07-D60	147	argillaceous limestone	0.2	-9.4
Wheeler Fm.	07-D61	147.5	lime mudstone	0.2	-9.1
Wheeler Fm.	07-D62	150.6	lime mudstone	0.2	-9.5
Wheeler Fm.	07-D63	152.1	lime mudstone	0.0	-9.2
Wheeler Fm.	07-D64	153.6	lime mudstone	0.5	-9.4
Wheeler Fm.	07-D65	154.8	lime mudstone	1.1	-8.7
Wheeler Fm.	07-D66	156.6	lime mudstone	0.5	-12.0
Wheeler Fm.	07-D67	158.1	lime mudstone	0.5	-9.0
Wheeler Fm.	07-D69	161.1	lime mudstone	0.4	-12.2
Wheeler Fm.	07-D71	164.1	lime mudstone	0.4	-12.8
Wheeler Fm.	07-D73	167.1	lime mudstone	1.0	-6.8

REFERENCES CITED

Ahlberg, P., Axheimer, N., Babcock, L.E., Eriksson, M.E., Schmitz, B., and Terfelt, F., 2009, Cambrian high-resolution biostratigraphy and carbon isotope chemostratigraphy in Scania, Sweden: first record of the SPICE and DICE excursions in Scandinavia: Lethaia, v. 42, p. 2-15.

Allan, J.R., and Matthews, R.K., 1982, Isotope signatures associated with early meteoric diagenesis: Sedimentology, v. 29, p. 797-817.

Allmendinger, R.W., Sharp, J.W., Von Tish, D., Serpa, L., Brown, L., Kaufman, S., Oliver, J., and Smith, R.B., 1983, Cenozoic and Mesozoic structure of the eastern Basin and Range Province, Utah, from COCORP seismic reflection data: Geology, v. 11, p. 532-536.

Álvaro, J.J., Bauluz, B., Subías, I., Pierre, C., and Vizcaïno, D., 2008, Carbon chemostratigraphy of the Cambrian-Ordovician transition in a midlatitude mixed platform, Montagne Noire, France: Geological Society of America Bulletin, v. 120, p. 962-975.

Babcock, L.E., Zhang, W., and Leslie, S.A., 2001, The Chengjiang Biota*:* Record of the Early Cambrian diversification of life and clues to exceptional preservation of fossils: GSA Today, v. 11, p. 4-9.

Babcock, L.E., Rees, M.N., Robison, R.A., Langenburg, E.S., and Peng, S.C., 2004, Potential Global Stratotype-section and Point (GSSP) for a Cambrian stage boundary defined by the first appearance of the trilobite *Ptychagnostus atavus*, Drum Mountains, Utah, USA: Geobios, v. 37, p. 149-158.

Babcock, L.E., Peng, S., Geyer, G., and Shergold, J.H., 2005, Changing perspectives on Cambrian chronostratigraphy and progress toward subdivision of the Cambrian System: Geosciences Journal, v. 9, p. 101-106.

Babcock, L.E., Robison, R.A., Rees, M.N., Peng, S., and Saltzman, M.R., 2007, The global boundary stratotype section and point of the Drumian Stage (Cambrian) in the Drum Mountains, Utah, USA: Episodes, v. 30, p. 85-95.

Berner, R.A., 2003, The long-term carbon cycle, fossil fuels and atmospheric composition: Nature, v. 426, p. 323-326.

Berra, F., 2007, Sedimentation in shallow to deep water carbonate environments across a sequence boundary: effects of a fall in sea-level on the evolution of a carbonate system (Ladinian-Carnian, eastern Lombardy, Italy): Sedimentology, v. 54, p. 721-735.

Bond, G.C., and Kominz, M.A., 1984, Construction of tectonic subsidence curves for the early Paleozoic miogeocline, southern Canadian Rocky Mountains – implications for subsidence mechanisms, age of breakup, and crustal thinning: Geological Society of America Bulletin, v. 95, p. 155-173.

Bond, G.C., Kominz, M.A., and Beavan, J., 1991, Evidence for orbital forcing of Middle Cambrian peritidal cycles: Wah Wah range, south-central Utah, *in* Franseen, E.K., Watney, W.L., Kendall, C.G.StC., and Ross, W., eds., Sedimentary modeling: computer simulations and methods for improved parameter definition: Kansas Geological Survey Bulletin, v. 233, p. 293-317.

Bond, G.C., Devlin, W.J., Kominz, M.A., Beavan, J., and McManus, J., 1993, Evidence of astronomical forcing of the Earth's climate in Cretaceous and Cambrian times: Tectonophysics, v. 22, p. 295-315.

Bosence, D., Cross, N., and Hardy, S., 1998, Architecture and depositional sequences of Tertiary fault-block carbonate platforms; an analysis from outcrop (Miocene Gulf of Suez) and computer modelling: Marine and Petroleum Geology, v. 15, p. 203-221.

Bottjer, D.J., Etter, W., Hagadorn, J.W., and Tang, C.M., 2002, Fossil-Lagerstatten: Jewels of the fossil record, in Bottjer, D.J., Etter, W., Hagadorn, J.W., and Tang, C.M., eds., Exceptional fossil preservation: New York, Columbia University Press, p. 1-10.
Brady, M.J. and Koepnick, R.B., 1979, A Middle Cambrian platform-to-basin transition, House Range, west central Utah: Brigham Young University Geology Studies, v. 26, p. 1-17.
Brasier, M.D., and Sukhov, S.S., 1998, The falling amplitude of carbon isotopic oscillations through the Lower to Middle Cambrian: northern Siberia data: Canadian Journal of Earth Sciences, v. 35, p. 353-373.
Brasier, M.D., Corfield, R.M., Derry, L.A., Rozanov, A.Yu., and Zhuravlev, A.Yu., 1994, Multiple δ13C excursions spanning the Cambrian explosion to the Botomian crisis in Siberia: Geology, v. 22, p. 455-458.
Brett, C.E., Allison, P.A., DeSantis, M.K., Liddell, W.D., and Kramer, A., 2009, Sequence stratigraphy, cyclic facies, and *lagerstätten* in the Middle Cambrian Wheeler and Marjum Formations, Great Basin, Utah: Palaeogeography, Palaeoclimatology, Palaeoecology, v. 277, p. 9-33.
Buggisch, W., Keller, M., and Lehnert, O., 2003, Carbon isotope record of Late Cambrian to Early Ordovician carbonates of the Argentine Precordillera: Palaeogeography, Palaeoclimatology, Palaeoecology, v. 195, p. 357-373.
Burchette, T.P. and Wright, P., 1992, Carbonate ramp depositional systems: Sedimentary Geology, v. 79, p. 3-57.
Burchfiel, B.C., Cowan, D.S., and Davis, G.A., 1992, Tectonic overview of the Cordilleran orogen in the western United States, *in* Burchfiel, B.C., Lipman, P.W., and Zoback, M.L., eds., The Cordilleran Orogen: Conterminous U.S.: Boulder, Colorado, Geological Society of America, The Geology of North America, v. G-3, p. 407-479.
Caldwell, C.D., 1980, Depositional environments of the Swasey Limestone: Middle Cambrian shelf carbonates of the Cordilleran miogeocline: Unpublished MS Thesis, University of Kansas, 84p.
Cartwright, J.A., Haddock, R.C., and Pinheiro, L.M., 1993, The lateral extent of sequence boundaries, *in* Williams, G.D. and Dobb, A., eds., Tectonics and Seismic Sequence Stratigraphy: Geological Society of London Special Publication 71, p. 15-34.
Catuneanu, O., Abreu, V., Bhattacharya, J.P., Blum, M.D., Dalrymple, R.W., Eriksson, P.G., Fielding, C.R., Fischer, W.L., Galloway, W.E., Gibling, M.R., Giles, K.A., Holbrook, J.M., Jordan, R., Kendall, C.G.St.C., Macurda, B., Martinsen, O.J., Miall, A.D., Neal, J.E., Nummedal, D., Pomar, L., Posamentier, H.W., Pratt, B.R., Sarg, J.F., Shanley, K.W., Steel, R.J., Strasser, A., Tucker, M.E., and Winker, C., 2009, Towards the standardization of sequence stratigraphy: Earth-Science Reviews, v. 92, p. 1-23.
Cooper, J.D., Miller, R.H., and Sundberg, F.A., 1982, Environmental stratigraphy of the lower part of the Nopah Formation (upper Cambrian), southwestern Great Basin, *in* Cooper, J.D., Troxel, B.W., and Wright, L.A., eds., Guidebook to selected areas in the San Bernardino Mountains, Mojave Desert, and southwestern Great Basin, Geological Society of America Cordilleran Section Annual Meeting Field Trip No. 9, p. 97-117.
Deuser, W.G., 1970, Isotopic evidence for diminishing supply of available carbon during diatom bloom in the Black Sea: Nature, v. 225, p. 1069-1071.
Droxler, A.W. and Glaser, K.S., 1990, Modern periplatform highstand shedding of two semidrowned or drowned shallow carbonate systems, Pedro Bank and the southern shelf of Jamaica, northern Nicaragua Rise:
Eberli, G.P. and Ginsburg, R.N., 1987, Segmentation and coalescence of Cenozoic carbonate platforms, northwestern Great Bahama Bank: Geology, v. 15, p. 75-79.

Elrick, M., and Hinnov, L.A., 1996, Millennial-scale climate origins for stratification in Cambrian and Devonian deep-water rhythmites, western USA: Palaeogeography, Palaeoclimatology, Palaeoecology, v. 123, p. 353-372.
Elrick, M., and Snider, A.C., 2002, Deep-water stratigraphic cyclicity and carbonate mud mound development in the Middle Cambrian Marjum Formation, House Range, Utah, USA: Sedimentology, v. 49, p. 1021-1047.
Embry, A., 1993, Transgressive-regressive (T-R) sequence analysis of the Jurassic succession of the Sverdrup Basin, Canadian Arctic Archipelago: Canadian Journal of Earth Science, v. 30, p. 301-320.
Evans, K.R., 1997, Stratigraphic expression of Middle and Late Cambrian sea-level changes-examples from Antarctica and the Great Basin, USA: University of Kansas, unpublished Ph. D. dissertation, 171 p.
Derry, L.A., Kaufman, A.J., and Jacobsen, S.B., 1992, Sedimentary cycling and environmental change in the Late Proterozoic: evidence from stable and radiogenic isotopes: Geochimica et Cosmochimica Acta, v. 56, p. 1317-1329.
Drewry, G.E., Ramsay, A.T.S., and Smith, A.G., 1974, Climatically controlled sediments, the geomagnetic field, and trade wind belts in Phanerozoic time: The Journal of Geology, v. 82, p. 531-553.
Flügel, E., 2004, Microfacies of carbonate rocks: Springer, New York, 976p.
Frakes, L.A., Francis, J.E., and Syktus, J.I., 1992, Climate modes of the Phanerozoic: Cambridge, U.K., Cambridge University Press, 274p.
Gaines, R.R., and Droser, M.L., 2003, Paleoecology of the familiar trilobite Elrathia kingii: an early exaerobic zone inhabitant: Geology, v. 31, p. 941-944.
Gaines, R.R., Kennedy, M.J., and Droser, M.L., 2005, A new hypothesis for organic preservation of Burgess Shale taxa in the Middle Cambrian Wheeler Formation, House Range, Utah: Palaeogeography, Palaeoclimatology, Palaeoecology, v. 220, p. 193-205.
Gawthorpe, R.L., Fraser, A.J., and Collier, R.E.L., 1994, Sequence stratigraphy in active extensional basins: implications for the interpretation of ancient basin-fills: Marine and Petroleum Geology, v. 11, p. 642-658.
George, A.D., Chow, N., and Trinajstic, K.M., 2009, Syndepositional fault control on lower Frasnian platform evolution, Lennard Shelf, Canning Basin, Australia: Geology, v. 37, p. 331-334.
Geyer, G., and Shergold, J., 2000, The quest for internationally recognized divisions of Cambrian time: Episodes, v. 23, p. 188-195.
Ginsburg, R.N., 1971, Landward movement of carbonate mud-new model for regressive cycles in carbonates [Abstr.]: American Association of Petroleum Geologists Bulletin, v. 55, p. 340.
Glumac, B. and Mutti, L.E., 2007, Late Cambrian (Steptoean) sedimentation and responses to sea-level change along the northeastern Laurentian margin: insights from carbon isotope stratigraphy: Geological Society of America Bulletin, v. 119, p. 623-636.
Glumac, B. and Spivak-Birndorf, M.L., 2002, Stable isotopes of carbon as an invaluable stratigraphic tool: An example from the Cambrian of the northern Appalachians, USA: Geology, v. 30, p. 563-566.
Glumac, B. and Walker, K.R., 1998, A late Cambrian positive carbon-isotope excursion in the southern Appalachians: relation to biostratigraphy, sequence stratigraphy, environments of deposition, and diagenesis: Journal of Sedimentary Research, v. 68, p. 1212-1222.
Goldhammer, R.K., Dunn, P.A., and Hardie, L.A., 1990, Depositional cycles, composite sea-level changes, cycle stacking patterns, and the hierarchy of stratigraphic forcing -

Examples from Alpine Triassic platform carbonates: Geological Society of America Bulletin, v. 102, p. 535-562.
Goldhammer, R.K., Lehmann, P.J., and Dunn, P.A., 1992, Third-order sequences and high frequency cycle stacking patterns in Lower Ordovician platform carbonates, El Paso Group (Texas)-implications for carbonate sequence stratigraphy, *in* Candelaria, M. P. and Reed, C. L., eds., Paleokarst, karst-related diagenesis and reservoir development-examples from Ordovician-Devonian age strata of west Texas and mid-continent: SEPM Field Trip Guidebook, Permian Basin Section, p. 59-92.
Goldhammer, R.K., Harris, M.T., Dunn, P.A., and Hardie, L.A., 1993, Sequence stratigraphy and systems tract development of the Latemar platform, Middle Triassic of the Dolomites (northern Italy): Outcrop calibration keyed by cycle stacking patterns, *in* Loucks, R., and Sarg, R., eds., Recent advances and applications of carbonate sequence stratigraphy: Tulsa, Oklahoma, American Association of Petroleum Geologists Memoir 57, p. 305-325.
Gomez, F.J., Ogle, N., Astini, R.A., and Kalin, R.M., 2007, Paleoenvironmental and carbon-oxygen isotope record of Middle Cambrian carbonates (La Laja Formation) in the Argentine Precordillera: Journal of Sedimentary Research, v. 77, p. 826-842.
Gradstein, F.M., Ogg, J.G., and Smith, A.G., 2004, Geologic time scale 2004: Cambridge University Press.
Grannis, J.L., 1982, Sedimentology of the Wheeler Formation, Drum Mountains, Utah: Unpublished M.S. Thesis, University of Kansas, Lawrence, Kansas.
Halgedahl, S.L., Jarrard, R.D., Brett, C.E., and Allison, P.A., 2009, Geophysical and geological signatures of relative sea level change in the upper Wheeler Formation, Drum Mountains, west-central Utah: A perspective into exceptional preservation of fossils: Palaeogeography, Palaeoclimatology, Palaeoecology, v. 277, p. 34-56.
Hamblin, W.K., 1965, Origin of “reverse drag” on the downthrown side of normal faults: Geological Society of America Bulletin, v. 76, p. 1145-1164.
Hintze, L.F., 1988, Geologic history of Utah: Brigham Young University Geology Studies Special Publication 7, 202p.
Hintze, L.F., and Robison, R.A., 1975, Middle Cambrian stratigraphy of the House, Wah Wah, and adjacent ranges in western Utah: Geological Society of America Bulletin, v. 86, p. 881-891.
Hintze, L.F., and Palmer, A.R., 1976, Upper Cambrian Orr Formation: Its subdivisions and correlatives in western Utah: US Geological Survey Bulletin 1405-G, 25p.
Hintze, L.F., and Davis, F.D., 2003, Geology of Millard County, Utah: Utah Geological Survey Bulletin 133, 305p.
Holmden, C., Creaser, R.A., Muehlenbachs, K., Leslie, S.A., and Bergström, S.M., 1998, Isotopic evidence for geochemical decoupling between ancient epeiric seas and bordering oceans: implications for secular curves: Geology, v. 26, p. 567-570.
Horodyski, R.J., and Knauth, L.P., 1994, Life on land in the Precambrian: Science, v. 263, p. 494-498.
Hotinski, R.M., Kump, L.R., and Arthur, M.A., 2004, The effectiveness of the Paleoproterozoic biological pump: A δ13C gradient from platform carbonates of the Pethei Group (Great Slave Lake Supergroup, NWT): Geological Society of America Bulletin, v. 116, p. 539-554.
Howley, R.A., 2002, Analysis of cyclic shallow-water carbonates: Cambrian Highland Peak Formation, eastern Nevada: Unpublished M.S. Thesis, University of Nevada Las Vegas, Las Vegas, Nevada, 254p.
Howley, R.A., Rees, M.N., and Jacobsen, E.A., 2001, Re-assessing reliability of meter-scale cyclic carbonates as recorders of orbital events – middle Cambrian Highland

Peak Formation, southern Nevada: Geological Society of America Abstracts with Programs, v. 33, p. A-68.
Howley, R.A., Rees, M.N., and Jiang, G., 2006, Significance of Middle Cambrian mixed carbonate-siliciclastic units for global correlation: southern Nevada, USA: Palaeoworld, v. 15, p. 360-366.
Hurtgen, M.T., Pruss, S.B., and Knoll, A.H., 2009, Evaluating the relationship between the carbon and sulfur cycles in the later Cambrian ocean: An example from the Port au Port Group, western Newfoundland, Canada: Earth and Planetary Science Letters, v. 281, p. 288-297.
Immenhauser, A., Kenter, J.A.M., Ganssen, G., Bahamonde, J.R., Van Vliet, D., and Saher, M.H., 2002, Origin and significance of isotope shifts in Pennsylvanian carbonates (Asturias, NW Spain): Journal of Sedimentary Research, v. 72, p. 82-94.
Immenhauser, A., Della Porta, G., Kenter, J.A.M., and Bahamonde, J.R., 2003, An alternative model for positive shifts in shallow-marine carbonate δ13C and δ18O: Sedimentology, v. 50, p. 953-959.
Irwin, H., Curtis, C., and Coleman, M., 1977, Isotopic evidence for source of diagenetic carbonates formed during burial of organic-rich sediments: Nature, v. 269, p. 209-213.
James, N.P., and Kendall, A.C., 1992, Introduction to carbonate and evaporite facies models, *in* Walker, R.G. and James, N.P., eds., Facies models – response to sea level change: Geological Association of Canada, p. 265-275.
Jiang, G., Kaufman, A.J., Christie-Blick, N., Zhang, S., and Wu, H., 2007, Carbon isotope variability across the Ediacaran Yangtze platform in South China: Implications for a large surface-to-deep ocean d13C gradient: Earth and Planetary Science Letters, v. 261, p. 303-320.
Jiang, G., Zhang, S., Shi, X., and Wang, X., 2008, Chemocline instability and isotope variations of the Ediacaran Doushantuo basin in South China: Science in China Series D-Earth Sciences, v. 51, p. 1560-1569.
Jiang, X., Chen, D., Qiu, L., Liang, H., and Ma, J., 2007, Source-controlled carbonates in a small Eocene half-graben lake basin (Shulu Sag) in central Hebei Province, North China: Sedimentology, v. 54, p. 265-292.
Kaufman, A.J., and Knoll, A.H., 1995, Neoproterozoic variations in the C-isotopic composition of seawater: stratigraphic and biogeochemical implications: Precambrian Research, v. 73, p. 27-49.
Kepper, J.C., 1969, Stratigraphy and petrology of a middle and upper Cambrian interval in the Great Basin: Unpublished PhD Dissertation, University of Washington, Seattle, 251p.
Kepper, J. C., 1972, Paleoenvironmental patterns in Middle to Lower Upper Cambrian interval in eastern Great Basin: American Association of Petroleum Geologists Bulletin, v. 56, p. 503-527.
Kepper, J.C., 1976, Stratigraphic relationships and depositional facies in a portion of the Middle Cambrian of the Basin and Range Province, *in* Robison, R.A., ed., Paleontology and depositional environments: Cambrian of western North America: Brigham Young University Studies in Geology, v. 21, p. 75-91.
Kepper, J.C., 1981, Sedimentology of a Middle Cambrian outer shelf margin with evidence for syndepositional faulting, eastern California and western Nevada: Journal of Sedimentary Petrology, v. 51, p. 807-821.
Knauth, L.P., and Kennedy, M.J., 2009, The late Precambrian greening of the Earth: Nature, v. 460, p. 728-732.
Kroopnick, P.M., 1974, The dissolved 02 – CO2 – 13C system in the eastern equatorial Pacific: Deep-Sea Research, v. 21, p. 211-227.

Koerschner, W.F. and Read, J.F., 1989, Field and modelling studies of Cambrian carbonate cycles, Virginia Appalachians: Journal of Sedimentary Petrology, v. 59, p. 654-687.
Kopaska-Merkel, D.C., 1988, Depositional environments and stratigraphy of a Cambrian mixed carbonate/terrigenous platform deposit: west-central Utah, USA: Carbonates and Evaporites, v. 2, p. 133-147.
Kouchinsky, A., Bengtson, S., Gallet, Y., Korovnikov, I., Pavlov, V., Runnegar, B., Shields, G., Veizer, J., Young, E., and Ziegler, K., 2008, The SPICE carbon isotope excursion in Siberia: a combined study of the upper middle Cambrian – lowermost Ordovician Kulyumbe River section, northwestern Siberian Platform: Geological Magazine v. 145, p. 609-622.
Langenburg, E.S., 2003, The Middle Cambrian Wheeler Formation: Sequence stratigraphy and geochemistry across a ramp-to-basin transition: Unpublished M.S. Thesis, Utah State University, Logan, Utah, 120p.
Leeder, M.R., and Gawthorpe, R.L., 1987, Sedimentary models for extensional tilt-block/half-graben basins, *in* Coward, M.P., Dewey, J.F., and Hancock, P.L., eds., Continental extensional tectonics: Geological Society, London, Special Publication 28, p. 139-152.
Lehrmann, D.J. and Goldhammer, R.K., 1999, Secular variation in parasequence and facies stacking patterns of platform carbonates-A guide to application of stacking-pattern analysis in strata of diverse ages and settings, *in* Harris, P.M., Saller, A.H., and Simo, J.A.T., eds., Advances in carbonate sequence stratigraphy-application to reservoirs, outcrops, and models: SEPM Special Publication 63, p. 187-225.
Levy, M., and Christie-Blick, N., 1991, Tectonic subsidence of the early Paleozoic passive continental margin in eastern California and southern Nevada: Geological Society of America Bulletin, v. 103, p. 1590-1606.
Liddell, W.D., Wright, S.H., and Brett, C.E., 1997, Sequence stratigraphy and paleoecology of the Middle Cambrian Spence Shale in northern Utah and southern Idaho: Brigham Young University Geology Studies, v. 42, p. 59-78.
Lindsay, J.F., Kruse, P.D., Green, O.R., Hawkins, E., Braiser, M.D., Cartlidge, J., and Corfield, R.M., 2005, The Neoproterozoic-Cambrian record in Australia: a stable isotope study: Precambrian Research, v. 143, p. 113-133.
Lohmann, K.C., 1977, Lower Dresbachian (Upper Cambrian) platform to deep-shelf transition in eastern Nevada and western Utah: an evaluation through lithologic cycle correlation: Brigham Young University Geology Studies, v. 23, p. 111-122.
Ludvigsen, R., and Westrop, S.R., 1985, Three new Upper Cambrian stages for North America: Geology, v. 13, p. 139-143.
MacNeil, A.J. and Jones, B., 2006, Sequence stratigraphy of a Late Devonian ramp-situated reef system in the western Canada sedimentary basin: dynamic responses to sea-level change and regressive reef development: Sedimentology, v. 53, p. 321-359.
McLeod, A.E., Dawers, N.H., and Underhill, J.R., 2000, The propagation and linkage of normal faults: insights from the Stratspey-Brent-Statfjord fault array, northern North Sea: Basin Research, v. 12, p. 263-284.
Melim, L.A., Westphal, H., Swart, P.K., Eberli, G.P., and Munnecke, A., 2002, Questioning carbonate diagenetic paradigms: evidence from the Neogene of the Bahamas: Marine Geology, v. 185, p. 27-53.
Miall, A.D., 2000, Principles of Sedimentary Basin Analysis: New York, Springer, 616p.
Miall, A.D., and Miall, C.E., 2001, Sequence stratigraphy as a scientific enterprise: the evolution and persistence of conflicting paradigms: Earth-Science Reviews, v. 54, p. 321-347.

Miller, J.F., Evans, K.R., Loch, J.D., Ethington, R.L., Stitt, J.H., Holmer, L., and Popov, L.E., 2003, Stratigraphy of the Sauk III interval (Cambrian-Ordovician) in the Ibex area, western Millard County, Utah and central Texas: Brigham Young University Geology Studies, v. 47, p. 23-118.

Miller, K.G., Kominz, M.A., Browning, J.V., Wright, J.D., Mountain, G.S., Katz, M.E., Sugarman, P.J., Cramer, B.S., Christie-Blick, N., and Pekar, S.F., 2005, The Phanerozoic record of global sea-level change: Science, v. 310, p. 1293-1298.

Mitchum, R.M., Vail, P.R. and Thompson, S., 1977, Seismic stratigraphy and global changes of sea level, part 2 – the depositional sequence as a basic unit for stratigraphic analysis, *in* Payton, C.E., ed., Seismic stratigraphy – applications to hydrocarbon exploration: American Association of Petroleum Geologists Memoir 26, p. 53-62.

Montañez, I.P. and Osleger, D.A., 1993, Parasequence stacking patterns, third-order accommodation events, and sequence stratigraphy of Middle to Upper Cambrian platform carbonates, Bonanza King Formation, southern Great Basin, *in* Loucks, R.G., and Sarg, J.F., eds., Carbonate sequence stratigraphy – recent developments and applications: American Association of Petroleum Geologists Memoir 57, p. 305-325.

Montañez, I.P., Osleger, D.A., Banner, J.L., Mack, L.E., and Musgrove, M., 2000, Evolution of the Sr and C isotope composition of Cambrian oceans: GSA Today, v. 10, p. 1-7.

Myers, K.J. and Milton, N.J., 1996, Concepts and principles of sequence stratigraphy, *in* Emery, D. and Myers, K.J., eds., Sequence Stratigraphy: London, Blackwell Science, p. 11-41.

Nagy, Z.R., Somerville, I.D., Gregg, J.M., Becker, S.P., Shelton, K.L., and Sleeman, A.G., 2005, Sedimentation in an actively tilting half-graben: sedimentology and stratigraphy of Late Tournaisian-Visean (Mississippian, Lower Carboniferous) carbonate rocks in south County Wexford, Ireland: Sedimentology, v. 52, p. 489-512.

Nystuen, J.P., 1998, History and development of sequence stratigraphy, in Gradstein, F. M., Sandvik, K.O. and Milton, N.J., eds., Sequence stratigraphy-concepts and applications, Norwegian Petroleum Society Special Publication 8: Amsterdam, Elsevier Science, p. 31-116.

Ogg, J.G., Ogg, G., and Gradstein, F.M., 2008, The Concise Geologic Time Scale: Cambridge University Press, 177p.

Osleger, D.A., and Montañez, I.P., 1996, Cross-platform architecture of a sequence boundary in mixed siliciclastic-carbonate lithofacies, Middle Cambrian, southern Great Basin, USA: Sedimentology, v. 43, p. 197-217.

Osleger, D.A., Montañez, I.P., Martin-Chivelet, J., and Lehmann, C., 1996, Cycle and sequence stratigraphy of middle to upper Cambrian carbonates, Bonanza King Formation, southern Great Basin, *in* Abbott, P.L., and Cooper, J.D., eds., Field Conference Guide 1996: Pacific Section AAPG GB73, p. 55-84.

Overstreet, R.B., Oboh-Ikuenobe, F.E., Gregg, J.M., 2003, Sequence stratigraphy and depositional facies of lower Ordovician cyclic carbonate rocks, southern Missouri, U.S.A.: Journal of Sedimentary Research, v. 73, p. 421-433.

Palmer, A.R., 1971, The Cambrian of the Great Basin and adjacent areas, western United States, *in* Holland, C.H., ed., Cambrian of the New World, New York, Wiley-Interscience, v. 1, p. 1-78.

Palmer, A.R., 1965, Trilobites of the Late Cambrian Pterocephaliid biomere in the Great Basin, United States: United States Geological Survey Professional Paper 493, p. 96-97.

Palmer, A.R., 1977, Biostratigraphy of the Cambrian System – a progress report: Annual Reviews of Earth and Planetary Sciences, v. 5, p. 13-33.
Palmer, A.R., 1984, The biomere problem: evolution of an idea: Journal of Paleontology, v. 58, p. 599-611.
Panchuk, K.M., Holmden, C.E., and Leslie, S.A., 2006, Local controls on carbon cycling in the Ordovician mid-continent region of North America, with implications for carbon isotope secular curves: Journal of Sedimentary Research, v. 76, p. 200-211.
Patterson, W.P., and Walter, L.M., 1994, Depletion of 13C in seawater ΣCO2 on modern carbonate platforms: significance for the carbon isotopic record of carbonates: Geology, v. 22, p. 885-888.
Peng, S. and Robison, R.A., 2000, Agnostid biostratigraphy across the middle-upper Cambrian boundary in Hunan, China: The Paleontological Society Memoir 53, Journal of Paleontology, 104p.
Peng, S.C. and Babcock, L.E., 2008, Cambrian Period, *in* Ogg, J.G., Ogg, G., and Gradstein, F.M., eds., A Concise Geologic Time Scale: Cambridge University Press, Cambridge, U.K., p. 37-46.
Peng, S.C., Babcock, L.E., Robison, R.A., Lin, H., Rees, M.N., and Saltzman, M.R., 2004, Global Standard Stratotype-section and Point (GSSP) of the Furongian Series and Paibian Stage (Cambrian): Lethaia, v. 37, p. 365-379.
Peng, S.C., Babcock, L.E., Zuo, J.X., Lin, H.L., Zhu, X.J., Yang, X.F., Robison, R.A., Chi, Y.P., Bagnoli, G., and Chen, Y., 2009, The Global boundary Stratotype Section and Point (GSSP) of the Guzhangian Stage (Cambrian) in the Wuling Mountains, northwestern Hunan, China: Episodes v. 32, p. 41-55.
Poole, F.G., Stewart, J.H., Palmer, A.R., Sandberg, C.A., Madrid, R.J., Ross, R.J., Hintze, L.F., Miller, M.M., and Wrucke, C.T., 1992, Latest Precambrian to latest Devonian time; development of a continental margin, *in* Burchfiel, B.C., Lipman, P.W., and Zoback, M.L., eds., The Cordilleran Orogen: Conterminous U.S., The Geology of North America Volume G-3, p. 9-56.
Posamentier, H.W, Jervey, M.T., and Vail, P.R., 1988, Eustatic controls on deposition 1 – conceptual framework, *in* Wilgus, C.K., Hastings, B.S., Kendall, C.G.St.C., Posamentier, H.W., Ross, C.A. and Van Wagoner, J.C., eds., Sea-level changes: An integrated approach: SEPM Special Publication 42, p. 109-124.
Pratt, B.R. and James, N.P., 1986, The St. George Group (Lower Ordovician) of western Newfoundland: tidal flat island model for carbonate sedimentation in shallow epeiric seas: Sedimentology, v. 33, p. 313-343.
Prave, A.R., 1999, Two diamictites, two cap carbonates, two δ13C excursions, two rifts: The Neoproterozoic Kingston Peak Formation, Death Valley, California: Geology, v. 27, p. 339-342.
Railsback, L.B., Holland, S.M., Hunter, D.M., Jordan, E.M., Díaz, J.R., and Crowe, D.E., 2003, Controls on geochemical expression of subaerial exposure in Ordovician limestones from the Nashville Dome, Tennessee, U.S.A.: Journal of Sedimentary Research, v. 73, p. 790-805.
Randolph, R.L., 1973, Paleontology of the Swasey Limestone, Drum Mountains, west-central Utah: Unpublished M.S. Thesis, University of Utah, Salt Lake City, Utah, 73p.
Rees, M.N., 1986, A fault-controlled trough through a carbonate platform – the Middle Cambrian House Range Embayment: Geological Society of America Bulletin, v. 97, p. 1054-1069.
Robison, R.A., 1960, Lower and middle Cambrian stratigraphy of the eastern Great Basin: Intermountain Association of Petroleum Geologists Eleventh Annual Field Conference, p. 43-52.

Robison, R.A., 1964, Middle – Upper Cambrian boundary in North America: Geological Society of America Bulletin, v. 75, p. 987-994.
Robison, R.A., 1976, Middle Cambrian trilobite biostratigraphy of the Great Basin: Brigham Young University Geology Studies, v. 23, p. 93-109.
Robison, R.A., 1982, Some middle Cambrian agnostoid trilobites from western North America: Journal of Paleontology, v. 56, p. 132-160.
Robison, R.A., 1984, Cambrian Agnostida of North America and Greenland – Part I, Ptychagnostidae: The University of Kansas Paleontological Contributions Paper 109, p. 1-59.
Robison, R.A., Rosova, A.V., Rowell, A.J., and Fletcher, T.P., 1977, Cambrian boundaries and divisions: Lethaia, v. 10, p. 257-262.
Rowell, A.J., Robison, R.A., and Strickland, D.K., 1982, Aspects of Cambrian agnostoid phylogeny and chronocorrelation: Journal of Paleontology, v. 56, p. 161-182.
Saller, A.H., Armin, R.A., Ichram, L.O., Glenn-Sullivan, C., 1993, Sequence stratigraphy of aggrading and backstepping carbonate shelves, Oligocene, Central Kalimantan, Indonesia, *in* Loucks, R.G. and Sarg, J.F., eds., Carbonate sequence stratigraphy: Recent developments and applications: American Association of Petroleum Geologists Memoir 57, p. 267-290.
Saltzman, M.R., 2005, Phosphorus, nitrogen, and the redox evolution of the Paleozoic oceans: Geology, v. 33, p. 573-576.
Sarg, J.F., 1988, Carbonate sequence stratigraphy, in Wilgus, C.K., Hastings, B.S., Kendall, C.G.St.C., Posamentier, H.W., Ross, C.A., and Van Wagoner, J.C., Sea-level changes-An integrated approach: SEPM Special Publication 42, p. 155-181.
Schlager, W., 1999, Type 3 sequence boundaries, in Harris, P.M. and Simo, J.A., eds., Advances in carbonate sequence stratigraphy: Application to reservoirs, outcrops and models, SEPM Special Publication 63, p. 35-45.
Schlager, W., Reijmer, J.G., and Droxler, A., 1994, Highstand shedding of carbonate platforms: Journal of Sedimentary Research, v. B64, p. 270-281.
Scotese, C.R., and Barrett, S.F., 1990, Gondwana's movement over the South Pole during the Paleozoic – evidence from lithological indicators of climate, in McKerrow, W.S. and Scotese, C.R., eds., Paleozoic paleogeography and biogeography: The Geological Society of London Memoir 12, p. 75-85.
Scotese, C.R. and McKerrow, W.S., 1990, Revised world maps and introduction, in McKerrow, W.S. and Scotese, C.R., eds., Paleozoic paleogeography and biogeography: The Geological Society of London Memoir 12, p. 1-21.
Smith, D.D., 2007, Sequence stratigraphy of the middle Cambrian Marjum Formation: response of sedimentary facies and biota to sea-level changes: Unpublished M.S. Thesis, Utah State University, Logan, Utah, 155p.
Spence, G.H. and Tucker, M.E., 2007, A proposed integrated multi-signature model for peritidal cycles in carbonates: Journal of Sedimentary Research, v. 77, p. 797-808.
Strother, P.K., Al-Hajri, S., Traverse, A., 1996. New evidence for land plants from the lower Middle Ordovician of Saudi Arabia: Geology, v. 24, p. 55–59.
Sundberg, F.A., 1991, Paleogeography of western Utah and eastern Nevada during the *Ehmaniella* biochron (Middle Cambrian), *in* Cooper, J.D., and Stevens, C.H., eds., Paleozoic paleogeography of the western United States – II: Pacific Section SEPM, v. 67, p. 387-399.
Sundberg, F.A., 1996, Morphological diversification of Ptychopariida (Trilobita) from the Marjumiid biomere (Middle and Upper Cambrian): Paleobiology, v. 22, p. 49-65.
Sundberg, F.A., 2005, The Topazan Stage, A new Laurentian stage (Lincolnian Series – "Middle" Cambrian): Journal of Paleontology, v. 79, p. 63-71.

Surge, D.M., Savarese, M., Dodd, J.R., and Lohmann, K.C., 1997, Carbon isotopic evidence for photosynthesis in Early Cambrian oceans: Geology, v. 25, p. 503-506.
Swart, P.K., 2008, Global synchronous changes in the carbon isotopic composition of carbonate sediments unrelated to changes in the global carbon cycle: Proceedings of the National Academy of Sciences, v. 105, p. 13741-13745.
Swart, P.K., and Eberli, G., 2005, The nature of δ13C of periplatform sediments: Implications for stratigraphy and the global carbon cycle: Sedimentary Geology, v. 175, p. 115-129.
Tearpock, D.J. and Bischke, R.E., 2002, Applied subsurface geological mapping with structural methods: Prentice Hall, 864p.
Theiling, B.P., Railsback, L.B., Holland, S.M., and Crowe, D.E., 2007, Heterogeneity in geochemical expression of subaerial exposure in limestones, and its implications for sampling to detect exposure surfaces: Journal of Sedimentary Research, v. 77, p. 159-169.
Tschanz, C.M., and Pampeyan, E.H., 1970, Geology and mineral deposits of Lincoln County, Nevada: Nevada Bureau of Mines and Geology Bulletin 73, 188p.
Tucker, M.E., and Wright, V.P., 1990, Carbonate sedimentology: Oxford, Blackwell Scientific Publications, 482 p.
Vail, P.R., Hardenbol, J., and Todd, R.G., 1984, Jurassic unconformities, chronostratigraphy, and sea-level changes from seismic stratigraphy and biostratigraphy, *in* Schlee, J.S., ed., Interregional unconformities and hydrocarbon accumulation: American Association of Petroleum Geologists Memoir 36, p. 129-144.
Vail, P.R., Mitchum, R.M. and Thompson, S., 1977, Seismic stratigraphy and global changes of sea level, part 3-relative changes of sea level from coastal onlap, *in* Payton, C.E., ed., Seismic stratigraphy-applications for hydrocarbon exploration: American Association of Petroleum Geologists Memoir 26, p. 63-81.
Van Wagoner, J.C., Mitchum, R.M., Campion, K.M., and Rahmanian, V.D., 1990, Siliciclastic sequence stratigraphy in well logs, cores, and outcrops: Concepts for high-resolution correlation of time and facies: American Association of Petroleum Geologists Methods Exploration Series 7, 55p.
Volkov, I.I., 2000, Dissolved inorganic carbon and its isotopic composition in the waters of anoxic marine basins: Oceanology, v. 40, p. 499-502.
Weissert, H., 1989, C-isotope stratigraphy, a monitor of paleoenvironmental change: a case study from the Early Cretaceous: Surveys in Geophysics, v. v. 10, p. 1-61.
Wilde, P. and Berry, W.B.N., 1984, Destabilization of the oceanic density structure and its significance to marine “extinction” events: Palaeogeography, Palaeoclimatology, Palaeoecology, v. 48, p. 143-162.
Wilson, P.A. and Roberts, H.H., 1992, Carbonate-periplatform sedimentation by density flows: A mechanism for rapid off-bank and vertical transport of shallow-water fines: Geology, v. 20, p. 713-716.
White, W.W., 1973, Paleontology and depositional environments of the Cambrian Wheeler Formation, Drum Mountains, west central Utah: Unpublished M.S. Thesis, University of Utah, Salt Lake City, 135p.
Xiao, H. and Suppe, J., 1992, Origin of rollover: American Association of Petroleum Geologists Bulletin, v. 76, p. 509-529.
Zecchin, M., 2005, Relationships between fault-controlled subsidence and preservation of shallow-marine small-scale cycles: examples from the lower Pliocene of the Crotone Basin (southern Italy): Journal of Sedimentary Research, v. 75, p. 300-312.
Zecchin, M., Massari, F., Mellere, D., and Prosser, G., 2004, Anatomy and evolution of a Mediterranean-type fault bounded basin: the lower Pliocene of the northern Crotone Basin (southern Italy): Basin Research, v. 16, p. 117-143.

Zhu, M.Y., Zhang, J.M., Li, G.X, Yang, A.H., 2004, Evolution of C isotopes in the Cambrian of China: implications for Cambrian subdivision and trilobite mass extinctions: Geobios, v. 37, p. 287-301.
Zhu, M.-Y., Babcock, L.E., and Peng, S.C., 2006, Advances in Cambrian stratigraphy and paleontology: integrating correlation techniques, paleobiology, taphonomy and paleoenvironmental reconstruction: Palaeoworld, v. 15, p. 217-222.
Zhuravlev, A. Y., and Wood, R.A., 1996, Anoxia as the cause of the mid-Early Cambrian (Botomian) extinction event: Geology, v. 24, p. 311-314.

VITA

Graduate College
University of Nevada, Las Vegas

Robyn A. Howley

Degrees:

Bachelor of Science, Geology, 1999
Salem State College

Master of Science, Geoscience, 2002
University of Nevada, Las Vegas

Special Honors and Awards:

The Honor Society of Phi Kappa Phi (since Spring 2008)
UNLV President's Graduate Fellowship (2007/08 academic year)
UNLV GPSA 1st Place Talk (2008 Science & Engineering Platform)
UNLV GPSA 2nd Place Talk (2007 Science & Engineering Platform)
UNLV GPSA graduate grant (Fall 2006 & Spring 2007)
SEPM-RMS Donald L. Smith Award - Honorable Mention (2006 & 2007)
National Association of Geoscience Teachers, FWS Graduate Scholarship (2006)
Geological Society of America Research Grant (2006)
American Association of Petroleum Geologists R.E.McAdams Memorial Grant (2006)
Institute for Cambrian Studies Research Grant (2006 & 2007)
Nevada Petroleum Society Graduate Scholarship (2005, 2006 & 2007)
UNLV Graduate College GREAT Assistantship (2001, 2006)
UNLV Geoscience Scholarship (Geological Society of Nevada Fund) (Summer 2006)
UNLV Alumni Association Most Outstanding Masters Thesis (9/2003)
UNLV College of Sciences Outstanding Masters Thesis (5/2003)
UNLV Geoscience Scholarship (Spring 2000, Summer 2001)
Geological Society of America Cordilleran Section Meeting Best Graduate Student Poster (2001)
Geological Society of America Travel Grant (2001)
Geological Society of America Research Grant (2000)
American Association of Petroleum Geologists Research Grant (2000)

Publications:

Howley, R.A. and Jiang, G., 2010, The Cambrian Drumian carbon isotope excursion (DICE) in the Great Basin, western United States: Palaeogeography, Palaeoclimatology, Palaeoecology, v. 296, p. 138-150.

Howley, R.A., Rees, M.N., and Jiang, G., 2006, Significance of Middle Cambrian mixed carbonate-siliciclastic units for global correlation: southern Nevada, U.S.A.: Palaeoworld, v. 15, p. 360-366.

Cizdziel, J.V., Wei, Y., Stetzenbach, K.J., Hodge, V.F., Cline, J., **Howley, R.**, and Phillips, F.M., 2008, Recent measurements of ^{36}Cl in Yucca Mountain rock, soil and seepage: Journal of Radioanalytical and Nuclear Chemistry, v. 275, n. 1, p. 133-144.

Howley, Robyn A. and Jiang, Ganqing, 2007, Sequence stratigraphy of the Middle Cambrian succession in eastern Nevada and western Utah: evidence for the

initiation and termination of the House Range Embayment: Geological Society of America Abstracts with Programs, v. 39, n. 6.

Howley, Robyn A., Johnson, Kimberly A., and Campbell, Brett D., 2007, Teaching Teachers through Field Experiences: A study on the Earth-system approach for Earth Science curriculum development: Geological Society of America Abstracts with Programs, v. 39, n. 6.

Howley, Robyn A., Jiang, Ganqing, and Rees, Margaret N., 2005, Significance of Middle Cambrian mixed carbonate-siliciclastic units for global stratigraphic correlation: southern Nevada, U.S.A.: Acta Micropalaeontologica Sinica, v. 22 supplement, p. 63-64. The 4th International Symposium on the Cambrian System, Nanjing, China, August 18-24, 2005.

Hanson, Andrew D., Druschke, Peter A., **Howley, Robyn A.**, Suurmeyer, Nathan R., Benneman, Bud, Erwin, Martin B., and McLaurin, Brett T., 2005, Deformation of the Miocene-Pliocene Muddy Creek Formation, southern Nevada: Lake Mead fault system, salt tectonics, or both?: Geological Society of America Abstracts with Programs, v. 37.

Snelson, Catherine M., McEwan, Darlene J., Hirsch, Aaron C., and **Howley, Robyn A**., 2005 Mapping fissures in Pahrump, Nevada using Geophysical methods: Geological Society of America Abstracts with Programs, v. 37.

Hirsch, A.C., McEwan, D.J., **Howley, R.A.**, Mehling, J.B., Snelson, C.M., and Drohan, P., 2004, A geophysical study of fissures in Pahrump, Nevada: Eos Trans. AGU, v. 85, Fall Meeting Supplement, Abstract H21E-1080.

Buck, B. J., Lawton, T. F., Merkler, D., **Howley, R. A.**, Khresat, S., Rawajfih, Z., Waidmann, B., and Hanson, A., 2003, Snowballs in the Devil's Anus and other adventures in the world of pedogenic sulfates, GSA Program with Abstracts, v 34, p. 257.

Steinberg, S., Rudin, M.J., Buck, B.J., Hanson, A.D., Hodge, V.F., Twichell, D.C., and **Howley, R.**, 2003, Investigation of organic matter in Lake Mead sediments using chemo-pyrolysis GCMS: 13th Annual West Coast Conference on Contaminated Soils, Sediments, and Water.

Zybala, J., Buck, B.J., **Howley, R.A.**, Twichell, D.C., Hickson, T.A., Hanson, A.D., Rudin, M.J., and Steinberg, S., 2003, Sediment Coring in Lake Mead Reservoir, NV and AZ: Implications for Deep Marine Sandstone Distributions, American Association of Petroleum Geologists Abstracts with Programs, p. 48.

Buck, B.J., Van Hoesen, J.G., Khresat, S., Rawajfih, Z., Merkler, D., Schiefelbein, I., **Howley, R.**, and Lawton, T., 2002, Genesis and morphology of pedogenic gypsum and other sulfate minerals, USA and Jordan: Soil Science Society of America Annual Meeting.

Howley, Robyn A., Shapiro, Russell S. and Rees, Margaret N., 2002, Carbonate depositional history refined by gamma radiation analysis - Middle to lower Upper Cambrian Highland Peak Formation, eastern Nevada: Geological Society of America Abstracts with Programs, v. 34.

Howley, Robyn A. and Rees, M.N., 2001, Sea level signatures and regional correlations elucidated by carbonate cycle architecture: Middle Cambrian Highland Peak Formation, eastern Nevada: Geological Society of America Abstracts with Programs, v. 33, p. 77.

Bailley, T.L., Gilbert, J.J., **Howley, R.A**., Rees, M.N., Schiefelbein, I.M., Taylor, W.J. and Van Hoesen, J.G., 2001, Geologic guide to Red Rock Canyon: Integrating research and education: Arizona-Nevada Academy of Science Abstracts with Programs, v. 36, p. 52.

Howley, R.A., Rees, M.N. and Jacobson, E.A., 2001, Re-assessing reliability of meter-scale cyclic carbonates as recorders of orbital events: Middle Cambrian Highland Peak Formation, southern Nevada: Geological Society of America Abstracts with Programs, v. 33, A68 and American Association of Petroleum Geologists Bulletin, v. 85, p. 1125.

Howley, Robyn A., 2000, Cyclic carbonate sedimentation in the Middle to early Late Cambrian, Highland Peak Formation, southern Nevada: Implications for interpreting eustasy: American Association of Petroleum Geologists Bulletin, v. 84, p. 1865.

Howley, Robyn A. and Rouleau, Danielle, 1999, Facies analysis of carbonate sediments from the Lee Stocking Island Region of the Bahama Bank: Salem State College Undergraduate Research Symposium.

Dissertation Title: Sequence & chemostratigraphy of the middle Cambrian succession, Nevada & Utah

Dissertation Examination Committee:
Chairperson, Ganqing Jiang, Ph.D.
Committee Member, Andrew Hanson, Ph.D.
Committee Member, Matthew Lachniet, Ph.D.
Committee Member, Steve Rowland, Ph.D.
Graduate Faculty Representative, Vernon Hodge, Ph.D.